UNIVERSIDAD NACIONAL DE COLOMBIA

Medición de campo magnético generado por descargas eléctricas atmosféricas en la ciudad de Bogotá

"Lightning magnetic field measuring system in Bogotá"

EE. Oscar Fernando Escobar Alvarado

Universidad Nacional de Colombia

Faculty of Engineering

Bogotá, Colombia

2013

Medición de campo magnético generado por descargas eléctricas atmosféricas en la ciudad de Bogotá

"Lightning magnetic field measuring system in Bogotá"

EE. Oscar Fernando Escobar Alvarado

Thesis for the degree of Master of Science in Electrical Engineering

Director:

Francisco José Román Campos, Ph.D.

Electromagnetic Compatibility Research Group

EMC-UNC

Universidad Nacional de Colombia

Faculty of Engineering

Bogotá, Colombia

2013

Acknowledgments

The author wants to express his deepest appreciation to all those who provided him the possibility to complete this thesis. A special gratitude to Professor Francisco Roman whose contribution in stimulating suggestions and encouragement, helped to develop my project.

Furthermore also the acknowledgement with much appreciation to the staff of Electromagnetic Compatibility Research Group EMC – UNC, who help to this project through their comments and advices and valuable time to discuss the results, especially to Eng. Herbert Rojas, Professor Francisco Santamaría, Eng. Carlos Rivera and Eng. Oscar Montero.

My acknowledgements to "Laboratorio de Ensayos Eléctricos Industriales – LABE" for the help provided for different tests and the invaluable support and comments of Professors Francisco Amórtegui, Fernando Herrera and Javier Araque.

I would like to thank my family and relatives, who have supported me during the whole process, in the difficult and good moments.

Finally extend the grateful for the support of "Dirección de Investigación Sede Bogotá – Universidad Nacional de Colombia", Faculty of Engineering, LABE and the Department of Electrical and Electronic Engineering of *Universidad Nacional de Colombia* who made possible the development of this research project.

Abstract

This thesis presents the configuration and performance of a lightning radiated electromagnetic field measuring system in Bogotá – Colombia. The system is composed by both magnetic and electric field measuring systems working as separated sensors. The aim of the thesis is the design and construction of a Magnetic Field Measuring System and the implementation of a whole lightning measuring system in Bogotá. The theoretical background, design process, construction and implementation of the system are presented and the analysis of signals obtained is discussed.

Keywords: Lightning in Bogota, Lightning measurement, Loop antennas, Magnetic Field Measuring System.

Spanish Abstract

Este trabajo de tesis presenta la configuración y desempeño de un sistema de medición de campos electromagnéticos radiados por las descargas eléctricas atmosféricas en la ciudad de Bogotá. El sistema está compuesto por sistemas de campo magnético y eléctrico integrados como sensores independientes. El objetivo de la tesis es realizar el diseño y construcción del Sistema de Campo Magnético y desarrollar la implementación completa de los sistemas para medición de descargas eléctricas atmosféricas en Bogotá. Son presentados el

marco teórico, el proceso de diseño, la construcción e implementación del sistema así como el análisis de las señales obtenidas.

Palabras Clave: Antenas tipo bucle, Descargas Eléctricas Atmosféricas en Bogotá, Medición de Rayos, Sistema de Medición de Campo Magnético.

Contents

Contents

Figures

Tables

Introduction

Characteristics of electric and magnetic fields produced by lightning discharges have been studied during the last century [1]-[3]. These characteristics are used to study the effects of lightning fields on electrical systems and equipment, especially in electronic circuits of high sensitivity as the equipment used in information technologies. However, deleterious effects of lightning are extensive, including the death or injury to people and animals, causing fire start, possible damage and destruction of structures, outages of power and communication lines, among others.

Due to these effects, lightning research has maintained a high dynamic, allowing that theories and measurement techniques have evolved greatly, understanding the phenomenon of lightning in a more accurate way, progress in the field of understanding the physical phenomenon as such, as well as measurement, detection, prediction and protection against this natural phenomenon. For the appropriate development of the above processes it is still a need to establish systems for measuring lightning signals, being able to determine the relevant features according the needs in the field of study (prediction, protection, localization, among others)

Atmospheric discharges produce electromagnetic fields propagating through the atmosphere above the ground near to light velocity; these electromagnetic fields induce currents and voltages on metal structures, facilities, electronic or any driver which is located in the spread area. Although these effects are undesirable on structures that can be affected, this property can be used for measuring the characteristics of lightning. Compared with other methods of direct lightning measurement, such as instrumented towers, measuring lightning electromagnetic fields is easier and cheaper.

Lightning characterization through its radiated magnetic field measurement has been developed and implemented for decades in several regions of the world [4]-[7]. It can be mentioned that lightning location systems are a

successful application of the distant measurement of lightning radiated electromagnetic fields [8]. Additionally, nowadays an important research topic [9]-[10] is the indirect determination of the lightning current amplitude by a distant measurement of the radiated electromagnetic fields.

Measurement techniques have been improved especially in instrumentation by increasing the bandwidth and resolution of the measuring equipment, allowing the registration of signals with more detail and improving the development of better measuring-, acquisition- and signal processing-systems.

The lightning activity in Colombia is very high due to its geographical location, allowing the use of lightning location systems (LLS) to study lightning discharges in a continuous way. Several lightning electromagnetic field measuring projects have been performed in the country mainly focused on prediction and detection of the atmospheric electrical activity. The Colombian System for Thunderstorm Information (SCITE) is the most important experience [11], using information from electrostatic field meters, lightning detection devices and high sensitivity cameras.

Measurements have also been developed with antennas for detection of electrostatic field and induced and radiated components, allowing the description of time variation in lightning signals. Two undergraduate thesis in *Universidad Nacional de Colombia*, shows the work developed for measure electric and magnetic field in the campus of the University during the 90s [12]-[13]. These works obtained descriptive rather than quantitative results, but it served as a first approach to the study of lightning in Bogotá and as a basis for further studies of characterization and description of application models.

Colombia has data activity detection of lightning and intra-cloud lightning provided by the Colombian Lightning location Network (RECMA), carrying out in accordance with SCITE mentioned above. These networks create an information system for detecting storms in the north-central region of the country, with some limitations in terms of effectiveness and location.

A new lightning detection system, already present in Europe, was brought to Colombia as private efforts. The LINET Network seeks to have greater reliability based on magnetic field measurement techniques and VLF / LF and an advanced algorithm for signal processing [14]. In September 2011 came into operation in Colombia the LINET network: The first nine sensors

(Bogotá, Tunja, Ibague, Rionegro, Barrancabermeja, Monteria, Cucuta, Barranquilla and Puerto Gaitán) provide real-time information of the lightning activity with efficiency greater than 90% for Cloud to Cloud (CC) and Cloud to Ground (CG) discharges in the central region of Colombia [15].

A lightning magnetic field measuring project is being developed at the Universidad Nacional de Colombia in Medellin. This measurement system uses lightning sensors for measuring atmospheric electric field (field mills and parallel plate antennas) and magnetic field (loop antenna) in order to characterize the atmospheric discharges in the area and implement a measurement network with other cities like Manizales and Bogotá [16]. This effort is also part of SCITE Network mentioned above.

Particularly, the EMC-UNC research group is measuring lightning electric and magnetic fields produced by lightning discharges [17]-[19], at the high altitude region of Bogotá-Colombia. Already in 2005, as part of the development of a postgraduate thesis, a Lightning Electric Field Measurement campaign was performed. A comparison between recorded signals in Bogotá and field records obtained in Sweden and Sri Lanka was developed, highlighting the analysis of times, multiplicity and waveforms of the recorded signals.

Although the projects already mentioned in the country, there is a continuing need of lightning characterization in Colombia, especially of the parameters derived from the measured waveforms mainly due to the possible spatial and temporal variation of these characteristics. Therefore, remains indispensable to establish a measuring system with constantly autonomous operation, in order to identify the variables of interest as the characteristic times, multiplicity, polarity, direction and, eventually supported by a Detection Network, lightning current values.

According to the reasons described above, the purpose of this thesis is to design, construct and implement a lightning magnetic field measuring system in Bogotá, Colombia, in order to analyse the electromagnetic behaviour of magnetic field signals and provide to EMC-UN Group a reliable lightning magnetic field measuring system for ulterior analysis and constant monitoring of thunderstorm conditions and signals.

This document is divided in 3 chapters, the first one is related to basic theory necessary for the development of the lightning measuring system. The second

chapter is intended to show the design, construction and implementation of electromagnetic field measuring system. The third chapter resumes the most important findings of measurements campaign made with the measuring system. The final chapter provide the conclusions of work and proposed future work.

Chapter 1

Atmospheric Electrical Discharges – Lightning

1.1. Lightning description

Lightning is a transient and high-current electric discharge occurred in the atmosphere and whose extension is measured in kilometres. These discharges are generally produced by electric charge separated in thunderstorm clouds, being the most common the *Cumulonimbus*, characterized for his vertical form formed by the water vapour carried by upward air currents. Although the atmospheric discharges are the most common, it is known that "Lightning-like electrical discharges can also be generated in the ejected material above volcanoes, in sandstorms and in nuclear explosions" [2].

A simple model of a thunderstorm cloud could be represented by a model that describe three charge centres: a negative region in the centre *N*, a positive region above this *P* and a second region smaller of positive charge in the lower part of the cloud *p*. See Figure 1.

Figure 1. Charge centres in a thunderstorm cloud. Picture taken from www.dlf.cz on January 2013 and adapted by the author.

There are several theories about how lightning flashes are initiated. In general, all of these theories agree in the existence of a region of the cloud where water drops, ice crystals and water vapour coexist in the presence of a high intensity electric field enough to allow the occurrence of a breakdown that initiate a chain of events that conform a whole flash. One of these theories that is normally discussed, suggest that the electrical potential between the positive and negative charges in the cloud above mentioned as *N, P* and *p*, eventually grows until defeat the air's resistance to electrical flow and initiate the lightning flash. The events and steps after the initiation are widely discussed in [1].

According with the start and end points of lightning and the type of charge that transport, it is possible distinguish three main types of flashes: intra-cloud (IC) flashes, which transports charge within a cloud between charge centres; cloud to cloud (CC) flashes occurs between two separate clouds that are at different electric potential; cloud to ground (CG) flashes could be of two types, negative in the case which transport negative charge from the cloud to the ground and positive flashes, which transport positive charge from the cloud to the ground. Other kind of flashes as cloud to air discharges, together with IC and CC flashes, are generally called cloud flashes or cloud discharges.

Cloud to ground (CG) against cloud discharges presents minor occurrence (approximately 75% of lightning are CC and IC), however, due to the severity of these effects in human and technological resources, the studies of lightning have been centred in CG flashes in order to understand the phenomena and, as an application, improve the lightning protection systems. Additionally, the study of cloud flashes is very restricted compared with CG flashes due to measurement limitations; nevertheless is an important field of study in the aircraft industry due the severity and effects over planes and air operations.

1.1.1. Cloud to Ground (CG) Flashes

CG flashes are classified in four types based in the direction of the initial leader and the polarity of charge transferred from the cloud to ground as is shown in Figure 2. In downward negative and positive – a) and c) in Figure 2 – the initial leader start his path from the cloud, either from the low or the high region of cloud where the positive and negative charge centres are

respectively present. According to the leader initial point, the charge transfer from the cloud to ground is negative for downward negative and positive charge for downward positive. For the case when the initial leader starts from ground (or a high structure attached to ground) in direction to the cloud, a transference of negative charge in upward negative and positive charge in upward positive is made – b) and d) in Figure 2 –.

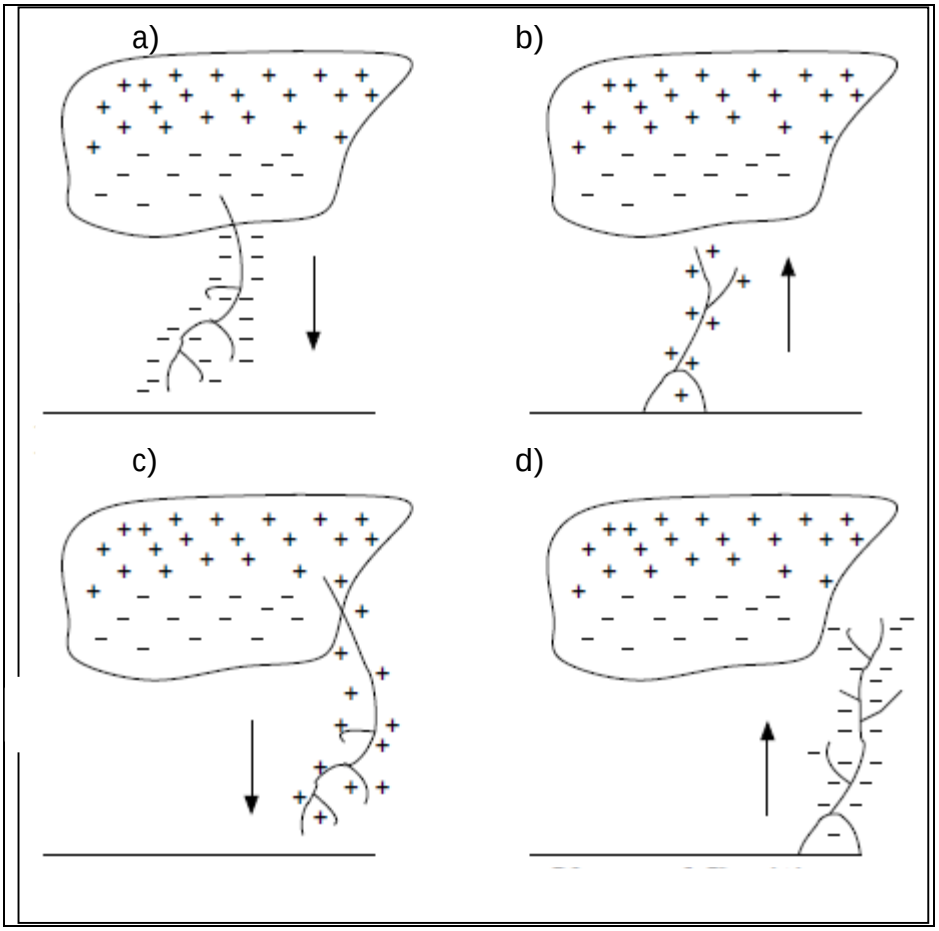

Figure 2. Types of Cloud to Ground (CG) Flashes. a) Downward negative, b) Upward negative, c) Downward positive, d) Upward positive. Adapted from [2].

The initial leader in a downward negative flash is initiated from within the cloud, through a process known as initial or preliminary breakdown. The initial breakdown is characterized by a series of pulses marking a transition from the initial breakdown to the initial leader.

After initial breakdown, the charged leader propagates in direction to an area of opposite charge, which are the base of the cloud for negative CG and the higher part of cloud for positive CG lightning. The leader is called "stepped"

because it has been observed optically to propagate in a discontinuous manner through the air before ionization. The stepped leader process can be viewed as a mechanism by which charge is removed from the cloud and deposited along a channel extending between cloud and ground [20]. The CG leader descends towards ground, typically exhibiting many branches as the lightning shown in Figure 3.

Figure 3. Downward lightning exhibiting many branches. Picture taken from http://www.moonraker.com.au/techni/lightning.jpg on March 2013.

During his travel to ground and when the stepped leader tip is still some hundreds of meters above ground, several upward leaders (positive or negative according to the polarity of the stepped leader tip charge) are initiated from objects on the ground and each propagate in direction to the stepped leader channel or one of its branches. An upward leader is initiated when the electric field at ground exceeds the required field for air breakdown, this due to the charge on the downward stepped leader. This event is considered as the beginning of the lightning attachment process.

When the two leaders combine to form a single channel, a potential discontinuity exist in the junction, this because the stepped leader channel is at some tens of megavolts and upward leader channel is nearly at ground potential. This large potential discontinuity then propagates in both directions from the attachment point. The downward wave, upon reaching the ground, reflects and propagates back up the channel towards the cloud. The

upward wave is known as the first return stroke and neutralizes most or all of the charge deposited by the stepped leader. The return stroke is responsible for the extraordinary visual and sound effects, as well as the damage and personal injury, associated with lightning.

Currents from return strokes have been measured using instrumented tall towers for direct impacts and calculations from electromagnetic measurements; nevertheless, the data provided by direct measurements is widely accepted for lightning characterization.

The characterization of negative downward lightning on Mount San Salvatore by Berger is the most recognized and still used results. The most representative parameters are: first-stroke currents have a median peak of about 30 kA, rise time of about 5.5 μs, and duration of half-peak width about 75 μs, either positive and negative downward lightning were measured. An example of measured signals is provided in Figure 4.

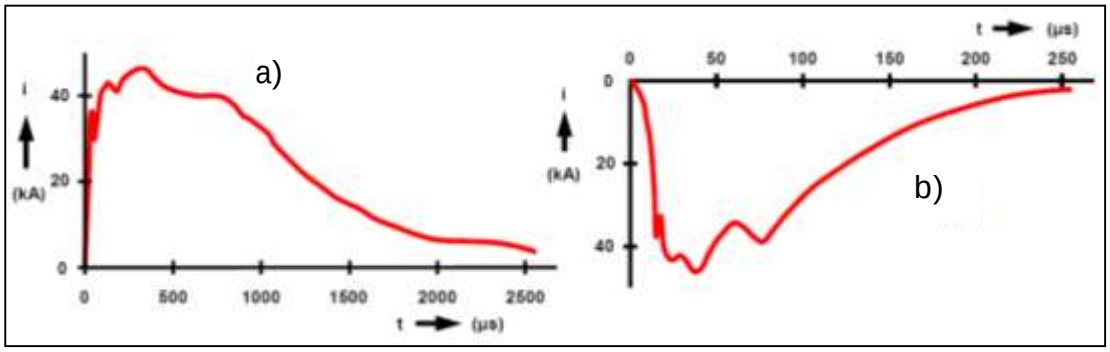

Figure 4. Return stroke currents of first strokes of (a) positive and (b) negative downward lightning. Adapted from [21].

After a no-current period of some tens of milliseconds one more subsequent leader/return-stroke sequences may follow the first. This subsequent event is present approximately in 80% of downward negative flashes according to Cooray [1]. In the work of Santamaria [17] developed in Bogotá, the author obtained a percentage of 40% of subsequent strokes in the case of negative downward lightning. The typical number of strokes per flash is 3 to 5, while in Bogotá Santamaria registered an average of 1.8 subsequent strokes per flash.

Downward positive cloud-to-ground lightning represents roughly 10% of all cloud to ground flashes being relatively low compared with negative lightning, being less observed and weakly understood. Downward positive lightning has

significant local and seasonal variability. For example, positive discharges may account for the majority of flashes in winter storms while negative lightning is dominant in summer thunderstorms.

Positive downward lightning presents higher charge transference from cloud to ground due to continue currents that follow the return strokes. This characteristic is important to understand the larger effects of positive rather than negative flashes on humans and equipment.

In the case of upward negative and positive lightning, most of these are developed in tall structures and towers from the top of the structure. At the top of structure the electric field increases and may be enhanced to such an extent that an upward leader starts. The upward lightning typically occurs in winter when the thundercloud base is lower and closer to the tower top, enabling the appearance of upward leaders from the structure towards the positive charge centre in the cloud as it is shown in Figure 5.

1.1.2. Cloud Flashes

The term cloud flashes is related to Intra-Cloud (IC) flashes that occurs between the negative and main positive charge of the cloud, Cloud to Cloud (CC) Flashes that occurs between the charge centres of two different thunderstorm clouds and Cloud to Air (CA) flashes that occurs between the thundercloud and surrounding air. Figure 6 shows these different flashes.

These kind of flashes are the types with most occurrence, however are the fewer studied and do not exist extensive literature of these. Studies about the spectrum frequency made by Cooray *et al* [22] or measurement campaigns of intra-cloud lightning discharges (CIDs) [23] are made, mainly in order to obtain a better understanding of cloud lightning discharges and estimate their peak currents.

Figure 5. Upward lightning from tall tower. Picture taken from jpgmag.com by Paul Romero

Figure 6. Types of Cloud Flashes. a) Cloud to Air flash (Brian Emfinger 2012), b) Cloud to Cloud flash (Scruffystu 2010) and c) Intra-Cloud (IC) flash (Samuel Barriclow 1999)

1.2. Lightning measurement

Measurements related with lightning have been made from eighteenth century, when Benjamin Franklin stated that thunderstorm clouds have electric charges of two different states (nowadays established as positive and negative charges) and their interaction between them and ground. The concept of the existence of two kind of charges was proposed by many

researchers but only after two centuries was possible to be obtained an evidence of this idea.

Although Franklin never could demonstrate this affirmation, he constructed a device known as Franklin bells that connected to other of his inventions, the lightning rod. This device is considered as the first attempt to measure, not only the possibility of existence of charges in a thunderstorm, but also for lightning as Franklin himself wrote, because sometimes the bells would ring when there was only a dark cloud above and no obvious thunder and lightning. Nevertheless, at other times the bells would be silent until a nearby flash of lightning started them ringing.

Modern methods of measure lightning are no worried only in the knowledge of its existence, also its characteristics, location and specific details. These characteristics are used analysis of lightning protection systems, lightning location or understanding of the physical phenomenon. For this objective, researchers used several techniques that could be classified in two types: direct and remote measurement. In next sections, some of these techniques will be presented briefly.

1.2.1. Direct Measurement

Direct measurement include the techniques where a structure is intended for the direct impact of lightning. These structures could be constructed for this objective or structures that according his dimensions, location or historically with high impact probability, could be struck for lightning. Examples of structures that are used due to high probability of impact are the CN Tower in Canada [24], Gaisberg Tower in Austria [25], Peissenberg Tower in Germany [26], Säntis Tower in Switzerland [27], Tokyo Skytree in Japan [28] and Ilyapa Project in Colombia [29]. Figure 7 shows an example of this kind of towers.

Other type of direct measurement is the triggered lightning, this technique is a method of artificially initiating a cloud-to-ground lightning flash. The technique involves launching a small rocket that extends upward a thin conducting wire, which can be grounded or ungrounded. If the wire is grounded, the flash is usually referred to as "classical" triggered lightning. Triggering with an ungrounded wire, having a gap of some hundreds of

meters or more between the bottom of the conducting wire and ground, is usually referred to as "altitude" triggered lightning [30].

Direct measurements techniques are used for understand the lightning channel-base current because most of the studies dealing with the electromagnetic effects of lightning are based on it. The most complete description of lightning return stroke currents is due to Berger et al [31] who measure natural lightning currents at the top of two 55-m high towers located on the Monte San Salvatore.

These techniques could be classified in two types: The first one is the use of resistive shunts intended for allow lightning current pass through the elements and measure the resulting voltage across the resistance. The high robustness and accuracy of the resistive shunt are crucial for the correct measurement of the lightning current parameters. Second main technique is based in the use of coils that surround the tower, building or descendant way of current in the structures. The most common used is the Rogowsky coil thanks to adequate characteristics for measure high speed current pulses as bandwidth, linear behaviour even when is subjected to large currents, among others. The main disadvantage is the requirement of use an integrator to obtain the current waveform because the voltage produced by a Rogowsky coil is proportional to the derivative current.

Despite the use of several towers around the world, direct measurement is expensive and requires an extensive use of high technology and maintenance. In addition, certain objectives of lightning studies as location systems are not suitable through instrumented towers. For these reasons, the remote measurement remains as an important source of information and the most extended technique of analysis and developments nowadays.

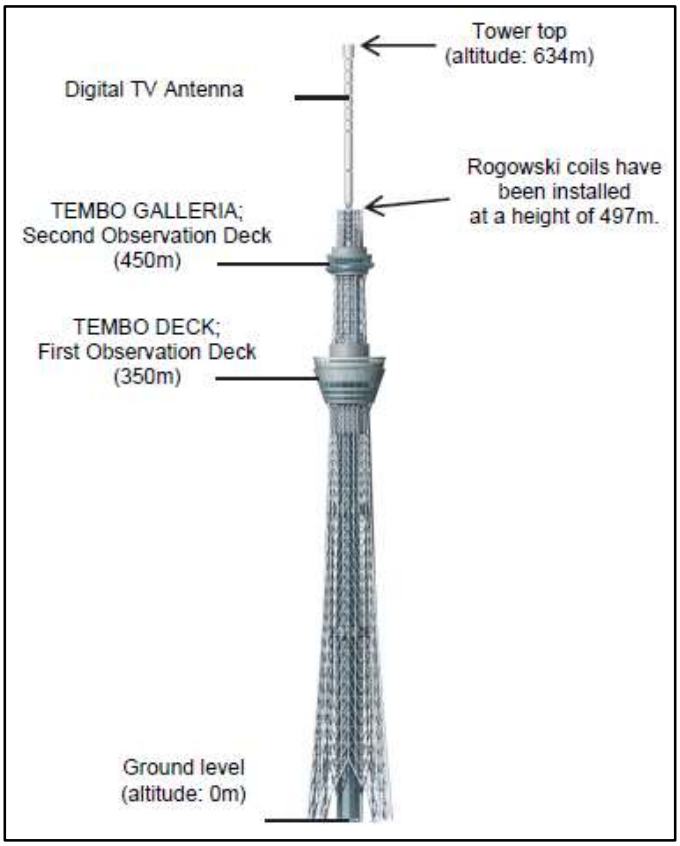

Figure 7. Schematic graphic of instrumentation in Tokyo Skytree Tower in Japan [28].

1.2.2. Remote Measurement

Measurement of Electric and Magnetic Fields are the main way to understand the lightning characteristics. Using Electromagnetic Field (EMF) sensors with different frequency ranges and bandwidths, the knowledge of EMFs produced by lightning has grown greatly and new applications and models have been proposed and established. Several types of systems has been used in the measurement of EMF lightning, allowing the analysis in different ways as near and far fields, nanoseconds range or Ultra High Frequency spectrum, obtaining new features and applying them in new concepts, standards and systems.

1.2.2.1. Electric Field Measuring Devices

Measurement of Atmospheric Electric Field is developed for both, slow and fast variations, from minutes or seconds for thunderstorm formation until milliseconds and microseconds related with behaviour of charge process and lightning propagation. The main methods used to measure such records are based on the measurement of the surface charge induced on a sensor surface.

From the development of Wilson in early twentieth century known as Portable Universal Electrometer [32], several approaches had been developed by other researchers using similar principles. The operation principle is based on the surface charge induction to generate a variable electric charge. The electric charge is induced on an electrode which is periodically covered and exposed to electric field through different mechanisms. These mechanisms vary from rotating shielding layers until mechanic arrays using spheres to produce a harmonic movement covering and uncovering the sensor surface converting the electric field into an AC voltage of modulated amplitude across a resistor. A diagram of electric field mill components is shown in Figure 8.

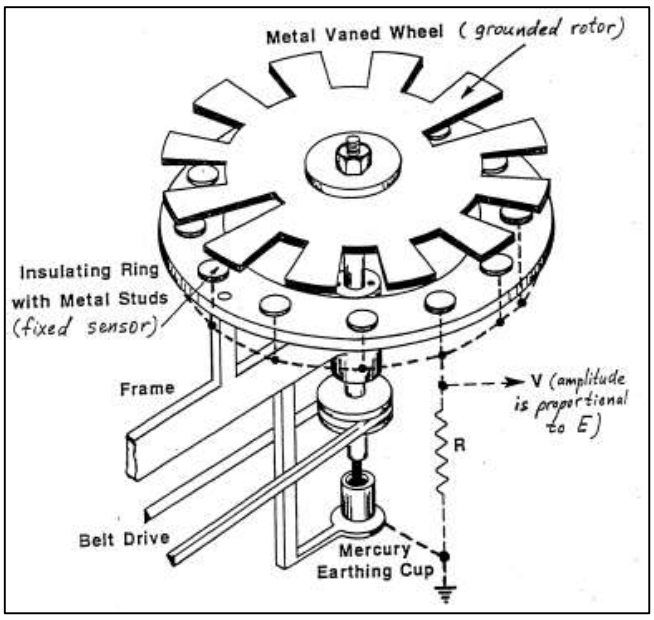

Figure 8. Electrostatic Flux meter (Field mill) [33]

The response time of electric field mill is determined by the rotation speed of top plate and number of segments into which the two plates are divided. According to these characteristics, the electric field measured varies from DC or relatively steady field until lightning field changes with an upper frequency of tens of kHz.

In order to measure fast electric field variations, devices based on radiation measurement have been used during several years. The principle of this type of sensors is that variation of atmospheric electric field with respect to time produces also the variation of electrical charge induced in an antenna and, grounding through an electrical circuit, generates a current proportional to

electric field. Antennas used for this configuration are for example flat plate, sphere or wire antennas as shown in Figure 9.

The charge induced on these antennas by the electric field is sensed and is necessary to integrate the current, *dQ/dt*, which is flowing to ground through electronic circuit. Using the relation between electric field and circuit voltage after integration, it is possible obtain the normal electric field to the plate:

$$E_n = \frac{V}{\left(\varepsilon_0 * \frac{A}{C}\right)} \quad (1)$$

Where (See Figure 10):

E_n: Normal electric field to plate,

V: Circuit voltage after integration,

ε_0: Vacuum permittivity,

A: Antenna area and

C: Capacitance.

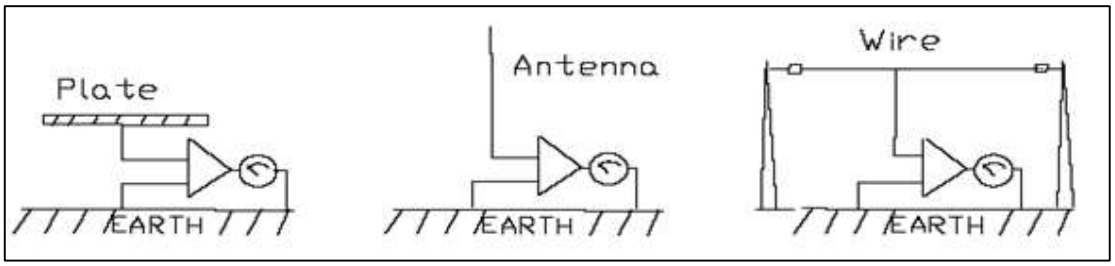

Figure 9. Antenna configurations for measuring electric field. Adapted from [17].

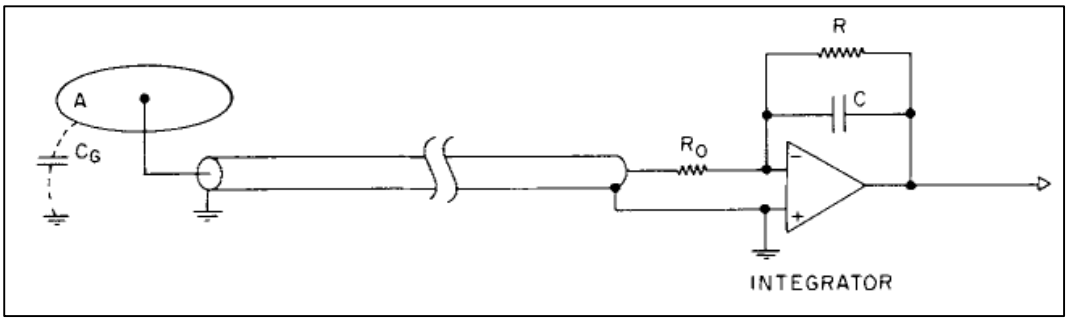

Figure 10. Electric field antenna system. Adapted from [3].

With these kind of antennas is possible to record the electric field component in only one direction. However, to measure simultaneously the three field components may combine different types of antennas or multiple thereof [34].

Flat plate antennas are often used to measure electric field changes from lightning. One of the commonly used types of flat plate antenna consists of a metallic box with a disk cut out of one of its sides, see Figure 11, as referenced by Pavanello [35]. Parallel flat antenna is used in this project and will be discussed with more details in Section 2.1.

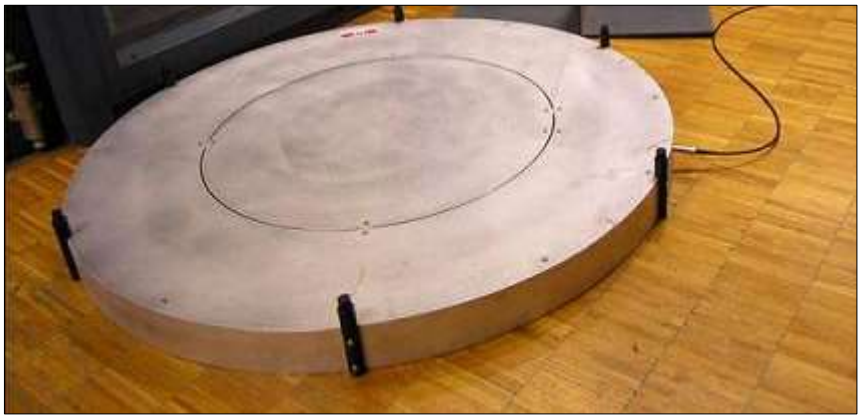

Figure 11. Electric field antenna [35].

1.2.2.2. Magnetic Field Measuring Devices

The simplest sensor for a magnetic field measurement is an open-circuited loop of wire. According to Faraday's Law, a varying magnetic field passing through an open circuited loop of wire will induce a voltage at the terminals of the wire. This induced voltage is equal to the loop area multiplied by the derivation of the magnetic flux density perpendicular to the loop surface. Thus the signal in a vertical loop antenna is proportional to the cosine of the angle between the lightning direction as viewed from the antenna and the plane of the loop antenna as follows:

$$V = A * cos\theta * \frac{dB}{dt} \tag{2}$$

Where:

V: Voltage at the terminals of the wire,

A: Area of the antenna,

θ*:* Incident angle of magnetic flux density and

B: Magnetic flux density.

In order to obtain a signal proportional to B is possible to integrate the differential antenna output over time. This procedure could be made using an electronical configuration or by numerical techniques. Krider and Noggle [36] proposed a wideband magnetic field measuring system formed from a single loop of 93Ω coaxial cable and electronic integration. The loop antenna referred in [36] is operated differentially and is shielded from electric fields with a grounded shield symmetrically broken at the top of the antenna. The schematic drawing of this system is shown in Figure 12. The magnetic field measurement characteristics using loops will be discussed in Section 2.2.

In addition to devices based on magnetic field loops, or some that operate with the same principle, several other types of sensors have been used to detect lightning magnetic fields. Williams and Brook [37] described magnetic field measurements made with a fluxgate magnetometer. In the case of relative low-frequency measurements, ballistic magnetometers that basically operate like compass needles have been used [38]. Other devices based on Hall Effect or other solid-state magnetometers could be used to measure lightning magnetic fields with very fast time response, but apparently have not been used for this purpose [3].

In [39] the authors describe several sophisticated geometries of loop-like antennas that make possible the extension of the upper frequency response above that of the conventional loop antenna, which are limited to the detection of wavelengths larger than the antenna size. A work about MultiGap Loop for Lightning measurement based on these geometries was design at the *Universidad Nacional de Colombia* with a cut-off frequency of 50 MHz [40]. Examples of these kind of sensors are shown in Figure 13.

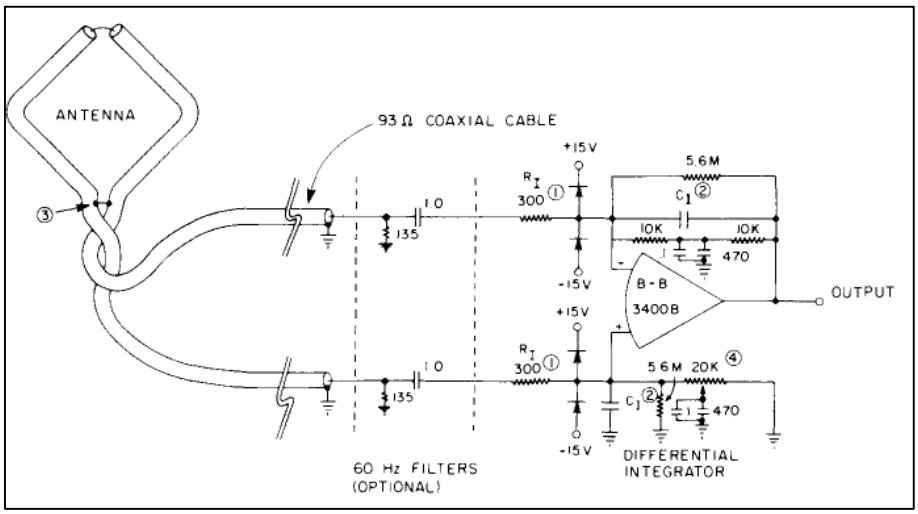

Figure 12. Magnetic field measuring system proposed by Krider and Noggle [36]. (1) 1% non-inductive resistors, (2) low-loss 1% capacitors: 100 to 10,000pF, (3) outside coaxial shields connected here, (4) adjust for optimum common mode rejection. All diodes 1N4447 and all capacitor values in microfarads.

1.3. Lightning Electromagnetic Fields

Lightning is a wideband event that radiates in a range of electromagnetic frequencies from Direct Current to X-ray. Nevertheless, the spectrum peaks of lightning processes are mostly in the radio-frequency spectrum at 5 to 10 kHz and 100 kHz to 200 kHz. For frequencies higher until 10 MHz, the spectral amplitude is approximately inversely proportional to the frequency, while to the range of 10 MHz to 10 GHz, the spectral amplitude is inversely proportional to the square root of frequency. For higher frequencies until 10^{16} Hertz the electromagnetic radiation of lightning is detectable, for example in the frequencies of visible light, however the mechanisms of radiation above 10 MHz are not completely understood [2].

Characterizations of lightning frequency spectrum have been made in several ranges from wideband measurements in determined ranges of frequencies, for example studies of cloud to cloud and cloud to ground lightning [41]-[42] and more specifics for Compact Intra-cloud Discharges (CID) for characterization and lightning location [23]. In the case of narrowband measurements, these are made in order to obtain frequency spectrums in detailed ranges as it is referenced in [43] and specific characteristics of lightning in reduce ranges as X-ray [44] and gamma-ray radiation.

Figure 13. Sensors of composite geometries for measure Magnetic Field. At left side B-Dot Sensor provided by Prodyn Technologies. At right side MGL design for lightning measurement [40].

Based on electromagnetic field measurements conducted with wideband antennas as referenced in section 1.2.2, Lin *et al.* [45] developed an extensive set of measurements in Florida and represented the "typical" electric and magnetic fields ranging from 1 to 200 km from negative return strokes. This characterization was presented as is shown in Figure 14 a) and b).

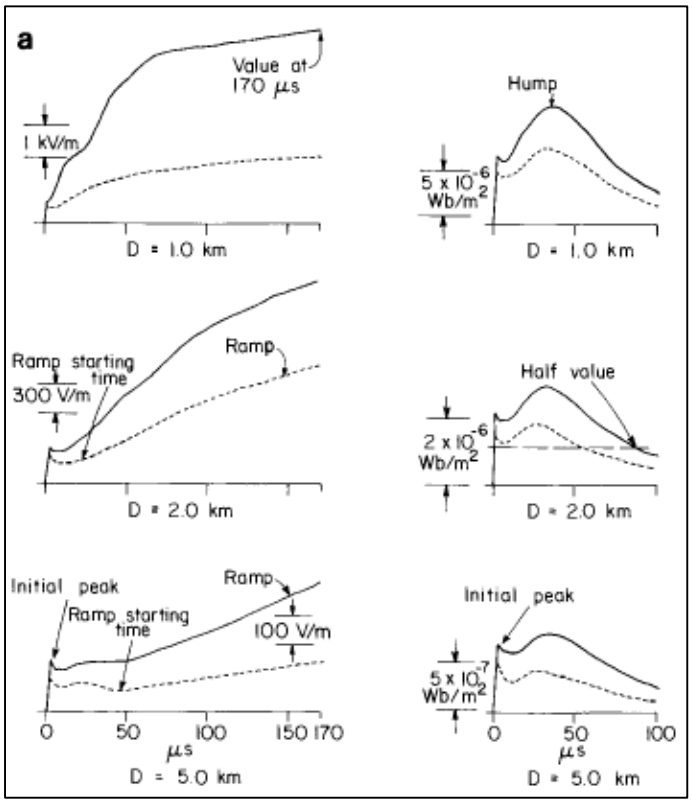

Figure 14 (a). Typical vertical electric field intensity (left column) and horizontal magnetic flux density (right column) for first (solid line) and subsequent (dashed line) return strokes at distances of 1, 2, and 5 km. The following characteristic features of the waveforms are identified: for electric field, initial peak, ramp starting time, ramp, and 170-μsec value; for magnetic field, initial peak, hump, and half-value. [45]

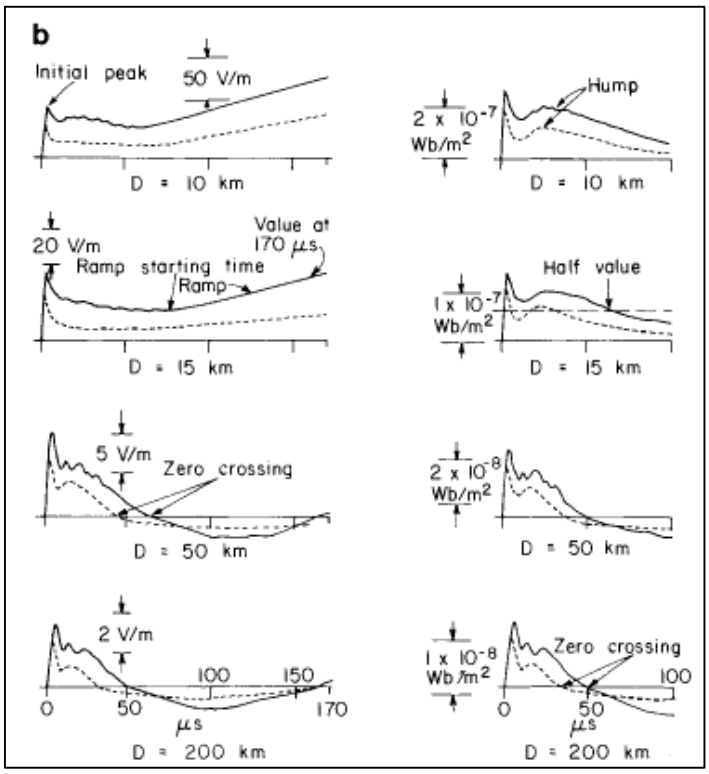

Figure 14 (b). Typical fields as described in a) for distances of 10, 15, 50, and 200 km. Characteristic waveform features identified in addition to those noted in a) are electric and magnetic field zero crossings. Adapted from Lin et al. [45].

From this characterization is possible affirm that:

- The initial rising portion and peak of the fields at each distance is due to the radiation component and decreases inversely with distance in the absence of significant propagation effects [45].
- After some tens of microseconds, the electric and magnetic fields within a few kilometres are dominated by the electrostatic and induction components, respectively [46].
- The close magnetic fields at similar times are dominated by the magnetostatic component of the total magnetic field, this component produces the magnetic field pronounced humps.
- Distant electric and magnetic fields have essentially identical wave shapes and are usually bipolar. The data suggest that at a distance of 50 km and beyond both electric and magnetic field wave shapes are composed primarily of the radiation component of the respective total fields [46].
- It is important to observe that whether the electric field at a given point on the waveform is radiation or not depends on the distance to

the return stroke, the location of the point of interest on the waveform and on the shape of the waveform [1].

In order to a better understanding of these affirmations, Santamaria [17] calculates the vertical electrical field and discriminate the electrostatic, induction and radiation components, using the Modified Transmission Line Model, linear (MTLL) as is explained by Cooray [1]. Calculating for distances from 50 meters to 200 kilometres, it is possible denote the previous statements through the graphics of Figure 15.

Other characterizations of lightning parameters have been made, especially for specific parameters as subsequent strokes, preliminary discharges, slow front in distant fields, derivative fields among others for both natural and artificially generated lightning. According to the scope of this work, these characterizations will not be considered.

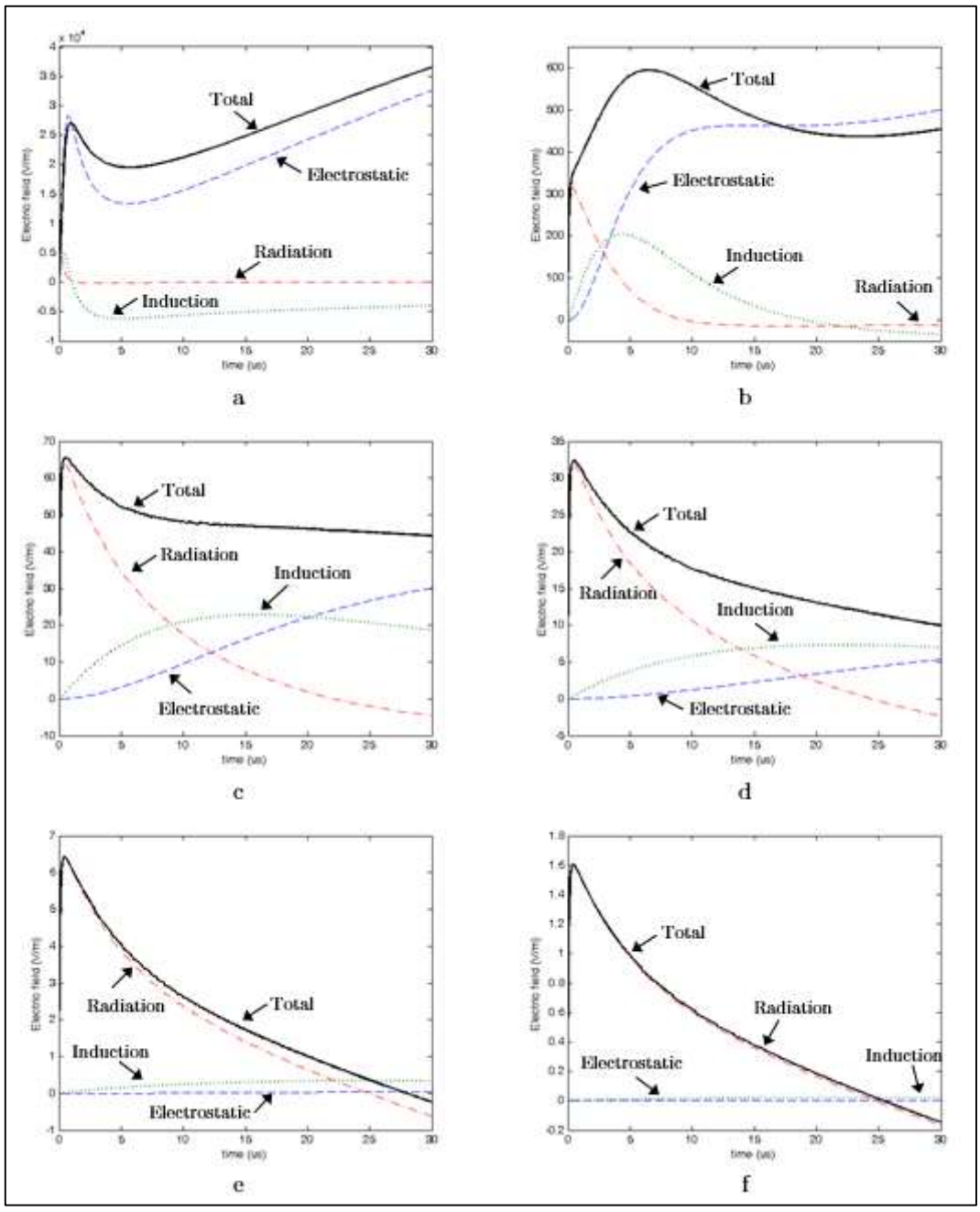

Figure 15. Vertical electric field components for different distances (r) from Modified Transmission Line Model, linear (MTLL), at a) 50 m, b) 1 km, c) 5 km, d) 10 km, e) 50 km, f) 200 km. Black line represent the total electric field, blue line the electrostatic field component, green line the induction field component and red line for radiation field component. Adapted from [17].

Chapter 2

Electromagnetic Field Measuring System

In order to characterize the electromagnetic fields generated by lightning in Colombia, as part of the continuous work of *Universidad Nacional de Colombia* and specifically of Electromagnetic Compatibility Research Group EMC-UNC, the design, construction and implementation of a Electromagnetic Field (EMF) Measuring System becomes as a necessary activity to continue the work developed and, based in new measurements, establish new research topics and new analysis of observations. As a starting point of start, the system was designed to cover a circle of 15 km radius, centred at the *Universidad Nacional de Colombia* as it is shown in Figure 16.

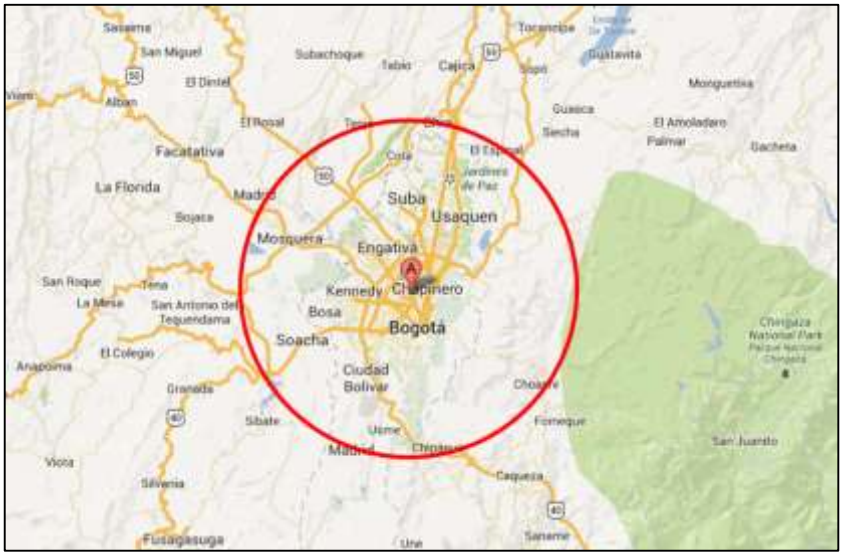

Figure 16. Covering area for Electromagnetic Field Measuring System. Map obtained from Google maps (maps.google.com).

This chapter describes the components of both, electric and magnetic measuring systems, the procedures used to design and calibrate each

measuring system and to establish the interaction of both systems to configure the implemented Electromagnetic Field Measuring System.

2.1. Electric Field Measuring System

An Electric Field Measuring System based on parallel-plate antennas was constructed following the *Universidad Nacional de Colombia* master thesis work [17] developed in 2005 (See Section 1.2.2.1). This electric field measuring system is composed by a parallel-plate antenna, an electronic circuit, two coaxial cables and an oscilloscope. Figure 17 shows the schematic of the original measuring system mentioned in [17].

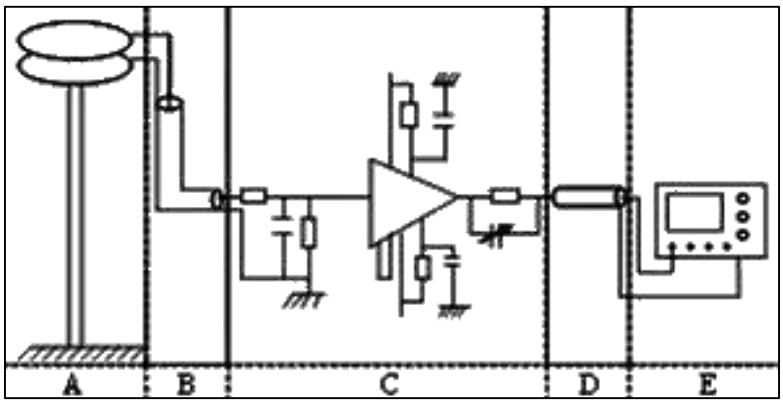

Figure 17. Schematic diagram of Original Electric Field Measuring System described in [17]. A) Parallel plate antenna, B) Coaxial cable 1, C) Electronic circuit, D) Coaxial cable 2 and E) Digital Oscilloscope.

In order to conserve the calibration characteristics and correction factors of the original system, the plate antenna characteristics, the coaxial cables and the electronic circuit were mainly reproduced from [17]. Table 1 shows the characteristics of the elements used in the electric field measuring system. Details of the acquisition system are shown in Section 2.2.4. Despite the changes in elements or characteristics, calibration procedures and system correction factors, except for the location factor, are very similar to those of original system.

In the case of the location factor was necessary to correct it to ensure a correct adjustment. In the measurement campaign made in 2005 the parallel plate antenna was located on the roof of a structure with a height near to 3

meters. In the present project, the antenna was located in 10 meters high building, near of some trees and structures of similar heights. The electric field antenna new location is shown in Figure 18.

Cerra and Pinzón [47]. In their graduate thesis work calculate the correction factor for the antenna location shown in Figure 18. Additionally, they calibrated again the antenna factor with the antenna geometrical characteristics. In order to improve the calculations mentioned in [17], a sensitivity analysis about the influence of metal structures and the system location was performed.

It is not intended explain all the performance of electric field measuring system in this section, nevertheless, as part of the whole system, the main characteristics must be taken into account for comparison and calibration of magnetic field system.

Table 1. Characteristics of elements of Electric Field Measuring System. Characteristics of elements marked with * are adapted from [17].

Components	Characteristics
Parallel Plate Antenna	• Two Circular Plates * • Diameter: 0,45 m * • Gap between plates: 0,03 m * • Metal base length: 0,80 m
Coaxial Cable 1	• Coaxial Cable RG 58/U • Double Shielding • Length: 20 meters • Characteristic Impedance: 50Ω
Electronic Circuit	• Buffer LH0033 * • Bandwidth: 100 MHz * • Slew Rate: 1,5 kV/µs *
Coaxial Cable 2	• Coaxial Cable RG 58/U • Single Shielding • Length: 0,4 meters • Characteristic Impedance: 50Ω

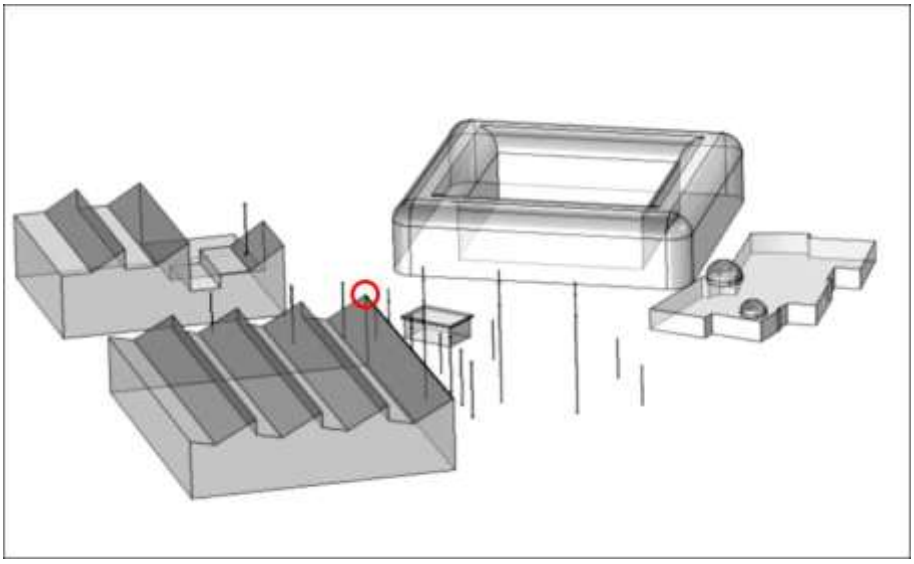

Figure 18. Three-dimensional model used to calculate the Electric Field Measuring System location factor. Red circle marks the antenna position on the building. Adapted from [47].

The Total correction Factor of the Measuring System (TF) is calculated as the product of the Measuring System Factor (MSF) and the Location Factor (LF).

$$TF = MSF * LF \tag{3}$$

The MSF is the relationship between the output voltage of electronic circuit and the incident electric field, providing a multiplication factor to be applied to obtained measure. This factor is obtained by calibrating the measuring system in a controlled environment. This can be done by immersing the system in a constant electric field while the output voltage is measured. Considering the same elements for the present application and a pre-test of electric field system (See Section 3.1), the MSF has the same value as in [17]:

$$MSF = 29{,}66 \tag{4}$$

The LF, second term of equation (3), was recalculated because the new antenna location is 7 meters higher than before and it is placed on the roof of another building. Based on this new characteristic, Cerra *et al.* performed new numerical simulations using following conditions:

- The building was modelled as a metal structure,
- The relative permittivity of the building concrete and surrounding trees were respectively 8 and 13.

- The background electric field of 1 [V/m] in volume of 150 x 150 x100 meters.

Simulation was implemented in the finite element method (FEM) software called Comsol Multiphysics. Figure 19 shows a detail of the simulated building structure. The obtained location factor LF is the following:

$$LF = 1{,}4324 \tag{5}$$

Based on these results, the Total correction Factor of the Measuring System is:

$$TF = 29{,}66 * 1{,}4324;$$

$$\boxed{TF = 42{,}485}$$

This TF will be used in the electric field calculation. Further details about the Electric Field System are given in references [17] and [47].

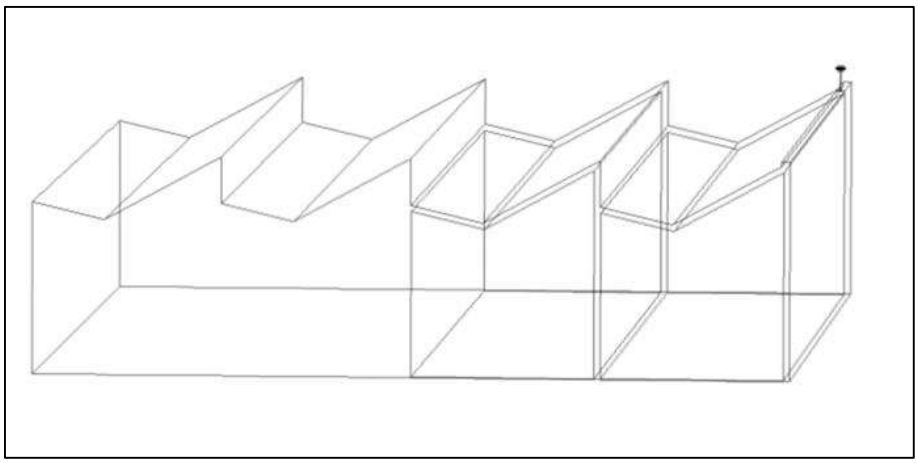

Figure 19. Building modelling using two solid sections and two sections with 30 cm. thickness walls [47].

2.2. Magnetic Field Measuring System

Measuring lightning radiated magnetic field produced is the most powerful technique to measure, locate or identify flashes. In section 1.2.2.2 the main systems used and the general principle of these devices were presented. In order to select the best sensor for the lightning measuring system, an

evaluation of the four main devices was performed. With the chosen sensor the characteristics of the electronic circuit, the acquisition system and the surrounding elements was obtained. This procedure is shown in this section.

2.2.1. Magnetic Sensors Evaluation

Four kinds of sensors were evaluated in order to select the best component for the Magnetic Field Measuring System. The evaluated sensors were chosen for its wide acceptance and use in the scientific community, the reliability of the measurements, previous works and feasibility of the construction or components acquisition. These sensors are the B-Dot Sensor, the Multi-Gap Loop, the Loop Antenna and the Monopole-Dipole antenna. This qualification was made using four rate parameters: Directivity, Cost, Reliability and Bandwidth. These rate parameters were evaluated using the labels high, medium or low according his characteristics regarding the parameters and avoiding the use of long explanations in order to facilitate the lecture.

2.2.1.1. Directivity

Lightning phenomena is unpredictable, at least to predict the exact lightning strike-point. Additionally, thunderstorms could occur in diverse locations, could follow different trajectories and have different intensities. For this reason a sensor is required with the possibility to measure electromagnetic fields coming from all directions. However, it is possible that more than one sensor can be used in order to obtain the total directivity.

It is necessary to clarify that the concept of directivity expressed here, is not the same approach used in antenna theory where directivity is a number determined by the ratio of the maximum radiation intensity to the average radiation intensity [48]. In the present case is defined in qualitative manner, being understood the best directivity for a sensor, or array of sensors, which could measure electromagnetic fields from all directions. In addition, the option of identify the origin of magnetic field is an excellent feature very useful in lightning measurement. Table 2 shows the evaluated sensor characteristics to obtain the directivity parameters.

Table 2. Directivity evaluation of analysed sensors.

Sensor / Characteristics	Directivity
Loop	**High:** Although the loop sensors are capable of measure the field normal to his axis, the array of two perpendicular loops is widely used for determine the direction of magnetic field origin.
Monopole – Dipole	**Medium:** The use of this kind of antenna is restricted because measure in all directions, but is necessary an array of several elements in order to know the direction of Magnetic Field.
B – Dot	**Medium:** B-Dot sensors includes structures constructed for measure magnetic field from all directions and other kind of B-Dots intended to measure in a specific direction. Is not possible determine the direction of radiation.
Multi Gap Loop	**Medium:** The Multi-Gap loop offers an omnidirectional measurement. Nevertheless, the complex geometries provide an additional challenge and it is not possible to determine the field direction.

2.2.1.2. Cost

The cost of the project must be evaluated in order to know the feasibility of purchasing or constructing the magnetic field sensors, which is determined by the quality and requirements of the measuring system. From the characteristics of each sensor, it was determined that the loop and the Multi Gap loop-sensors could be constructed following the required quality parameters. In addition, the acquisition possibilities of this kind of sensors for lightning applications is limited. In the case of B-Dot and Monopole – Dipole antennas, was suggested the evaluation only for purchase, in the case of B-Dot for the complex construction and calibration and monopole – dipole antennas for reliability. Table 3 shows the cost evaluation of the selected sensors.

Table 3. Cost evaluation of analysed sensors.

Sensor / Characteristics	Cost
Loop	**Low:** Construction of loop antennas for lightning application is feasible and reliable using quality materials and making an adequate calibration or model of antennas array.
Monopole – Dipole	**Medium:** The purchase of these kind of antennas is feasible but more of them are designed for EMC tests and special fabrication is expensive.
B – Dot	**High:** B-Dot sensors are constructed by few companies and are expensive. Nevertheless, as part of equipment of EMC group, a B-Dot Model B-100 could be used for the lightning magnetic field system.
Multi Gap Loop	**Medium:** Construction of Multi-Gap loop sensor requires materials and manufacture costs near to 2 million COP. This calculation is based in [12], where a MGL was constructed with fewer size and similar specifications.

2.2.1.3. Reliability

The reliability is defined in this project is considered according the level of theoretical support of sensor for calibration through circuit or mathematical models, numerical simulations and calibration tests. The most level implies e.g. that sensor is widely support by the theory without several suppositions or not requirements of special infrastructure for calibration tests. The evaluation of this parameter for the different sensors is shown in Table 4.

Table 4. Reliability evaluation of analysed sensors.

Sensor / Characteristics	Reliability
Loop	**High:** Loop antennas are one of the most used sensors in all kind of applications thanks to its easy construction, single circuit model and low affectation by nearby structures
Monopole – Dipole	**High:** Monopole and dipole antenna are the simplest highly used in radio and telecommunications. Antenna model and calibrations are widely known.
B – Dot	**High:** B-Dot sensors has an theoretical support provided mainly by Baum notes and articles [49], intended for phenomenon similar to lightning in some features and high range frequencies.
Multi Gap Loop	**Medium:** Due to complex structures, and although theoretical work on B-Dot sensors, the MGL is extremely variable with geometrical parameters, being necessary the use of calibration test with precision in order to obtain reliable results.

2.2.1.4. Bandwidth

The spectrum peaks of lightning processes are mostly in the radio-frequency spectrum at 5 to 10 kHz and 100 kHz to 200 kHz. Nevertheless events at intermediate frequency ranges have been measured and new measurements in Ultra High Frequency (UHF) range shown lightning characteristics suitable of analysis [50]. Based on several studies of lightning frequency ranges, and as it is shown in Figure 20, 30 [MHz] was selected as superior limit for the lightning measuring system. This selection means that it will be possible the measurement in the range from some [kHz], according technology selected, and 30 MHz as upper limit, from ULF to HF frequency ranges shown in Table 5. The evaluation of sensors using Bandwidth criteria is shown inTable 6.

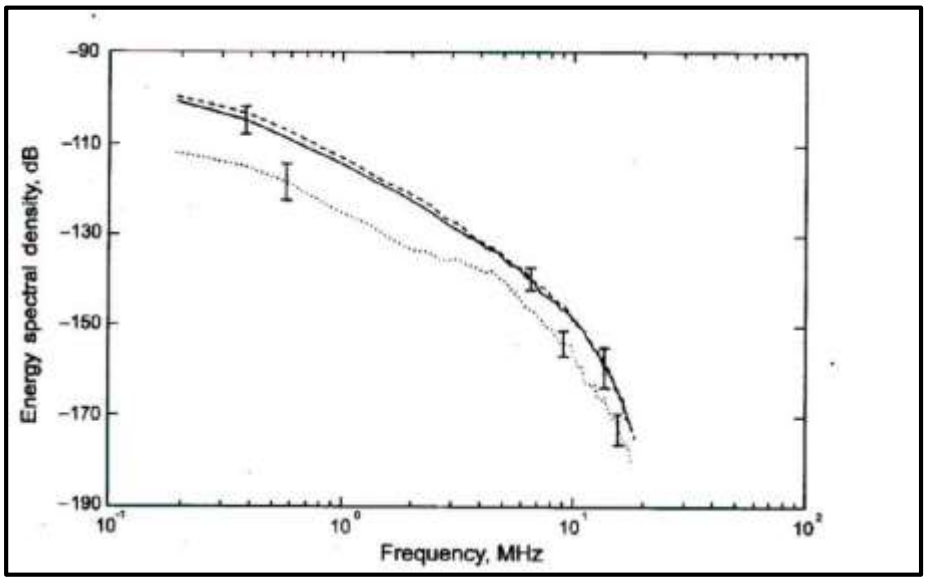

Figure 20. Lightning Frequency Spectrum by [51]. Notice the decay after some tens of Megahertz.

Table 5. Frequency band designations according to International Telecommunications Union (ITU) radio regulations.

Designation		Frequency	Wavelength
ELF	extremely low frequency	3Hz to 30Hz	100.000km to 10.000 km
SLF	superlow frequency	30Hz to 300Hz	10.000km to 1.000km
ULF	ultralow frequency	300Hz to 3000Hz	1.000km to 100km
VLF	very low frequency	3kHz to 30kHz	100km to 10km
LF	low frequency	30kHz to 300kHz	10km to 1km
MF	medium frequency	300kHz to 3000kHz	1km to 100m
HF	high frequency	3MHz to 30MHz	100m to 10m
VHF	very high frequency	30MHz to 300MHz	10m to 1m
UHF	ultrahigh frequency	300MHz to 3000MHz	1m to 10cm
SHF	super high frequency	3GHz to 30GHz	10cm to 1cm

EHF	extremely high frequency	30GHz to 300GHz	1cm to 1mm

Table 6. Bandwidth evaluation of analysed sensors.

Sensor / Characteristics	Bandwidth
Loop	**High:** Good noise relation at least 10:1 in the frequency range, but poor at high in broad-band designs [52]. Use of single or multiple turns in loop is an important characteristic to evaluate during the design.
Monopole – Dipole	**Low:** The radiation efficiency and gain characteristics of both of these elements are strongly influenced by their electrical length which is related to the frequency of operation. Are often used in UHF and SHF ranges for optimal characteristics in portable equipment, therefore for use in lower frequencies (HF) the wavelength is very long, being necessary antennas of several meters of length.
B – Dot	**High:** B-Dot sensors are designed for ultra-fast impulses with rise times of some hundreds of [ps], being intended and designed for high operation frequencies in a wide spectrum.
Multi Gap Loop	**High:** MGL sensors could be designed using a parameter of maximum frequency response in the order of GHz, because as the case of B-Dots, are created for measure transient signals of low duration.

2.2.1.5. Evaluation of the Sensor Parameters

Table 7 shows a resume of the qualitative qualifications obtained from the analysed sensors. For each evaluated parameter: Directivity, Cost, Reliability and Bandwidth, the sensors with the best qualification were highlighted (using bold letters). Using this criteria, the best sensor to be designed and constructed is the loop, and actually for the present research should be a crossed loop antenna. Nevertheless, it is necessary to understand why the other options were not implemented.

Monopole – Dipole antennas are impractical because of the fact that to improve directivity and to get the minimal features for lightning measurement, it is required the use of several antennas or an array of them.

In addition, electrical length is also an important parameter for the antenna configuration, being at least 10 meters for the frequency range of interest, which is impractical for location and construction in vicinity of the *University Campus*.

B-Dot sensors. The use of B – Dot sensors was initially proposed due to existence of a Prodyn sensor in the Electromagnetic Compatibility Research Group, being possible to be adapted, if required. The sensor Model B-100 is a full cylinder loop that measures the time rate-of-change of a magnetic field with a wiring configuration that causes any electric fields to be effectively cancelled out, being magnetic fields the only output of the sensor. This sensor is weather protected and has SMA connectors on the output; its bandwidth is greater than 2.6 GHz and it is able to measure signals with a rise time of 0.13 ns. This B-Dot sensor is shown in Figure 21.

Despite the excellent characteristics of the B-Dot Sensor presented above, the sensor not measure any orthogonal field component because its construction, output configuration and measurement position (the rotation axis of the sensor has to be parallel to the incident magnetic field, note the arrow indication in the Figure 21) being unfeasible the covering of all lightning flashes that could be surrounding it.

MGL-Sensor. In the case of the MGL sensor, needless to say that it is normally used in high frequency applications. The MGL sensor design and construction is relatively simple compared with others B-dot sensors. For this reason a MGL Sensor for lightning measurement was design in the EMC group [40].

Table 7. Sensor Parameters qualification for the evaluated sensors. Bold qualifications are the best for each parameter.

Antenna/Factor	Directivity	Cost	Reliability	Bandwidth
Loop	**High**	**Low**	**High**	**High**
Monopole – Dipole	Medium	Medium	**High**	Low
B – Dot	Medium	High	**High**	**High**
Multi Gap Loop	**High**	Medium	Medium	**High**

Figure 21. Prodyn B-Dot Sensor Model B-100.

The MGL designed in the EMC Group for lightning magnetic field measurement, shows a good agreement between theoretical and numerical simulation results. The 50 [MHz] bandwidth was covered and gave an adequate sensor response under magnetic field signal of lightning characteristics. However, the designed Sensor was 0,3 meters in diameter and 0,28 meters in length, which is very large and because its geometry requires a precision and high technology construction, which is not achievable in the university facilities. In addition, this kind of sensor is more suitable for direct lightning current measurements, instead of radiated lightning fields. The reason is that due to the wide frequency response of MGL, it is necessary to introduce noise rejection electronics treatments to reduce its effect on the output signal that is be strongly affected by the environment signals as FM and AM broadcast.

According to the evaluation of each sensor, the best option is to design, construct and implement loop sensors, in a two crossed loop configuration, with weather protection, an upper bandwidth limit of 30 MHz and with a reliable construction by using high quality materials.

2.2.2. Antenna Design and Construction

Several researchers have used crossed loop antennas to characterize naturally or artificially generated lightning magnetic field signals [46]-[54], to support mathematical models of propagation [55] or to localize lightning by using direction finding (DF) [56]-[57] or Time of Arrival (TOA) techniques [58]. As it is mentioned in Section 1.2.2.1, Magnetic field sensors in addition with electric field measuring devices and electric and magnetic field derivative antennas, narrowband antennas, high speed video cameras, X-ray sensors [44] among others, are frequently used as part of the Lightning Measuring Stations.

The lightning measuring station is located on the top of a 10 m tall building located in the *Universidad Nacional de Colombia* in the city of Bogota (2600 meters above sea level). See Figure 22. This location was selected because the building's height provides a visible point in all directions without several obstacles, however the building distorts the measurement of electric field mainly, situation that was resolved with the numerical simulations developed in section 2.1. In addition this location is easily accessible from an office of EMC group that will be used as the central station to adequate the acquisition devices.

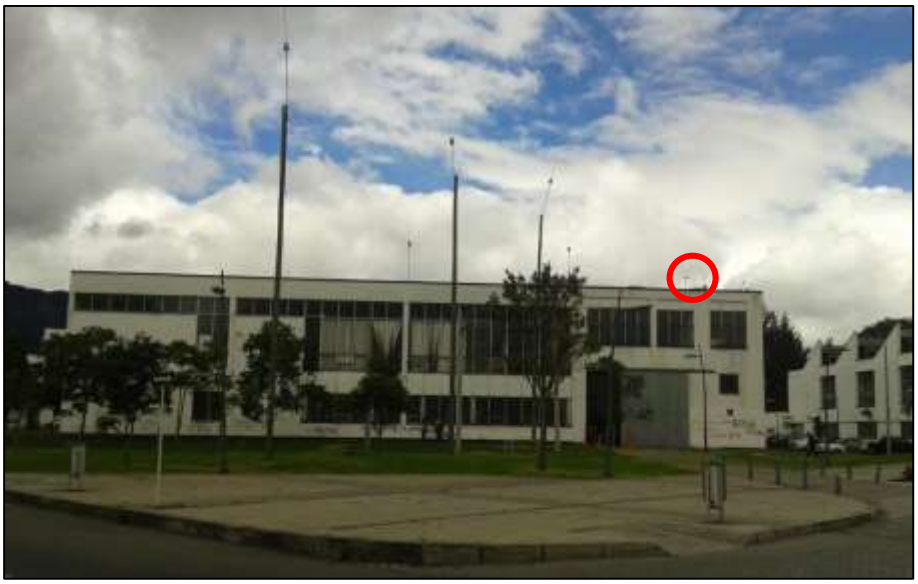

Figure 22. Location of Electromagnetic Field System.

2.2.2.1. Loop antennas

Two crossed loop antennas were used to measure simultaneously both the perpendicular and the parallel lightning radiated magnetic field components. For this objective is necessary understand the theoretical background of loop antennas and provide a solution based on magnetic field system requirements.

A single-turn loop antenna could be constructed as a metallic conductor which forms a circle or square. Faraday's law states that the sum of tangential electric fields around any closed contour is equal to the negative time rate change of the magnetic flux which is enclosed by that contour. This affirmation could be expressed in terms of closed integration path as it is shown in (6):

$$\oint E \cdot dl = -\frac{d}{dt}\oint B \cdot dS \tag{6}$$

As it is stated in [59], on the contour enclosed by the conductor there is not tangential electric field so that the left side of equation (6) is equal to zero, thus the magnetic flux change inside the loop is zero for a perfect conductor.

In order to use the loop as an antenna it is necessary to form the terminals with a gap in the conductor and an element that acts as a load. If a resistor is inserted into the break in the conducting loop and exists an incident field, currents flowing in the loop could be measure through a voltage drop across the resistor, obtaining a quantitative value of the incident field. This voltage signal is proportional to the product of the loop area and the time rate of change of the magnetic field in the optimum loop orientation.

The discussion of loop antennas is conveniently divided according to the electrical size [60]. Electrically small loops, those whose total conductor length is small compared with the wavelength in free space, less than 0.1 times the wavelength is generally accepted, are the most frequently encountered in practice. For example, they are commonly used as receiving antennas with portable radios, as directional antennas for radio-wave navigation, and as probes with field-strength meters. Electrically larger loops, particularly those near resonant size (circumference of loop/wavelength ≈ 1), are used mainly as elements in directional arrays.

The loop can act as a transmitter or receiver according the application. For this case the loops are used as a sensor meaning that has to act as a receiver. Small transmitting antenna is not adequate from the point of view of

efficiency because much of the generated power is wasted in heating in the ohmic resistance. On the other hand, acting as receiver the small antenna is very satisfactory because sensitivity is a more important factor than power efficiency.

The radiation pattern and Gain of a small loop is the same of a short dipole oriented normal to the plane of the loop but with Electric and Magnetic fields interchanged. If the normal direction to the plane of the loop is the *z* axis the radiated electromagnetic fields are given by:

$$E_\phi = 120 * \pi * \frac{\pi * N}{r} * \frac{A}{\lambda^2} * I * sin\theta \quad (7)$$

And

$$H_\theta = -\frac{\pi * N}{r} * \frac{A}{\lambda^2} * I * sin\theta = \frac{E_\phi}{120 * \pi} \quad (8)$$

Where:

r = distance from the antenna

I = antenna current

N = number of turns of the loop

A = area of loop

λ = wavelength

An example of radiation pattern for horizontal gain with angle θ=0 is shown in Figure 23.

The axial current distribution in an electrically small loop is supposed to be uniform; that means that the current has the same value at any point along the conductor. For single-turn loops, measurements suggest that this is a good assumption provided the total length of the conductor (N × circumference) is small compared with the wavelength in free space, typically ≤ 0.1λ. With a uniform current assumed, the electrically small loop antenna is simply analysed.

When the electrically small loop is used as a receiving antenna, the voltage developed at its terminals $V_{1\text{-}2}$ is proportional to the component of the incident magnetic flux density normal to the plane of the loop B_z^i:

$$V_{1-2} = j * \omega * N * A * B_z^i \quad (9)$$

Where the incident field is assumed to be uniform over the area of the loop.

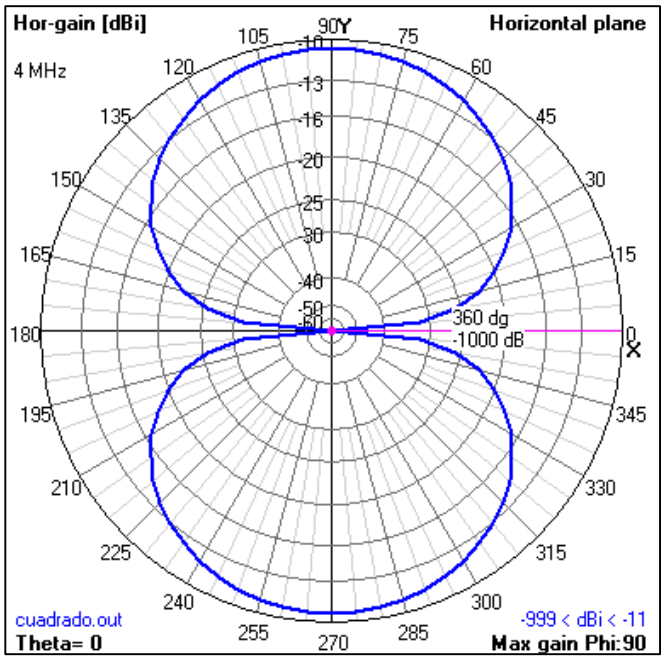

Figure 23. Radiation pattern for horizontal gain with angle θ=0 [16].

If a relation between the incident electric and magnetic fields at the centre of the loop is known, $V_{1\text{-}2}$ can be expressed in terms of the magnitude of the incident electric field E_i and an effective height h_e. In case of an incident linearly polarized plane wave with the vector k_i and the orientation shown in Figure 24:

$$V_{1-2} = j * \omega * N * A * B^i * cos\Psi_i * sin\theta_i = h_e(\Psi_i, \theta_i)E^i \quad (10)$$

In which:

$$h_e(\Psi_i, \theta_i) \equiv \frac{V_{1-2}}{E^i} = j * \beta * N * A * cos\Psi_i * sin\theta_i \quad (11)$$

Where

β= 2* π/ λ propagation constant of an electromagnetic wave.

The voltage across an arbitrary load impedance Z_L connected to the terminals of the loop with input impedance Z is determined from the Thévenin equivalent circuit shown in Figure 25.

$$V_L = \frac{V_0 * Z_L}{Z + Z_L} \quad (12)$$

Circuital model for loop antenna will be discussed in Section A11 using the parameters of constructed antennas.

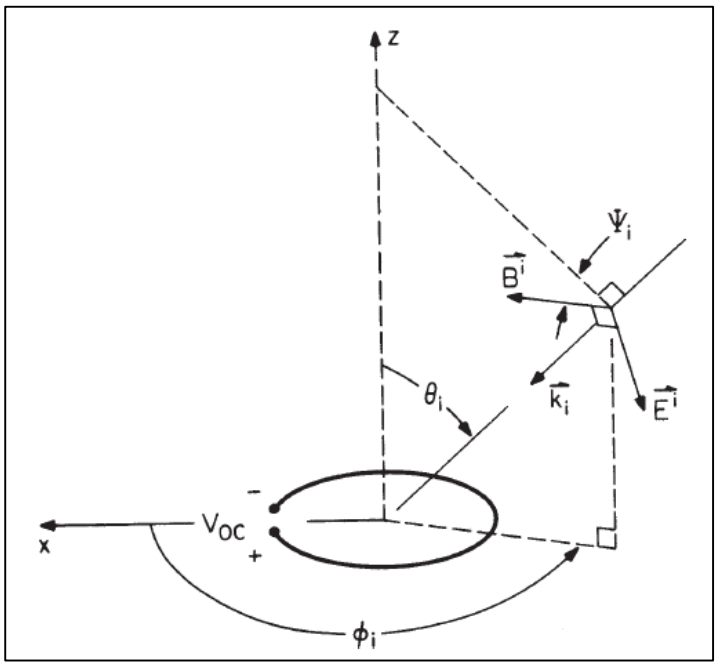

Figure 24. Plane-wave field incident on receiving loop [60].

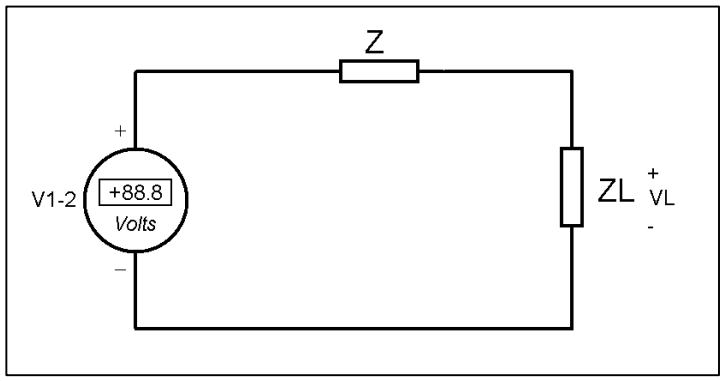

Figure 25. Thévenin equivalent circuit for the receiving loop.

For the application in this project, the most appropriated kind of antenna is the so called thin-wire loop antenna. The thin-wire loop antenna is constructed using only a single turn of conducting wire as it is shown in Figure 26. This kind of antennas is specially used in direction-finding systems and communications in the UHF band (See Table 5), as well as probes for magnetic field intensity measurement.

If we consider a thin-wire electrical small loop with circular shape as it is shown in Figure 26 and it is illuminated by an uniform plane wave incident at angle θ_i with respect to the axis of the loop (*z* axis) and polarized at an angle Ψi with respect to the *y* axis, the electric field vector of the incident plane-wave field could be expressed as:

$$\boldsymbol{E^i} = E^i(-sin\Psi_i cos\theta_i \hat{\boldsymbol{a}}_{\boldsymbol{x}} + cos\Psi_i \hat{\boldsymbol{a}}_{\boldsymbol{y}} + sin\Psi_i sin\theta_i \hat{\boldsymbol{a}}_{\boldsymbol{z}}) \quad (13)$$

Where the incident azimuthal angle was taken as Φ_i=0 without any loss of generality.

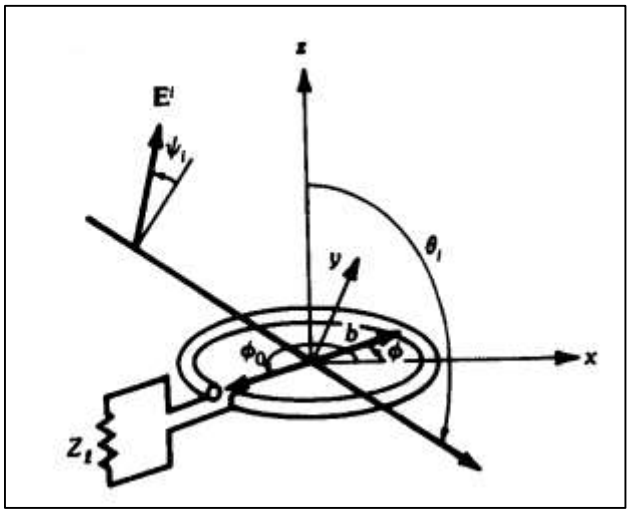

Figure 26. Circular thin-wire loop antenna acting as a receiver [61].

In order to obtain a geometrical symmetry of the loops related to the perpendicular plane, the position of terminals is a determining factor. This could be accomplished by using the so-called shielded loop. Figure 27 is an example of a shielded receiving loop whose external surface is symmetrical about the *yz* plane.

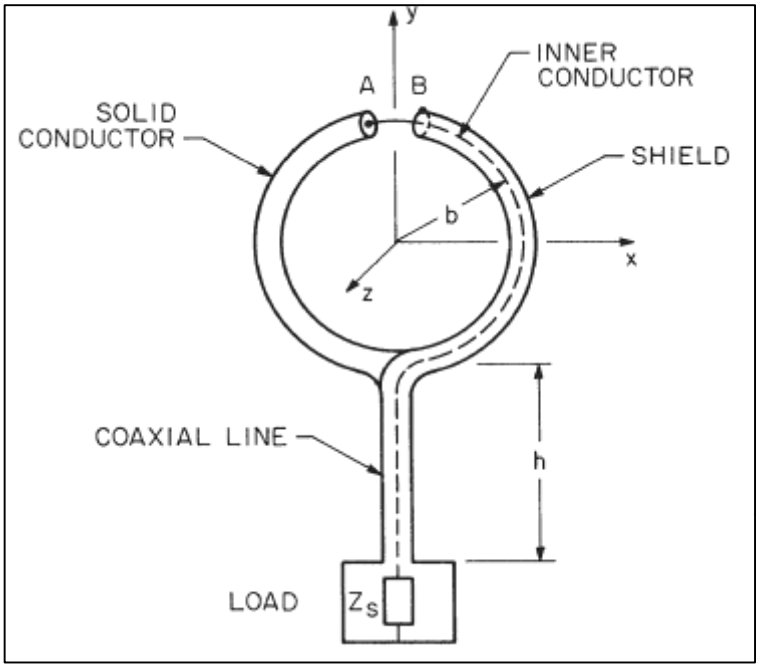

Figure 27. Shielded loop antenna as is described in [60].

The thickness of the metal forming the shield is chosen to be several skin depths; this prevents any direct interaction between the currents on the internal and the external surfaces of the shield. This kind of condition could be achieved using a quality coaxial cable.

In order to obtain a balanced version of the loop shown in Figure 27, and use it in the application for lightning measurement, coaxial cables are connected as it is shown in Figure 28, ensuring a differential measurement between the two terminals. The incident field produces a current on the internal conductor of the shield; the current passes through the effective impedance Z_s, producing a voltage $V_{1\text{-}2}$ that could be determined using equations (8) and (10).

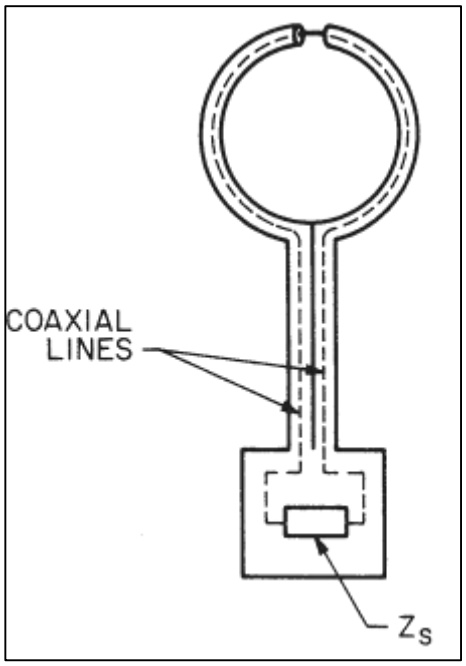

Figure 28. Balanced shielded loop antenna [60].

To illustrate a typical use of the shielded loop, consider the electrically small receiving loop placed in an incident linearly polarized electromagnetic plane wave with the wave vector k_i, as in Figure 29. This is the same geometry as in Figure 24, except that the terminals of the loop are at the angle $\Phi = \Phi_L$ instead of Φ=0, and $\Phi_i = \pi$, Ψ_i=0.

The voltage at the open-circuited terminals of the electrically small loop, determined from the Fourier-series analysis, is approximately:

$$V_{1-2} = j * \omega * A * B^i(sin\theta_i - 2 * j * \beta * r * cos\Phi_L) \qquad (14)$$

Where *r* is the loop radius. For many applications the second term is negligible because $\beta * b \ll 1$ for an electrically small loop, however, this will also decrease the sensitivity for the smaller loop area. For example, the sensitivity of the antenna in the direction finder is decreased by this term because it fills in the nulls of the $sin\theta_i$ field pattern (See Figure 23). An alternative is to make this term zero ($\beta * b$) by placing the terminals of the loop precisely at $\Phi_L = \pm\pi/2$ where $cos\Phi_L = 0$. This can be accomplished by using a shielded loop as in Figure 27 or Figure 28.

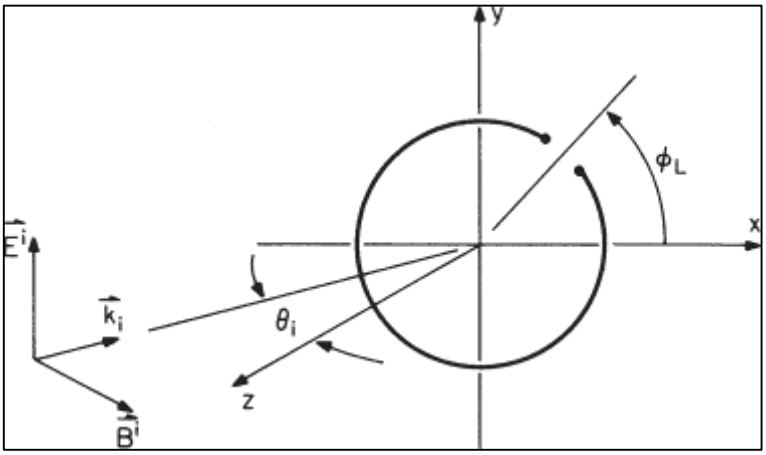

Figure 29. Receiving loop in plane-wave incident field [60].

2.2.2.2. Crossed loop antennas

For construction of crossed loop antennas the parameters related in sections 2.2.1 and 2.2.2 were analysed and considered in order to obtain a couple of similar antennas with required characteristics for lightning application. The use of two crossed loops is necessary in order to achieve the directivity condition which is to detect magnetic field signals in all directions.

According to bandwidth analysis developed in 2.2.1.4 an upper frequency of 30 MHz for antenna response was selected. To meet with this requirement it is necessary to take into account the value of the antenna circumference and his relation with the selected wavelength necessary to comply the characteristic of electrically small loop:

$$\frac{C}{\lambda} \leq 0{,}1 \qquad (15)$$

Where *C* is the loop-antenna circumference.

The compliance with (13) allows the analysis as small loop using the equations and parameters related in previous sections. In addition to this

condition, the antennas are selected to be thin-wire and shielded loops following the results and analysis of theoretical background and recommendations according the application (See Section 2.2.2.1).

Using (13) and parameters selected:

$$\frac{C}{\lambda} \leq 0{,}1 \rightarrow C \leq 0{,}1 * \lambda \rightarrow C \leq 0{,}1 * \frac{3e8\left[\frac{m}{s}\right]}{30e6\left[\frac{1}{s}\right]} \rightarrow C \leq 1[m]$$

In order to avoid boundary effects due to loop-antenna geometry that could generate interference or noise in the measurements, a circular shape was selected for loops construction taking into account the need to ensure the construction quality. Using a circular shape the circumference is given by:

$$C = 2 * \pi * r \tag{16}$$

Thus:

$$2 * \pi * r \leq 1 \rightarrow r \leq \frac{1}{2 * \pi} \rightarrow r \leq 0{,}159[m]$$

Therefore the loop antenna radio is chosen in 15 [cm], being able to be analysed as electrically small loop for frequencies lower than 31,83 [MHz].

The construction of antennas was made using the concepts presented by Krider and Noggle in [36] and shown in Figure 12. Antennas are constructed with a single turn of a coaxial cable BEDEA RG-62 with characteristic $\text{impedance of } 93\ [\Omega]$. The importance of the coaxial cable quality and characteristic impedance is the uniformity between the internal and external conductors. Because of the construction of a coaxial structure with wire and pipe could introduce strong variability in the calculus of antenna parameters. In addition the lower impedance of a coaxial cable loop results in a reduced antenna output at high frequencies, but the response is still adequate for lightning application.

A mechanical shielding is necessary to protect the coaxial cable from weather and mechanical stresses such as wind or birds. A reinforced flexible tube for steering fluid pressure composed by 4 layers of PVC was used as a shielding. A half inch diameter was selected to allow insertion of the coaxial cable, however the crimp of connectors must be made after the coaxial cable insertion as it is detailed in this section. Figure 30 shows the crossed loop antennas final design concept recreated through a CAD application using two of these antennas in perpendicular configuration.

The coaxial cable shield is discontinuous at the top of the antenna to prevent the flow of the induced currents in the shield loop. Any transient or 60-Hz background electric field detected at the separation of the shield appears equally on both signal inputs and is rejected by the electronic circuit as a common-mode signal. This coaxial cable gap was made as it is shown in Figure 31.

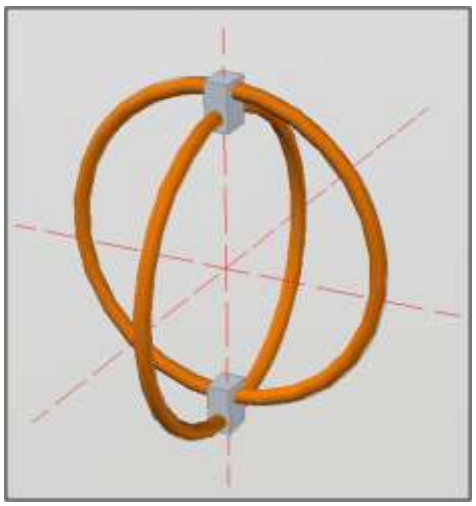

Figure 30. Antenna loop design concept.

In order to protect the coaxial cable and prepare the antennas for installation, they are inserted in the mechanical shielding before crimping the connectors and ensuring the same size to obtain similar antennas. 20 centimetres of coaxial cable are additionally left outside the protecting shielding for crimping the connectors and for the connection with the electronic circuit. See Figure 32.

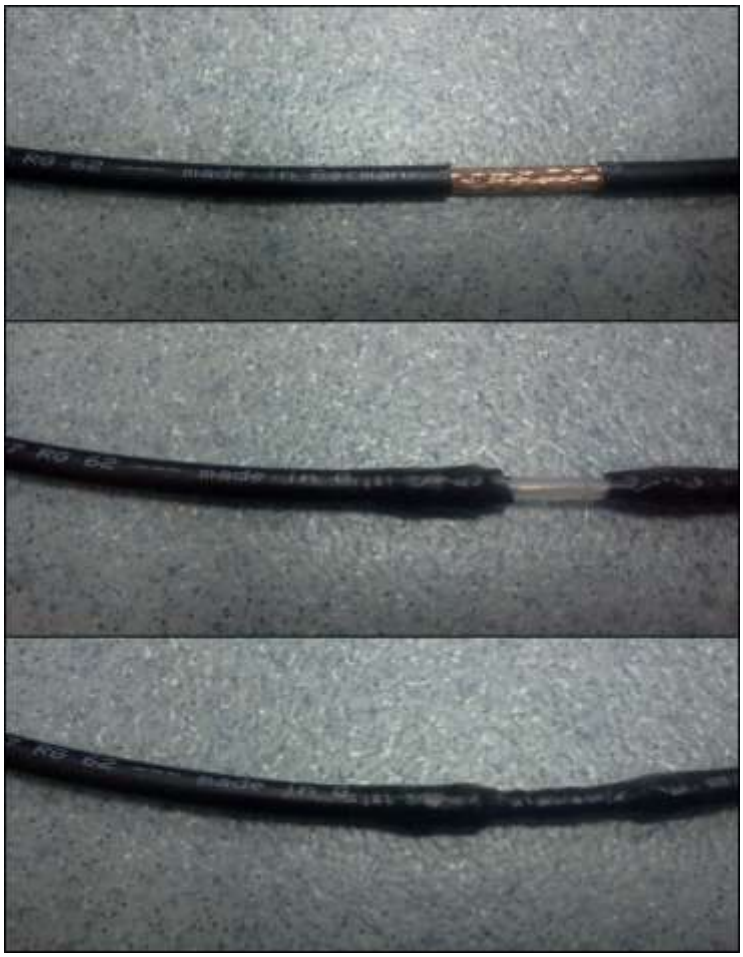

Figure 31. Construction of Coaxial Cable Gap for Loop Antennas.

Figure 32. Coaxial cable inside mechanical shielding pipe before crimping the connectors.

BNC Straight Crimp Plug from Amphenol® Connex connectors with contact finish in gold and RoHS Compliant with adequate response for frequencies until 4 GHz were used. These connectors were crimped with coaxial cable inside a mechanical shield as it is shown in Figure 33.

In order to protect the electronic circuitry from interference and weather conditions and act as a base of the crossed-loop antennas, an EMC-safe cabinet was used for their installation. The antennas constructed using weather resistant materials, were assembled in the top of an EMC box in a crossed configuration as indicated in Figure 30, Figure 34 and Figure 35. The loops-antenna axes were respectively oriented in the North-South (NS) and East-West (EW) directions in their final emplacement. See Figure 34.

The coaxial cables terminals are inside the EMC cabinet in order to connect with electronic circuit. A final view of Crossed-Loop Antennas is shown in Figure 35.

Figure 33. Loop antenna with terminal connectors prepared for installation.

Figure 34. Final view of crossed loop antennas with 90° alignment.

Figure 35. Crossed loop antennas constructed and installed in EMC-safe cabinet.

2.2.3. Electronic Circuitry

To eliminate the need of an input impedance matching and to avoid the amplification of the signals (NS and EW), provided by the loop-antennas, they are connected to an instrumentation amplifier. These instrumentation amplifier is placed inside of the mentioned EMC-safe cabinet shown in Figure 35.

2.2.3.1. Design

The instrumentation amplifier is a voltage-voltage differential amplifier whose gain can be set very accurately and has been optimized to operate according to their own specification even in a hostile environment. It is an essential element of the measurement systems, which is assembled as a functional block that offers its own functional features independent of the other elements with which it interacts [62].

In addition, the instrumentation amplifiers must have following characteristics:

- Their differential is gain accurate and stable.
- The differential gain is controlled using only an analogue element.

- Common mode gain is lower respect to differential amplifier resulting in high Common Mode Rejection Ration (CMRR) in all the frequency range.
- High input impedance to avoid impedance matching effects.

The basic differential amplifier constructed with a single operational amplifier satisfies some of the characteristics of the instrumentation amplifier, but not all for example:

- To modify the differential gain it is necessary to change two components values in order to maintain the common gain equal to zero.
- The input impedance is very low.

Due to the mentioned reasons a more effective solution was proposed avoiding the use of a single differential amplifier in the electronic circuit design.

The configuration most used as instrumentation amplifier is constituted by three operational amplifiers used in accordance with the scheme of Figure 36. An instrumentation amplifier is a type of differential amplifier with two input buffer amplifiers, which eliminate the need for input impedance matching and are intended to be used whenever acquisition if a useful signal is difficult.

Instrumentation amplifiers must have extremely high input impedances because the source impedances may be high or unbalanced. Bias and offset currents are low and relatively stable so that the source impedance do not need to be constant. Additional characteristics include very low DC offset, low noise, high open-loop gain and common-mode rejection ratio. Instrumentation amplifiers are used where great accuracy and stability is required.

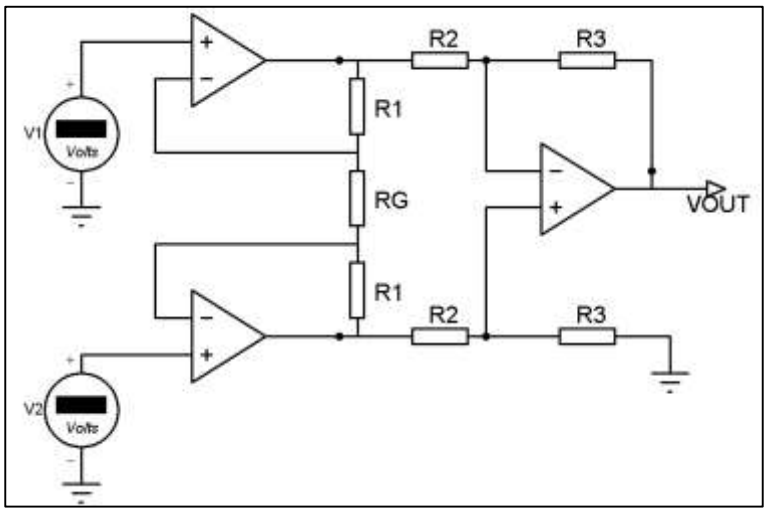

Figure 36. Three operational amplifiers in instrumentation amplifier configuration used as base of circuitry design.

The circuit analysis will be considered using the symmetry properties and using superposition. Simplifying the analysis for lightning application and, for the case when all resistances have the same value:

$$Vout = \frac{(V_2 - V_1)}{R_g}(R_g + 2R_1)$$

$$Vout = (V_2 - V_1)\left(\frac{R_g}{R_g} + \frac{2R_1}{R_g}\right)$$

$$Vout = (V_2 - V_1)\left(1 + \frac{2R_1}{R_g}\right) \quad (18)$$

In order to obtain a circuit variable gain for analysis and flexibility, a trimming potentiometer of 20 [kΩ] and resistances of 10 [kΩ] were used to obtain an output voltage for the potentiometer nominal value according to (15):

$$Vout = (V_2 - V_1)\left(1 + \frac{2 * 10e3}{20e3}\right) \rightarrow Vout = 2 * (V_2 - V_1)$$

As it can be seen in Figure 38, the minimum gain obtained using the circuit will be 2. Figure 38 shows the circuit gain obtained for different potentiometer values. It is necessary to highlight that potentiomenter values lower than 2 [kΩ] could be dangerous for circuit and generate over-currents that could damage the components.

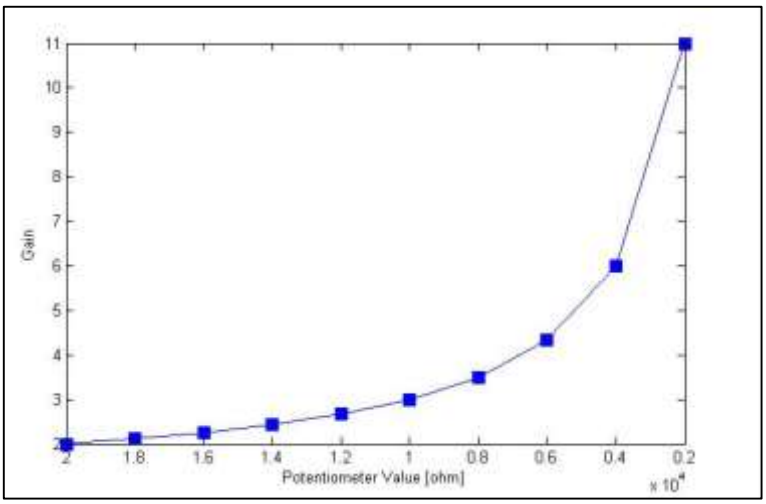

Figure 37. Instrumentation Amplifier Gain with different potentiometer values. Notice that for values lower than 2 [kΩ] (right extreme of Figure) the circuit gain raise in exponential manner, being dangerous for circuit integrity.

The gain selection depends on the antenna response to the magnetic field intensities. According to the strike distance, lightning current amplitude, propagation constants of media among others, the magnetic flux density varies from 10^{-5} to 10^{-11} Tesla. Using well defined values for these parameters and varying the lightning impact distance from 10 meters to 10 [km] and number of return strokes, Rai *et al.* [63] calculated magnetic flux density values for a time of 0,5 [μs] as it is shown in Table 8.

Table 8. Magnetic flux density in Teslas calculated for time of 0,5 [μs]. Adapted from [63].

Number of Return strokes	Distance 10 metres	Distance 100 metres	Distance 1 kilometre	Distance 10 kilometres
Primary	$17{,}1.10^{-5}$	$17{,}1.10^{-7}$	$17{,}1.10^{-9}$	$17{,}1.10^{-11}$
First	$17{,}4.10^{-5}$	$17{,}4.10^{-7}$	$17{,}4.10^{-9}$	$17{,}4.10^{-11}$
Second	$17{,}5.10^{-5}$	$17{,}5.10^{-7}$	$17{,}5.10^{-9}$	$17{,}5.10^{-11}$
Third	$17{,}7.10^{-5}$	$17{,}7.10^{-7}$	$17{,}7.10^{-9}$	$17{,}7.10^{-11}$

Despite being a statistic made four decades ago, could be used as first approximation in order to configure the electronic circuit, in addition, the distances used in [63] are approximately the same that the considered in this project application (15 kilometres). Using equations shown in Section 2.2.2.1

and (15) it is possible obtain an adequate voltage range for loop-antenna and electronic circuit.

Because the circuit acts as a follower providing a gain and there is not integration for obtain magnetic flux, for each antenna sensor is possible calculate the voltage in the terminals using only:

$$V = f * K * A * cos\emptyset * \frac{dB}{dt} \quad (19)$$

Where:

K: Gain of Electronic Circuit (established according (15))

A: Area of antenna sensor (knowing that radius is 15 centimetres, is possible obtain the area using $A = \pi * r^2 = \pi * 0{,}15^2$

$\rightarrow A = 0{,}0707\ m^2$)

∅: Is the angle of incidence

Using the angle of incidence where the induction is greater (0°) and a fixed gain of 5, the maximum value of voltage could be calculated with the values of Table 8 for each distance. In addition, using the information of main frequency component of lightning reported in ranges with centres in 7,5 and 150 kHz, the calculated voltage is shown in Table 9.

Table 9. Calculated voltage from electronic circuit at two main frequencies [V].

Number of Return strokes	**10 m 7,5 kHz**	10 m 150 kHz	**100 m 7,5 kHz**	100 m 150 kHz	**1 km 7,5 kHz**	1 km 150 kHz	**10 km 7,5 kHz**	10 km 150 kHz
Primary	45,3 $.10^{-2}$	9,1	45,3 $.10^{-4}$	9,1 $.10^{-2}$	45,3 $.10^{-6}$	9,1 $.10^{-4}$	45,3 $.10^{-8}$	9,1 $.10^{-6}$
First	46,1 $.10^{-2}$	9,2	46,1 $.10^{-4}$	9,2 $.10^{-2}$	46,1 $.10^{-6}$	9,2 $.10^{-4}$	46,1 $.10^{-8}$	9,2 $.10^{-6}$
Second	46,4 $.10^{-2}$	9,3	46,4 $.10^{-4}$	9,3 $.10^{-2}$	46,4 $.10^{-6}$	9,3 $.10^{-4}$	46,4 $.10^{-8}$	9,3 $.10^{-6}$
Third	46,9 $.10^{-2}$	9,4	46,9 $.10^{-4}$	9,4 $.10^{-2}$	46,9 $.10^{-6}$	9,4 $.10^{-4}$	46,9 $.10^{-8}$	9,4 $.10^{-6}$

According to the calculated voltage in the electronic circuit, the selected gain of 5 provides safety over the possibility of over-voltages in the circuit.

Nevertheless, for the peak at 150 kHz and close distances to objective of this measuring system (15 km), the induced voltage is of only some microvolts being very low in order to ensure the correct measurement. In addition, the probability of lighting at less than 10 meters is very low according to statistics to Bogota (1 discharge per kilometre square per year in Bogota [64]).

According to the results shown in Table 9 and the reasons presented above, the electronic voltage gain was established in the range of 5 to 10. Low values for distant lightning can be enhanced through the use of an adequate acquisition system.

2.2.3.2. Construction and tests

Several prototypes of electronic circuit were constructed and tested in order to ensure the reliability and response of circuit elements. The first prototypes were constructed using DIP (Dual in-line Package) technology due to the installation simplicity and the whole circuit was configured in breadboards. For the final construction, the SMD (Surface Mount Device) technology was selected increasing the circuit reliability, the accuracy in the values of the elements and the elimination of disturbances in the output circuit. The EMC-safe cabinet should protect the circuit against the electromagnetic environmental noise.

The main element of electronic circuit is the operational amplifier, being selected according to required characteristics as bandwidth, slew rate, power supply voltage and input bias current, among others. Two different types of operational amplifiers were selected; one for the input buffer amplifiers and other for the differential ones.

For the input buffer amplifiers following important characteristic must be highlighted: a low input bias current avoiding that the signal will be loaded down by the amplifier input; adequate input common mode voltage range to allow signal measurements without saturation or affectation provide by the amplifier. For these reasons, the Texas Instruments Amplifier THS-3001 (420-MHz high-speed current-feedback amplifier) was selected with input bias current of 15 [A] and input common-mode voltage range of ±13,2 [V]. Other important characteristics are a 420 [MHz], bandwidth of a Slew rate of 6500 [V/us], a power supply of ±16 [V] and an input voltage noise of 1,6 [$\mathrm{nV}/\sqrt{\mathrm{Hz}}$].

To differential amplifier stage, it is necessary take into account: -the common-mode input range to avoid signal saturation, -high slew rate to ensure fast signal measurements and -low input voltage noise to ensure adequate behaviour in high frequencies (> 10 [kHz]). The Texas Instruments Amplifier THS-3061 (low-distortion, high slew rate, current-feedback amplifiers) was implemented for the differential amplifier stage with a common-mode input range of ±13,1 [V] and a slew rate of 7000 [V/us]. Additional characteristics are 300 [MHZ] bandwidth, a supply voltage of ± 15[V] and an input voltage noise of 2,6 $[\mathrm{nV}/\sqrt{\mathrm{Hz}}]$.

Circuits for two antennas were terminated on its characteristic impedance at both inputs of the instrumentation amplifier, to prevent any overshoot or ringing in the *dB/dt* waveform. These circuits are identical (See Figure 38).

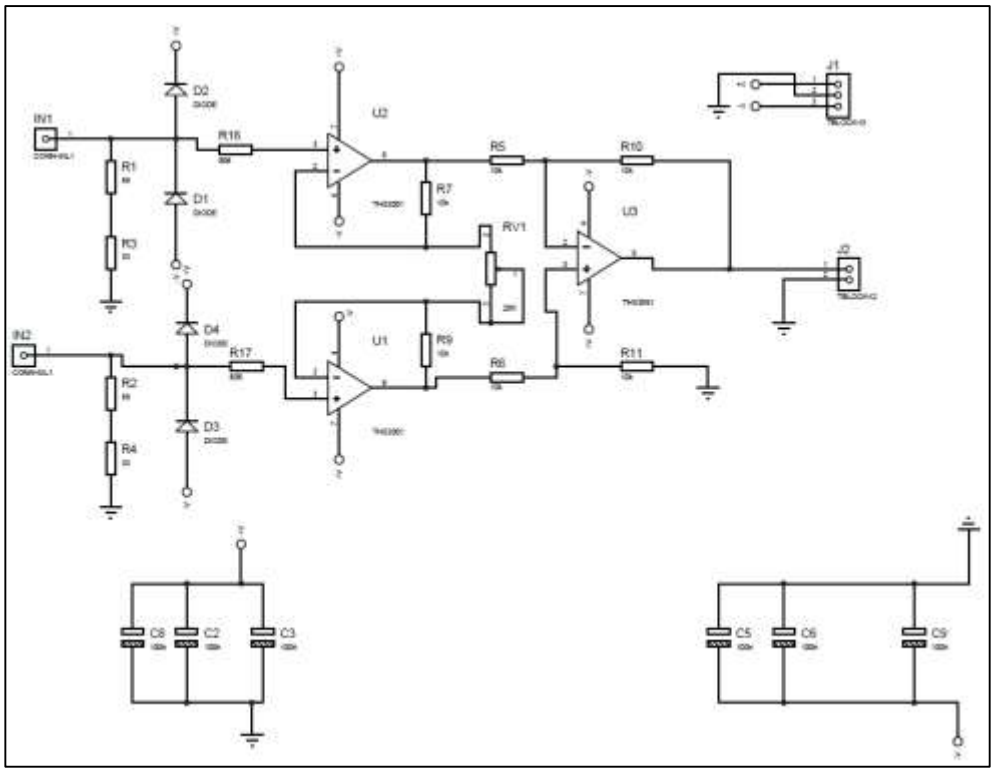

Figure 38. Scheme of Electronic Circuit in Instrumentation Amplifier configuration.

Protecting diodes are installed to protect each circuit against overvoltages. The Buffer amplifiers are connected to the input through 806 $[\Omega]$ resistors and to the instrumentation amplifier described above. For flexibility of circuit and to obtain a circuit gain of 6, a potentiometer is installed in the gain resistor and configured together with the 10 $[\mathrm{k}\Omega]$ resistors. Capacitors are implemented in the supply voltage inputs in order to diminish the possible

power supply fluctuations that could affect the operational amplifiers and the output waveform.

The DC power supply for each polarity is provided by rectification of the commercial power line provided by a transformer. The PCB (printed circuit board) was performed using EMC techniques by the use of ground planes and adequate distances between the tracks and both the power supply and the signals. The final implementation is shown in Figure 39.

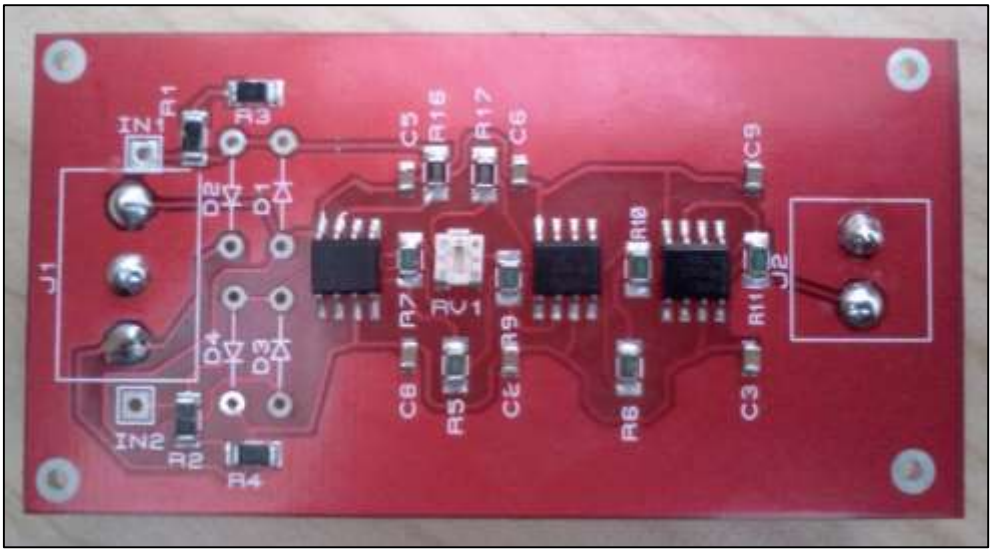

Figure 39. Final implementation of circuit with SMD elements.

The crossed loop antennas are connected with female RGB led strip needle connectors welded to the substrate and directly connected with the central conductor of the coaxial cables. The output of the electronic circuit, the same kind of connectors are used in the substrate. The coaxial cable that transport the signal to the acquisition system are connected with BNC chassis connectors.. Tests were performed in order to measure the quality of electronic circuit. Using known voltage inputs, the noise measured at electronic circuit output was always within 5 [mV] and without any disturbance in waveform. The circuit gain was measured and remained stable in the calculated range. For the specific case of gain 6, 10 measurements were made using 4 kind of voltage inputs were used: square, sinusoidal, DC and open. For a DC input to 3 [MHz] for square and sinusoidal inputs, the obtained range of gains was 6 ± 0,3.

The passive antenna response was tested using a high voltage impulse generator. An impulse was generated and its magnetic field was measured

with the antenna connected to its electronic circuit. The EMC-safe cabinet was used to avoid the influence of electric field in the system. Figure 40 shows the impulse measured by antenna connected to its electronic circuit.

Despite of the correct measurement of the generated impulse, there was not available an active antenna with a high performance response to be used as reference for comparison. For this reason, both, the circuital model and antenna calibration were made to ensure the correct response of the loop antennas.

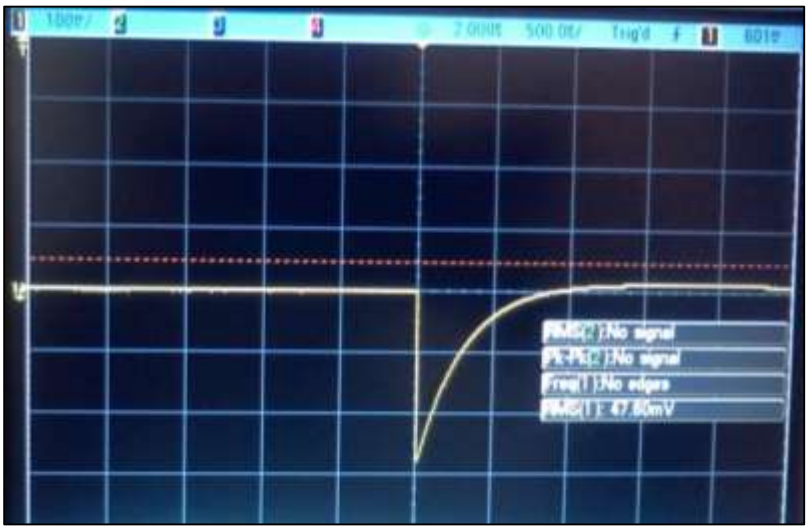

Figure 40. Measured signal of impulse generator with the loop antenna connected to its electronic circuit.

2.2.4. Acquisition System

Two acquisition systems were implemented in order to obtain the best performance, allowing different sample rates and specific analysis of lightning signals to be captured.

High speed system consist of an oscilloscope for detailed analysis in short times of microseconds, measuring parameters as rise time and pre-discharges. The slower system is used in ranges of hundreds of milliseconds and is able to obtain statistics of number of flashes, polarity and multiplicity.

The measured signals are transmitted to the high speed recording system which consists of a 4-channel Oscilloscope Agilent DSO 6104A, 1 GHz Bandwidth and 4 GSa/s sample rate as shown in Figure 41. The oscilloscope

is connected to a computer and the signals are acquired with a maximum resolution of 250 ps.

Figure 41. Oscilloscope Agilent DSO 6104A used for acquisition of signals at high speed rate.

A second acquisition system was used consisting in an Agilent Instruments Data-Acquisition Device (DAQ) U2300A with 3MSa/s sampling rate in each channel and 16-bit resolution.

Due to the fact that both systems have different input impedances it is difficult its connection in parallel mode. For this reason the high speed rate system will be used for determine the performance of system for microseconds ranges and slow speed rate system is intended to perform the measurements of parameters for complete flashes in a range of hundreds of microseconds.

Figure 42. DAQ Agilent U2331A used for acquisition of signals at low speed rate.

The acquisition system were selected, among other characteristics mentioned above, for its capability to integrate one electric field signal and two magnetic

field signals in the same time scale, thanks to the several input channels of both systems.

For the two systems is possible the communication with a central computer that allows the reception and analysis of data through an interface developed in the commercial software Labview®. This software structure of the data acquisition was developed offline due to the short interval between several lightning flashes being unrealizable the online processing. This limitation was overcome by saving each lightning flash data as files and making the post-processing in other central unit.

With the data file of each flash, the software structure was developed as it is shown in Figure 43. The procedure could be divided in three stages detailed as follows:

- Signal configuration: This stage consists in taking the signal from the text file and convert it into a data vector of adequate size for next stages, conserving the time stamp and value of corresponding voltage for each signal.
- Signal filtering: In order to sift out the undesired signal components, it is necessary to remove the low frequency component and apply a filter. The low frequency component of the signal should be removed before the integration stage, for this reason a math script node was added with *detrend* function to remove the trend of the signal. A Chebyshev type of digital band-pass filter is adopted in the signal processing procedure with a high cut-off frequency of 10 MHz and low cut-off frequency of 300 Hz. The order of the filter is six. In addition to this filtering procedure, an adaptive filter in Fractional Fourier Domain was implemented [19] comparing the results and validating the accuracy of method for filtering undesirable signal components.
- Signal Integration: According to calculations and models evaluated in previous sections, the loop antennas measured voltage is proportional to the derivative of the magnetic flux, therefore to obtain the magnetic flux density, the signal should be integrated. This integration of the signal can be achieved by a numeric integration through a virtual instrument in Labview®.

This processing method is used for signals from both slow and high speed rate systems and is compared with filtering method proposed by Rojas *et al.* [19] and it is shown in Section 3.2.

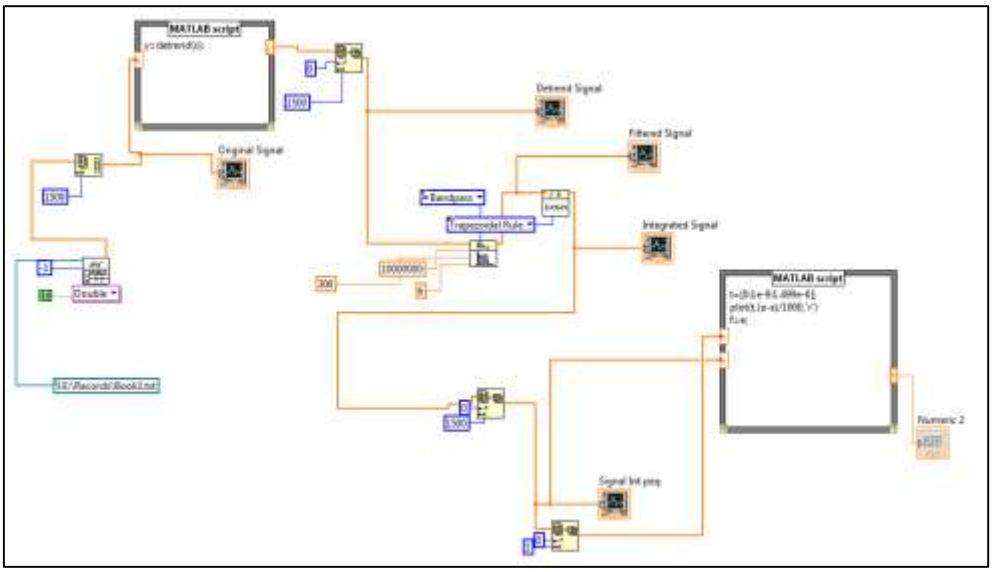

Figure 43. Block diagram of signal processing procedure for each channel.

Chapter 3

Electromagnetic Field Measurements

Both, the acquisition and the Electric Field Systems were installed and tested during four months in the Camilo Torres building at the *Universidad Nacional de Colombia* in Bogota from October 2011 to February 2012. Figure 44 show the location of electric field antenna and the acquisition system. Measurements of electric field were performed verifying the proper functioning of system in order to implement it in a new configuration.

Figure 44. Electric field sensor and acquisition system located in Camilo Torres building.

For the electromagnetic field measuring system was selected the location shown in Figure 18. The sensors and antennas with their corresponding electronic circuits were installed on the roof of the building (See Figure 45 and Figure 46). Sensors and antennas were connected through shielded coaxial cables to the Base Station where the acquisition system and the post-processing unit were located (See Figure 47). To ensure noise-free measurements, connections between roof and base station were performed using Belden Coaxial Cable an Amphenol connectors. Additionally, to avoid

environmental electromagnetic noise, a metallic case was used to cover the cables. To synchronize this measuring station with the future ones, a GPS Module Receiver using an M12M Timing Oncore™ for synchronization will be used.

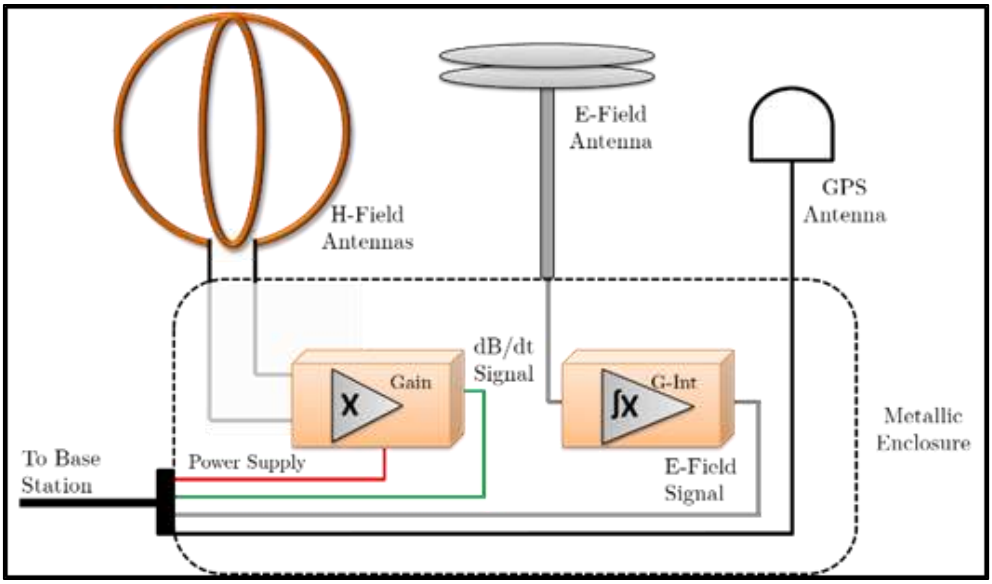

Figure 45. Scheme of Lightning Electromagnetic Field Measuring system installed in the 411 building Roof. The sensors installed in the roof of building (H-Field Antennas and E-Field Antenna) are connected to electronic amplifier circuits and in the specific case of the electric field to integrate it. . The signals are transported to the Base Station with coaxial cables placed in a metallic case.

To characterize and calibrate the measuring system, lightning data was recorded with a high speed rate system during the lightning seasons from January to June 2013. However, during the subsequent months, the complete system continued registering new events. Table 10 resume the lightning signals recorded, including the lightning electric field measuring system testing.

All the records are constituted by two magnetic field signals and one of electric field. These signal are captured using the high rate acquisition oscilloscope DSO 6104A, generating three files in txt format in the same time scale. These files are accurately compared in the same sub-microseconds time base by using a specific application developed in Labview®.

Figure 46. Electric and magnetic field sensors located on the roof of 411 building. Note the H-Field and E-Field Antennas and the EMC-safe cabinet to protect the electronic circuit on the base of the magnetic field antennas. The shielded cables from each sensor to the base station (grey colour), can be seen under the shielded box.

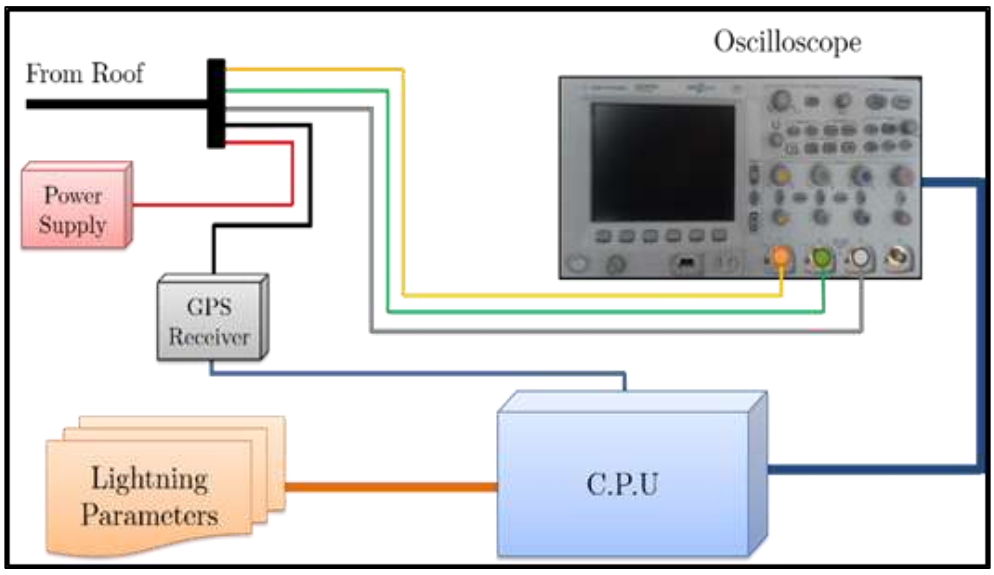

Figure 47. Scheme of the Electromagnetic Field Measuring System in the Base Station. The signals from the roof sensors enter the Base Station through shielded cables and are acquired by the Oscilloscope, at a 4Ghz/s rate. This data is transferred to the computer by using a Labview® algorithm. Details of this algorithm are shown in Figure 43.

Table 10. Lightning Records obtained from Measuring System.

Date	Number of Flashes	Comments
Oct 2011 – Feb 2012	86	Electric Field (Camilo Torres Building)
December 20th 2012	2	Magnetic Field (411 Building)
January 2013	11	Magnetic Field (411 Building)
February 2013	59	Magnetic Field (411 Building)
March 2013	22	Magnetic Field (411 Building)
April 2013	98	54 Records with Simultaneous E and B Field
May 2013	19	Simultaneous E and B Field

The computer in the Base Station is connected to both, the oscilloscope through LAN connection and Internet by Wireless LAN connection. The use of these communication media allows the acquisition of data and continuous upload of text files to a cloud server through a free software application for remote control. This application could share the saved files and allows the control of the computer in the base station through other computers connected to internet with a username and correspondence password, avoiding the need of on-site change of parameters of acquisition as resolution time and scales, among others.

3.1. Magnetic and Electric Field Records

Examples of captured oscilloscope lightning signals are shown in Figure 48 and Figure 49. Figure 48 shows a lightning electric field signal measured in

October of 2011 during the electric field measuring system test. See Figure 44. The signal analysis allows the calculation of parameters as rise time, FWHM (full width at half maximum) and zero cross time, which permitted the evaluation of the results against the expected values. The measured signals shown an adequate behaviour of electric field system since the obtained values are in the range of ±15% of standard values for lightning signals.

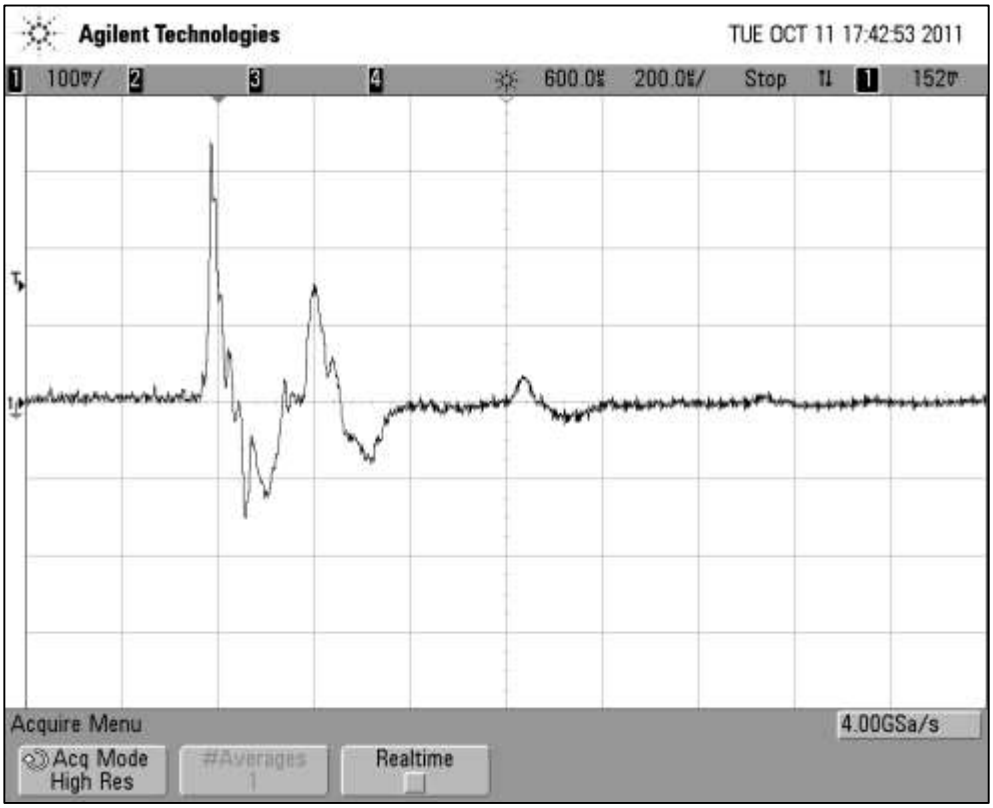

Figure 48. Oscilloscope Capture (Acquisition System) of Lightning Electric Field Signal on Oct 11 2011 using a Window of 2 ms and 4G Samples.

Using the electromagnetic system shown in Figure 46, 86 waveforms were captured and analysed in order to evaluate the resulting parameters and compare with expected values, performing a test for the system calibration. These measurements were a complement to the calculation of the system measuring factors mentioned in Section 2.1.

Figure 49 shows a signal registered on May 3, 2013. The yellow and green signals are from magnetic field antennas in North–South and East–West directions respectively. The waveforms from magnetic field shown a variation between positive and negative values proportional to the magnetic field

derivative, behaviour expected and that after numerical integration tend to resemble the electric field signal at least in the first microseconds of the phenomenon.

Magenta signal is from electric field antenna after the integration via an electronic circuit. In this particular case, two strokes were recorded with more than 40 ms between them and showing the dominance of the electrostatic component resulting in the long duration of each stroke.

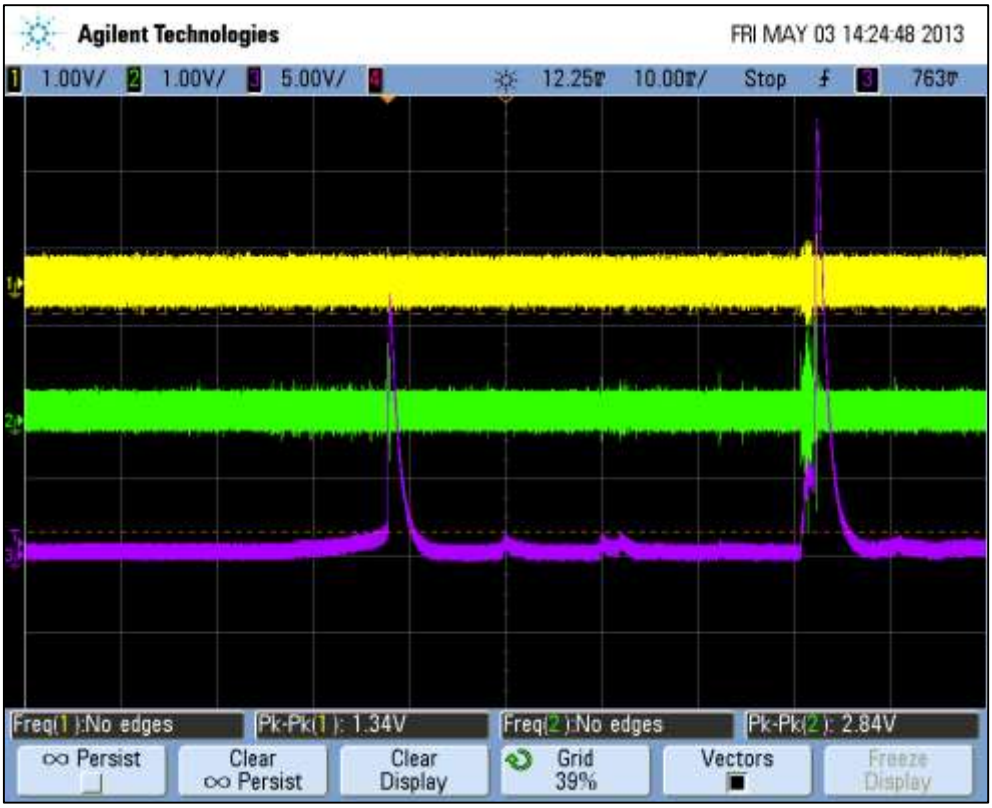

Figure 49. Oscilloscope Capture (Acquisition System) of two strokes on May 3rd using a Window of 100 ms and 1MSamples. Yellow and green signals are from magnetic field antennas and the magenta one is from the electric field antenna.

Two time windows were used for calibration purposes. The first time window was established in 100 [ms] in order to observe different strokes for the same flash and evaluate parameters as multiplicity, polarity and relative magnitudes, recognizing the system ability to measure these characteristics.

The second time window was established in 5 [ms] to observe the detail of waveforms and obtain parameters as rise-time, FWHM, zero cross time, among others, allowing temporal parameters analysis and the comparison with other measurement systems through the micro-second variables. This

time window is still too long for the typical lightning signal (1,2/50 us) but was chosen due to the predominance of electrostatic component in electric field signal that increment the visualization time. An example of this time window configuration is shown in Figure 50.

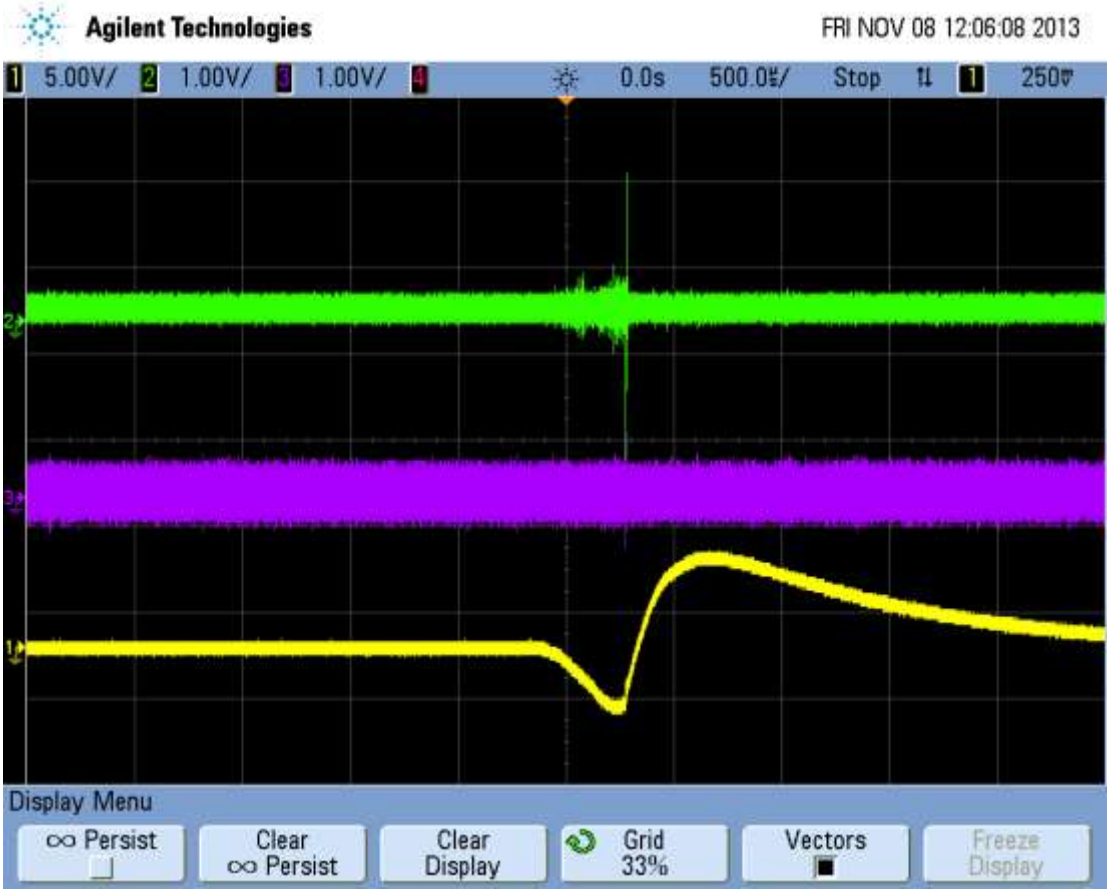

Figure 50. Oscilloscope Capture (Acquisition System) of two strokes on November 8 using a Window of 5 ms and 1MSamples. Magenta and green signals are from magnetic field antennas and the yellow one is from the electric field antenna. Notice the predominance of electrostatic component in the electric field.

Using the txt files created for each set of signals, the magnetic field files are processed as it is related in Section 2.2.4. The detail of entrance signals is shown in Figure 51, denoting the high electromagnetic environmental noise and correspondence between the N-S and E-W loops and differences in peaks and values due to different illumination angle according the direction of the lightning flash. This characteristic is used to obtain the direction of lightning flash using both magnetic field signals. See Section A22.

In the next section the processing method is described in detail, while the filtering process is specially evaluated. The two signals previously shown in

Figure 50 are treated in this chapter as examples of the processing procedure, nevertheless all the captured signals were evaluated and their results were used for the statistics in the different stages of the processing process.

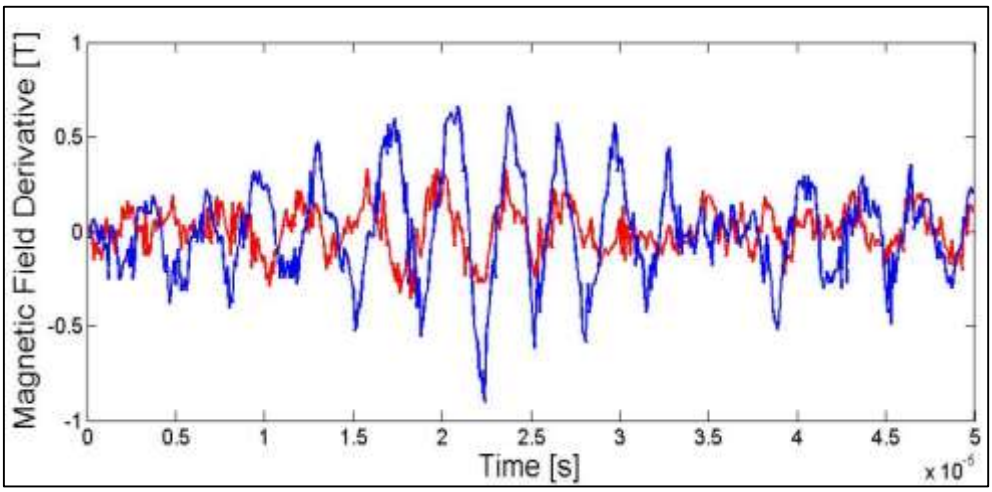

Figure 51. Magnetic field derivative of two loops for flash shown in Figure 50. Blue signal is from N-S loop and red signal is from E-W loop. Notice the correspondence between the two signals and difference in values due to the flash direction.

3.2. Processing Method

The measured signals in Figure 49 and Figure 50 contains environmental electromagnetic noise in addition to some other noise components mainly produced by the measuring system itself. Nevertheless, the influence of electromagnetic signals produced by FM (frequency modulation) broadcasting is clearly the most representative noise. This could be evidenced in the signal itself and by treating the signal through a Fourier Transform to obtain the main frequencies that contribute to the signal.

The green signal of Figure 49 corresponding to the magnetic field derivative of the N-S loop is presented in Figure 52. A detail of this signal is shown in Figure 53, showing the waveform obscured by high frequency components.

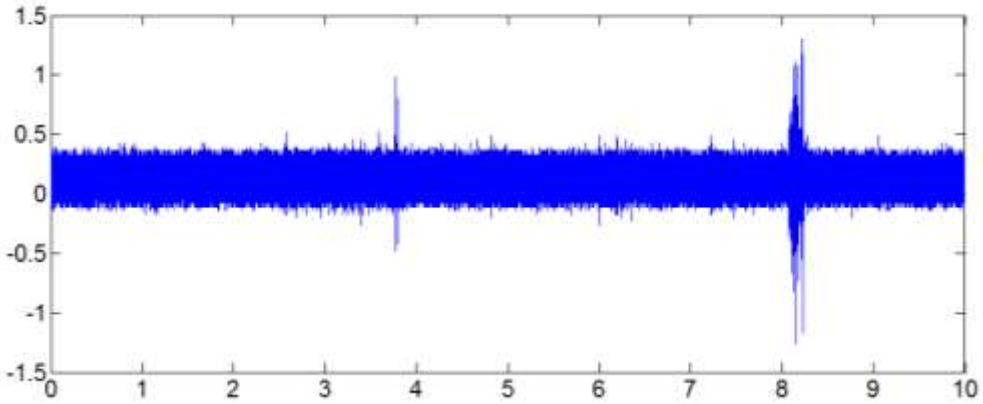

Figure 52. Magnetic field derivative of N-S loop (green signal of Figure 49)

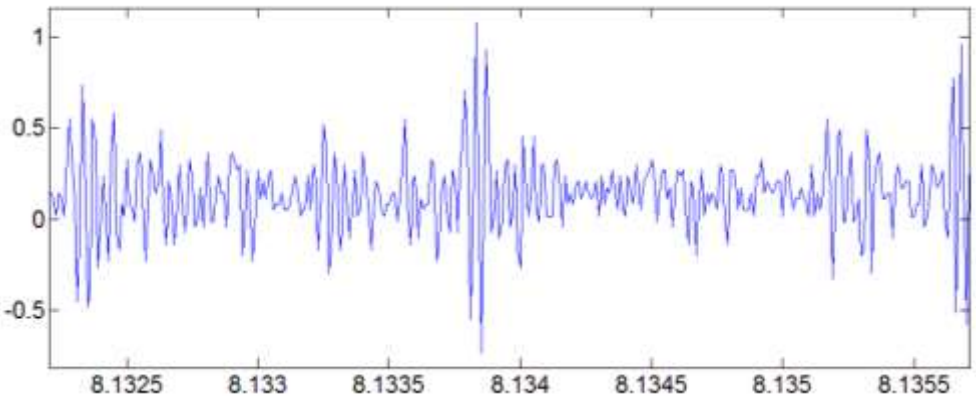

Figure 53. Zoom of Magnetic field derivative shown in Figure 52.

In order to evaluate the specific frequency ranges to be filtered, and to probe the influence of FM broadcasting in the total noise of the measured signal, the Fourier Transform was applied to the magnetic field derivative of Figure 52 and the magnitude of the single-sided power spectrum was plotted. See Figure 54. There is a specific range of frequencies located at the right side of Figure 54 comprising from 87 to 108 MHz approximately, which corresponds to FM broadcasting as previously proposed. It is necessary to highlight that the low frequency component of the signal should be removed before the signal pass to the next stage of the processing procedure, avoiding errors in the integration stage due to offset values.

A filtering procedure which uses a Chebyshev filter was developed in Labview®. This procedure is similar to the one described by Zhou et al. [66]. By using a Virtual Instrument, the Chebyshev Filter was implemented with following characteristics: order 6, low cut-on frequency of 300 Hz and high

cut-off frequency of 10 MHz. The Fourier Transform was applied and magnitude power spectrum is shown in Figure 55.

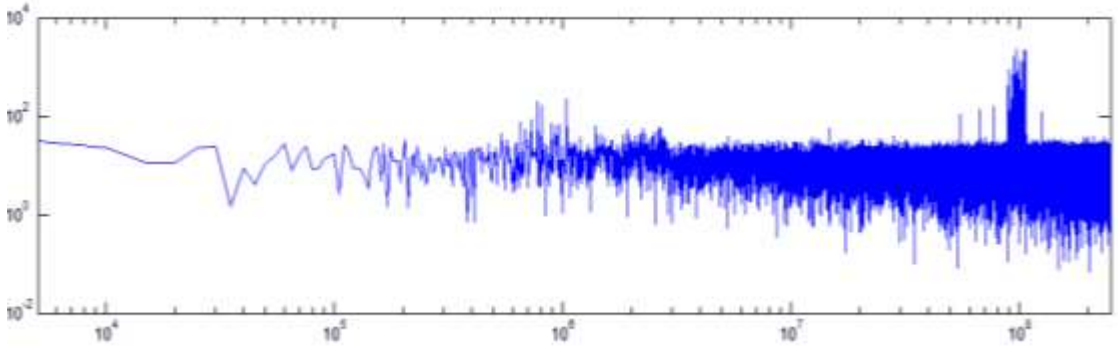

Figure 54. Magnitude of the single-sided power spectrum of signal shown in Figure 52. X-axis denotes the frequency and Y-axis shows the magnitude of power spectum in dB.

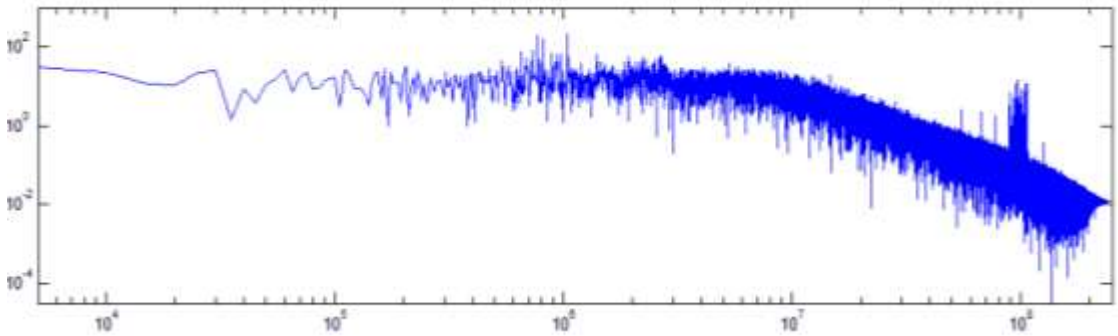

Figure 55. Magnitude of the single-side power spectrum after filtering process of signal shown in Figure 52. X-axis denotes the frequency and Y-axis shows the magnitude of power spectum in dB.

It is plausible that the filter implemented could reduce the influence of the noise high frequency components. Nevertheless, the frequency range adopted for the filtering process was established basically from the knowledge of the system restrictions and the Fourier Transform evaluation of the signal. Additionally it was assumed that the lightning main components are in the range of hundreds of kilohertz as it is mentioned in Section 1.3. This selection could derivate in errors for two reasons:

- Neglecting frequency components that are directly related with the signal of interest, or
- Keeping frequency components of noise that are not part of the desired measurement.

For the Chebyshev filter used in this application, several test were developed in order to probe the best configuration for lightning signals, obtaining the cut-on and cut-off frequencies at 300 [Hz] and 10 [MHz] respectively.

In order to separate the original signal from the undesired components, and to compare the ability of the designed filter mentioned above, an adaptive filter in the Fractional Fourier domain (FRFd) was adopted.

The fractional Fourier transform (FRFT) is a generalization of the conventional Fourier transform (FT). This type of filters avoids the difficulties of adaptation in a time-varying signal environment by transforming these signals to FRFd, where the signals vary slowly. The presence of undesired signals that distorted the original lightning electric and magnetic field signal suggests that the FRFT can be successfully used in the denoising process of the measurements and the improvement on its application depends on the selection of a suitable fractional order. The filtering process using the fractional Fourier transform is described with detail in [65].

Figure 56 shows the induced measured voltage signature acquired in February 2013, by the magnetic field antenna. The sampling rate is 1 GS/s and the length of the recorded signal is 20.000 points.

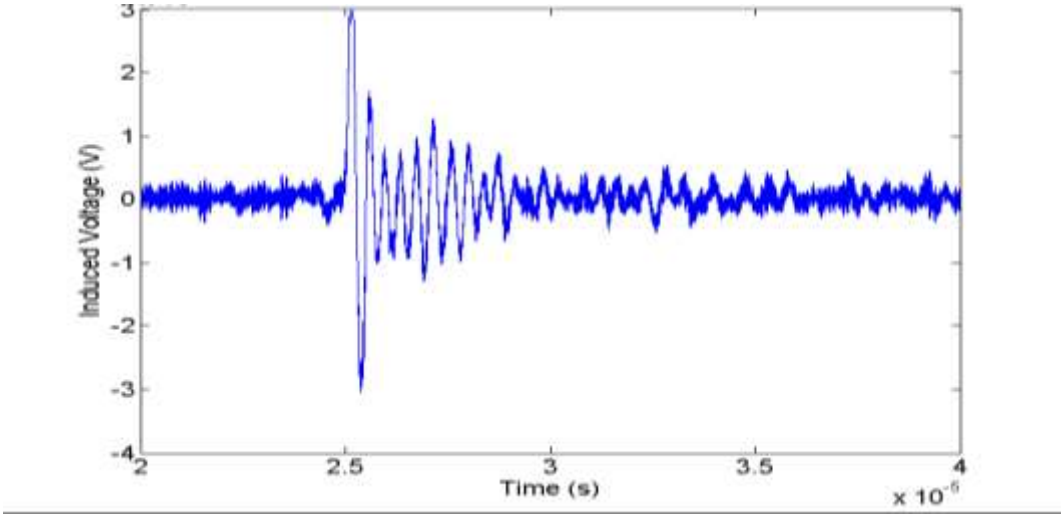

Figure 56. Voltage signal induced in the loop before filtering.

The signal is processed through the signal processing procedure developed in Labview shown in Figure 43. The result of the filtering process is shown in Figure 57. The noise of the signal is sensibly reduced and a function to remove trend effects in the data was performed in order to minimize the effect of low frequency component in the integration stage.

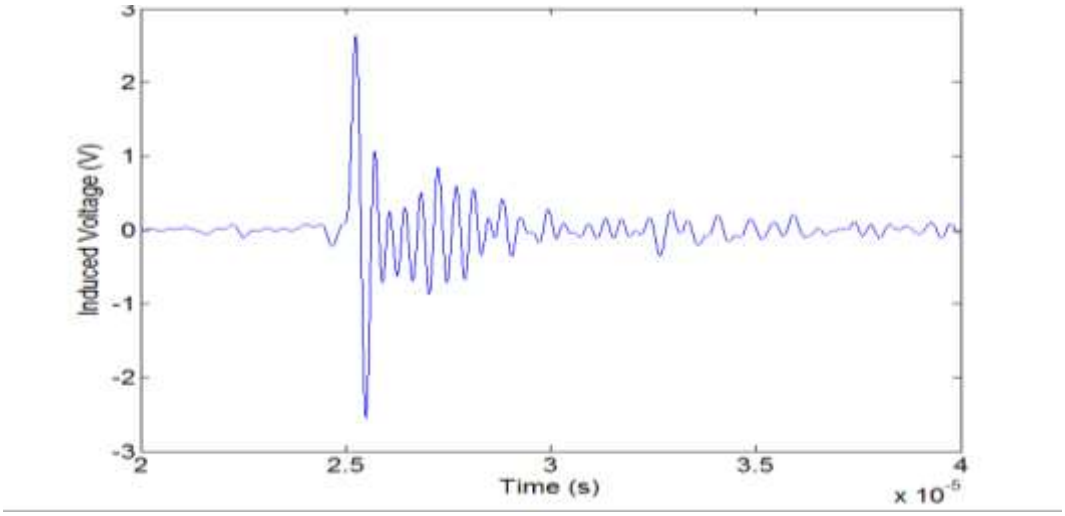

Figure 57. Voltage signal induced in the magnetic loops after Chebyshev filtering procedure.

After the Chebyshev filter the signal denoised is integrated and the magnetic flux density of lightning is obtained. The result is shown in Figure 58.

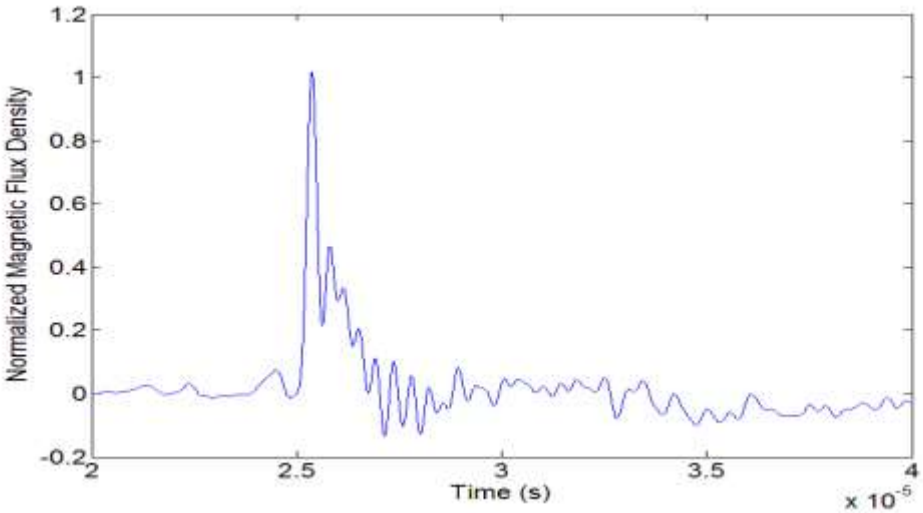

Figure 58. Normalized magnetic field signal after the integration procedure with Chebyshev filter.

The described process starts with the induced voltage measured data on the loops and finish with the desired measure, the magnetic flux density. The

latter is useful for comparison with the electric field, with other measuring systems and with the literature and the related normative.

For comparison with the Chebyshev filtering procedure, the FRFd adaptive filter is configured with following parameters: fractional order $\alpha = 0.2$; adaptive algorithm Normalized leakage LMS (NL-LMS); normalized step-size $\mu_{NL-LMS} = 1.25$; leakage factor $\gamma = 0.9975$; stabilization factor $\beta = 1 * 10^{-17}$; number of coefficients is 4.

The signal before and after the FRFd filtering procedure is respectively shown in Figure 56 and Figure 59. Another important stage of the signal processing procedure is the integration of the signal captured by the antenna. Knowing that the induced voltage at the measuring loops is proportional to the magnetic flux derivative, the lightning magnetic field must be obtained by integrating the measured induced voltage. This integration is numerically performed by using a Matlab® routine which also removes the low frequency component present in the filtered signal before the integration stage.

A numerical integration replaces the use of an integration circuit in the measuring system. The use of a new hardware in the measuring system, such as an integrating circuit, could introduce undesired noise components (electric noise), which could obscure features of the measured signal. Figure 60 shows the output signal after the numerical integration procedure.

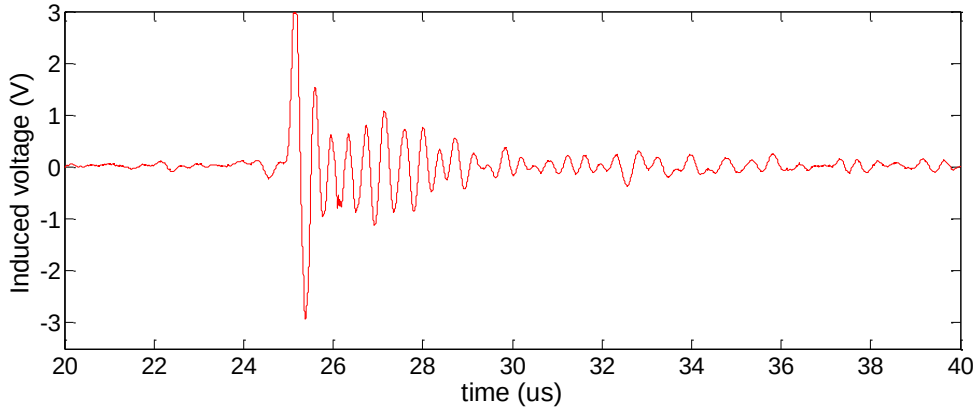

Figure 59. Voltage signal induced in the magnetic loops after FRFd filtering procedure.

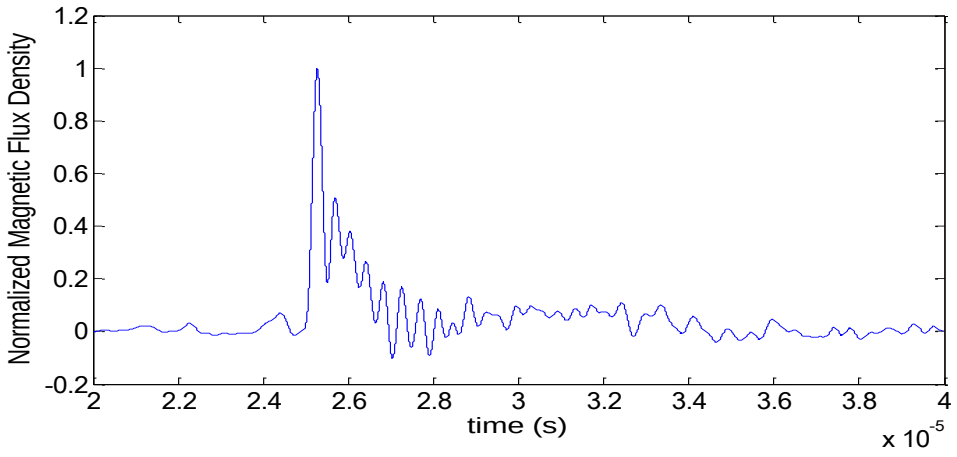

Figure 60. Normalized magnetic field signal after the integration procedure with FRFd filter.

The evaluation of the measured signal and the filters performance was satisfactory, revealing that it is possible use both of them for processing the data. It is plausible that the similarities between the signals shown in Figure 58 and Figure 60, obtained with the two kind of filters, nevertheless the resulted signal using both filtering process shown the influence of a high frequency signal considered as noise, are incomparable for this specific case. For this reason, in order to compare the results, the signal captured in May 3rd of 2013 is filtered using the two methods (See Figure 49). The result after integration of signals is shown in Figure 61.

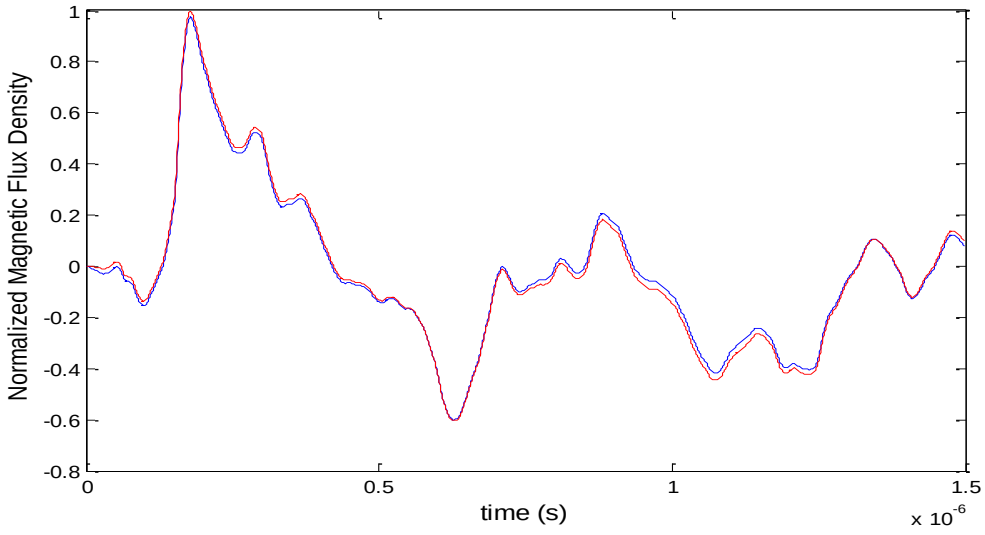

Figure 61. Normalized magnetic field signal comparison between the two filtering methods. FRFd technique (blue line) and Chebyshev filter (red line) of a first stroke in May 3rd of 2013.

According to the results in Figure 61, there are some differences in specific times that must be evaluated. To compare the two signals using numerical values, three parameters of the signal were selected for evaluation: Peak value, zero crossing time and rise-time. The evaluation of these parameters is shown in Table 11. This results shown that differences between two filter techniques are bigger in the case of rise-time, but still remain acceptable for the other two evaluated parameters.

Table 11. Signal parameters evaluation of the two filtering techniques

Parameter	FRFd	Chebyshev	Difference (%)
Rise – time	2,8 [us]	3,0 [us]	6,67
Zero cross time	42,0 [us]	42,3 [us]	0,71
Peak value	0,9743	1	2,57

According to the results and analysis of the measured signals, it is possible to conclude that filtering process using either, Chebyshev or FRFd method, are satisfactory to process the lightning signals measured with the Electromagnetic Field Measuring System. Similarly, the designed software to process the measured signals is suitable to be use and the obtained results at the end of the process show reliable information for system evaluation and future construction of a database with lightning information for Bogotá and surroundings.

3.3. Comparison of Electric and Magnetic Field records

The comparison between the measured magnetic and electric fields is useful for the determination of the constructed magnetic field system performance versus the results of an electric field system previously tested and configured. If the radiated electromagnetic fields are from far field, it is expected a similarity between both, the magnetic and the electric fields in all the visualization time. In this case, due to the configuration of the Lightning Electromagnetic Field Measuring System, it is only intended to measure in a

radius of 20 kilometres, where the electrostatic component of electric field is dominant and similarities are expected only for the first microseconds. See Section 1.3.

The previously comparisons were made using only the signal processed from one of the loops, generally the one with the higher peak. However, the electric field signal should be compared with the total magnetic flux density given by the combination of both orthogonal loops. These two magnetic field signals are combined as vectors to obtain the total magnetic field component transverse to the propagation path.

Figure 62 shows the magnetic and electric field records of the first 150 microseconds of the second stroke of a flash recorded in May 3rd of 2013 at 14:24:48 (See Figure 49). According to the magnetic and electric field characteristics registered, the lightning strike was located between 15 to 20 kilometres. This is mainly due to the fact that in the electric field signature the electrostatic component was evident as it is described in several electromagnetic models of return stroke [46] and also by Lin *et al.* in [45]; a similar behaviour between E and B is expected during the first microseconds.

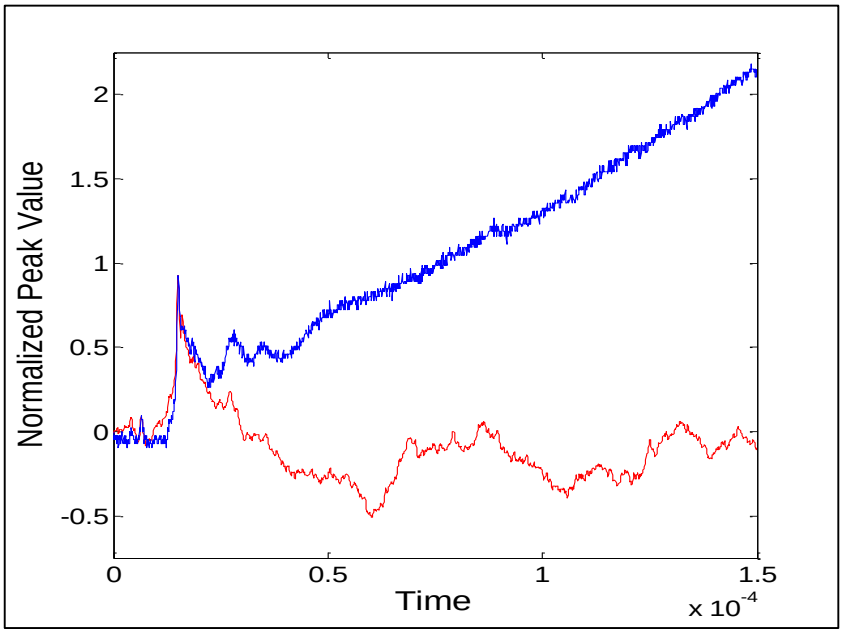

Figure 62. Magnetic Field Signal (red line) and Electric Field Signal (blue line) of second stroke showed in Figure 49. Note the correspondence in the first 25 microseconds before the electrostatic component starts dominating.

The resulting waveforms of magnetic flux density are similar and shown and adequate agreement in all the visualization time. Figure 62 shows a good

correspondence between both signatures, but with some differences especially in the parameter rise time. This difference could be explain by the different characteristics of both measuring system, the response time of the electronic components and the different nature of both sensors.

Other example of comparison between electric and magnetic field, but in this case using the signals of the orthogonal loops without combination, was developed using the normalized peak value of the flash shown in Figure 50. The result of this comparison is shown in Figure 63. The noise present in the electric field signal is related to the oscilloscope measuring range, which was established in 5 Volts per division. This voltage range was chosen to capture the whole event in the oscilloscope range and without saturating the measuring electronic circuit. Nevertheless, it is possible to recognize the similarities between both magnetic field signals and its correct relation with the electric field.

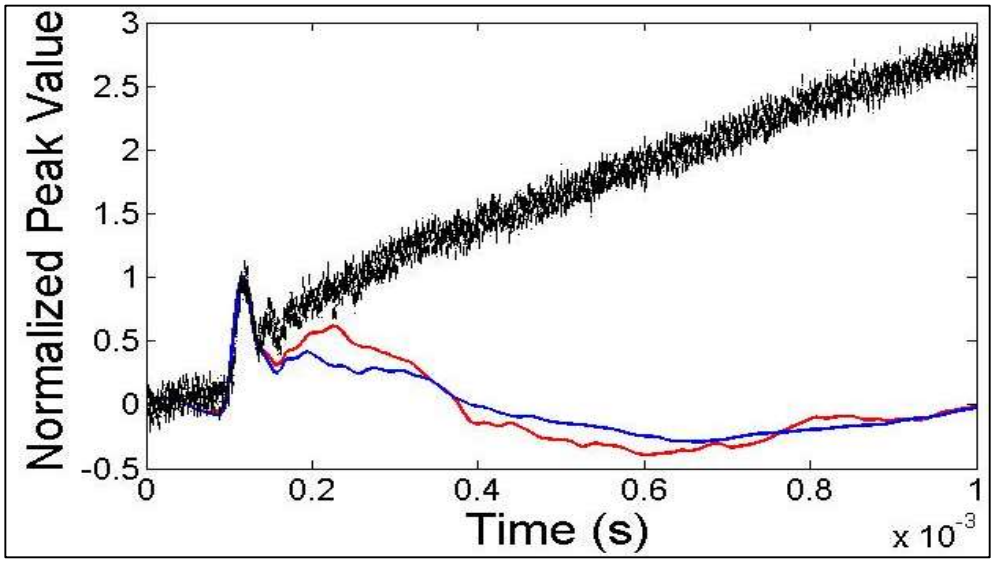

Figure 63. Magnetic Field Signal of N-S loop (red line), E-W loop (blue line) and Electric Field Signal (black line) of flash showed in Figure 50. Note the correspondence in the first $150\ \mathrm{s}$ before the electrostatic component starts dominating

Despite the observed differences between the magnetic and electric field especially in rise-time, the results and behaviour of system are satisfactory and consistent with the expected values. Through the comparison of the lightning magnetic and electric field signals, it is possible to guarantee that the magnetic field system is reliable for measuring lighting.

Chapter 4

Conclusions and Future work

4.1. Conclusions and Future Work

The Lightning Electromagnetic Field Measuring System (LEMFMS) developed in the present investigation requires some improvements to obtain reliable measures and stringent statistics of lightning in Bogota and surroundings. The following characteristics should be implemented in order to obtain better results:

- A GPS module for the LEMFMS would be implemented to synchronize with future measuring stations and to obtain additional parameters as lightning location and lightning current. In addition, the time stamp provides a precise comparison value with other lightning systems
- Optical fibers in replacement of coaxial cables should improve the high frequency system response in the ranges of lightning signals and it should discriminate between Cloud to Ground and Cloud to Cloud flashes
- Acquisition systems of LEMFMS using automatic data should be implemented, improving the data capture through an additional method as remote control

4.2. Conclusions

A Lightning Electromagnetic Field Measuring System was constructed and its performance was tested as part of the Electromagnetic Compatibility Research Group EMC-UNC interest on investigating the lightning activity in

Bogotá. This lightning investigation seeks to understand the behaviour of lightning activity in Bogotá and surroundings. Additionally, in this investigation the characteristics and parameters of captured lightning signals will be obtained, the results will be compared with other measuring systems and features as pre-discharges, noise discrimination of lightning and treatment, among others, could be obtained and analyzed.

The Measuring system complies with the proposed objectives in terms of measuring parameters, time scales and ranges, providing the base for a complete analysis of lightning phenomena in the EMC-UNC group. This achievement was obtained through the research and consulting of national and international developments, understanding the recent advances in the research topic and implementing the best option according with functionality and costs.

From this process is possible ensure that high technologies for lightning measuring are possible of construction and implementation in Colombia, providing the means to a deeper study and research of this phenomena in our country.

The main conclusions of this project are:

- To understand the principles of lightning measurement and to construct an adequate information background for the research project, plentiful literature related to lightning, antennas and acquisition systems was revised and analysed
- An evaluation of studies on lightning phenomena in Colombia during the last 25 years was performed, obtaining the state of art in our country and raising the advances and challenges on lightning research in Colombia
- Several magnetic field sensors were evaluated and each one was evaluated in the performance to measure lightning signals, selecting loop antennas as sensors for Magnetic Field System and constructed using resistant and good quality materials
- Calibration of magnetic loop antennas was performed using theoretical and laboratory tests and antenna factor were calculated in the interested frequency range
- Electronic circuit was designed, constructed and tested to match the sensor impedance with acquisition system, reducing noise, avoiding reflections and undesired frequency components

- Available devices for acquisition system were tested and evaluated for the use with LEMFMS, selecting the frequency ranges and acquisition sampling according to desired signal analysis
- LEMFMS was constructed and components assembled, obtaining a modular and robust system, weather protected and suitable for maintenance and repair labours
- A LEMFMS was installed and start-up of system was performed in *Universidad Nacional de Colombia*, forming the basis for a complete system for lightning characterization in Bogota
- A lightning measuring campaign was performed during several months of 2013, being possible the analysis and evaluation of Magnetic Field System behaviour and obtaining a sufficiently set of signals for measure the performance of the whole system
- Comparison between Electric and Magnetic Field signals was achieved, obtaining adequate agreements and comparable results to evaluate the Magnetic Field System performance and obtaining statistics for lightning behaviour in Bogota and surroundings, constructing a database, amenable to improvements in order to establish a complete and reliable lightning database
- Algorithms for lightning parameters measuring, lightning discrimination and lightning direction were evaluated and some of them were implemented obtaining preliminary successful results
- Two filtering techniques were tested using lightning signals obtained with LEMFMS, evaluating the performance and comparing the obtained results

4.3. Publications

4.3.1. Ariza, D.; Roman, F.; Montero, O.; Escobar O.; F. Santamaria, "Behavior of corona current and atmospheric variables under thunderstorm conditions: thunderstorm prediction algorithm" Proc. of 31st International Conference on Lightning Protection, Vienna, Austria, September 2012.

In order to develop an algorithm to predict thunderstorms, atmospheric data is continuously recorded in Bogota Colombia, from July to November, 2011. The recorded variables are corona current, natural electric field, atmospheric pressure, ambient temperature and air humidity. From this large amount of recorded data, 22 thunderstorm events are selected to be analyzed in the present paper. The transition of the measured variables from fair weather- to thunderstorm conditions are presented and discussed. The recorded significant changes in the atmospheric data can be used to develop a thunderstorm predicting algorithm. The lightning electromagnetic field signals captured would be analyzed and related to the atmospheric variables.

4.3.2. Escobar, O., Rojas, H., Román, F. and Cortés, C., "Lightning Magnetic Field Measuring System in Bogotá – Colombia, Signal Processing Method" in XII International Symposium on Lightning Protection (SIPDA), October 2013.

This paper presents the configuration and performance of a magnetic field measuring system in Bogotá – Colombia and describes the signal processing procedure based on adaptive filters using the fractional Fourier Transform (FRFT) compared with traditional filters and the application of a numerical integration method to reduce the noise present in the recorded lightning signals.

4.3.3. Rojas, H., Santamaría, F., Escobar, O. and Román, F. Lightning research in Colombia, Part 1: Lightning parameters and protection systems and Part 2: Lightning measurements and overvoltage mitigation. Pending for publication.

This paper review summarizes the most important studies on lightning phenomena in Colombia during the last 25 years. Due to the extent of topic, this review has been divided in two parts to give a depth treatment to specific aspects and advances in lightning research. Lightning parameters and lightning protection systems are presented in Part I, while lightning discharge measurements, lightning discharge modeling and mitigation of lightning overvoltages mitigation are given in Part II of this work study. The paper

concludes with the advances and challenges on lightning research in Colombia.

Annex 1: Antenna Calibration

Loop antennas are used to measure the magnetic field emitted from a widely variety of devices as power transmission lines, antennas and so on. The antenna factor of a receiving loop antenna must be accurately calibrated as one of the main antenna's characteristics. In order to check the factor of the antenna that, combined with the electronic circuit factor, gives the factor to convert the voltage measured in the acquisition system and the magnetic flux, two approach were used: circuital model and calibration as antenna.

A11. Circuit Model

The circuit model provides the behaviour of loop antenna evaluated in terms of frequency for the particular interest in this project. From the analysis of the Thévenin equivalent circuit shown in Figure 64, its possible obtain the relationship between magnetic field flux density and voltage in terminals of loop antennas as was shown in Section 2.2.2.1.

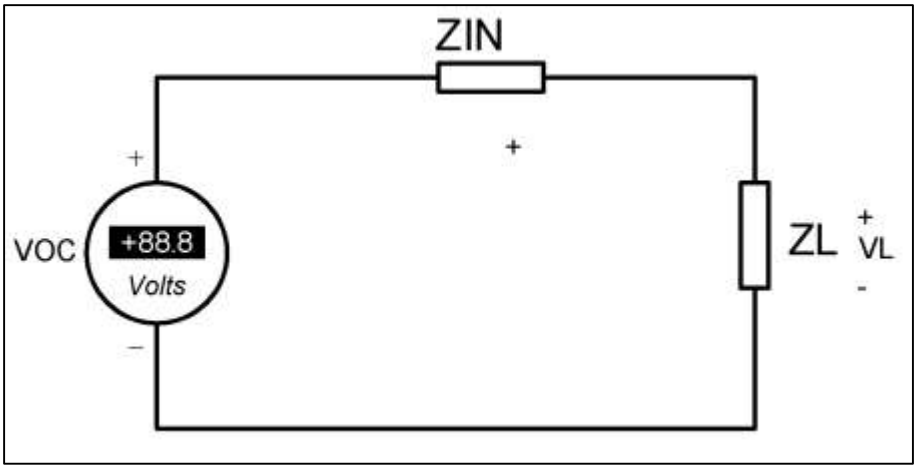

Figure 64. Thévenin equivalent circuit for loop antenna

From circuit of Figure 64 is possible define:

$$V_{OC} = j * \omega * \pi * a^2 * B_z^i \quad (20)$$

and

$$V_L = \frac{V_0 * Z_L}{Z_{in} + Z_L} \tag{21}$$

Where Z*in* corresponds to impedance of loop antenna and is modelled as is shown in Figure 65 with the full loop antenna model. The impedance of loop antenna could be modelled using a combination of resistances, inductances and capacitances proper of cable and antenna's geometry. In the next sections the different parameters are calculated and impedance model will be obtained.

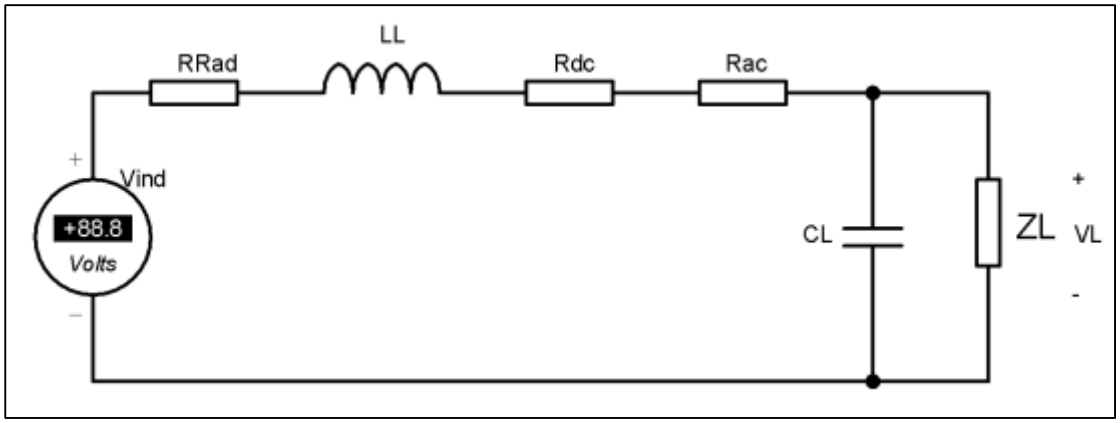

Figure 65. Loop antenna model shown in Figure 64 with Zin elements included.

A12. Resistance

Resistance will be composed by radiation resistance and ohmic resistance. Radiation resistance is defined as the energy losses during the transformation of electromagnetic energy to electric energy and is mainly important for the transmitter antennas. In the case of receiver antennas is considered but represent a minimal part of total resistance component.

Radiation resistance is calculated for a single-turn loop as [53]:

$$R_{Rad} = \eta * \left(\frac{2 * \pi}{3}\right) * \left(\frac{k * S}{\lambda}\right)^2 \cong 320 * \pi^4 * \left(\frac{S^2}{\lambda^4}\right) \tag{22}$$

Where:

R_{Rad}: is the radiation resistance of the loop,

S: is the area of the loop and

λ: is the wavelength

For the case of N-turn loop the ohmic resistance for an antenna with loop radius *a*, wire radius *b* and loop separation 2**c*, is given by:

$$R_{ohmic} = \frac{N * a}{2 * \pi * b} * R_S * \left(\frac{R_p}{R_0} + 1\right) \quad (23)$$

Where:

R_S: is the surface impedance of conductor,

$$R_s = \sqrt{\frac{\omega * \mu_0}{2 * \sigma}} \quad (24)$$

R_p: is the ohmic resistance per unit length due to the proximity effect and

R_0: is the ohmic skin effect resistance per unit length [Ω/m].

$$R_0 = \frac{N * R_s}{2 * \pi * b} \quad (25)$$

In the case of single-turn loop constructed for this project, the term R_p/R_0 tends to zero because do not exist the proximity effect between turns for be only one turn (N=1). For this reason the equation (23) is calculated as:

$$R_{ohmic} = \frac{a}{b} * R_S \rightarrow R_{ohmic} = \frac{a}{2 * \pi * b} * \sqrt{\frac{\omega * \mu_0}{2 * \sigma}} \quad (26)$$

Table 12 shows the geometrical parameters provided by the manufacturer of coaxial cable checked by direct measurement, in order to calculate the resistance parameters of equations (22) and (26), along with the radius value of the loop corresponding to 0,15 [m], therefore:

$$R_{Rad} = 320 * \pi^4 * \left(\frac{(\pi * 0{,}15^2)^2}{\lambda^4}\right) \rightarrow R_{Rad} = \frac{0{,}1557}{\lambda^4}$$

In the case of maximum value of frequency in the range selected, 30 MHz, the radiation resistance corresponds to 15,57 [μΩ] and will be demonstrated that corresponds to a minimal part of total resistance component.

Table 12. Geometrical parameters of coaxial cables RG-62 of BEDEA used for the construction of loop antennas [72].

Parameter	Value
Inner conductor (diameter) StCub: Copper weld wire bare	0,65 [mm]
Insulation	3,71 [mm]
Outer Conductor	3,71 to 6,15 [mm]

CuGb: Copper braiding	
Sheathing (diameter)	6,15 [mm]
DC Resistance inner conductor	150 $[\Omega/\mathrm{km}]$
DC Resistance outer conductor	8 $[\Omega/\mathrm{km}]$
Capacitance	42,5 [pF/m]
Velocity ratio	0,83 [v/c]

The value of conductivity of copper weld wire was based on the value for copper and efficiency of copper weld referred in 10% to 30% respect to copper [73]. In this case the value used is $5{,}7*10^6$ [S/m].

In the case of ohmic resistance:

$$R_{AC} = \frac{0{,}15}{2 * \pi * 0{,}00065} * \sqrt{\frac{\omega * 4 * \pi * 10^{-7}}{2 * 5{,}7 * 10^6}}$$

$$R_{AC} = 36{,}728 * \sqrt{\omega * 1.1 * 10^{-13}}$$

In the case of maximum value of frequency in the range selected, 30 MHz, the ohmic resistance corresponds to $167{,}24$ $[\mathrm{m}\Omega]$. For DC resistance calculation, the generic formula was used:

$$R_{DC} = \frac{1 * l}{\sigma * A} \tag{27}$$

Where:

l: Loop length,

σ: Copper weld conductivity and

A: Transversal area of wire.

And with parameters of Table 12 is obtained:

$$R_{DC} = \frac{1 * 2 * \pi * 0{,}15}{5{,}7 * 10^6 * \pi * 0{,}00065^2} \rightarrow R_{DC} = 0{,}124572[\Omega]$$

Comparing this result with the value provided by the manufacturer:

$$R_{DC} = 150 * \frac{2 * \pi * 0.15}{1000} = 0{,}1414[\Omega]$$

Is possible conclude that the value assumed for conductivity of copper weld wire is correct and the ohmic resistance for AC values is correctly used.

A13. Inductance

For the calculus of loop inductance is possible use [53]:

$$L_L = \mu_0 * a * \left(\ln\left(\frac{8 * a}{b}\right) - 2\right) \tag{28}$$

Calculating:

$$L_L = 4 * \pi * 10^{-7} * 0{,}15 * \left(\ln\left(\frac{8 * 0{,}15}{0{,}00065}\right) - 2\right) \rightarrow L_L = 1.0407[\mu H]$$

A14. Capacitance

Capacitance value of the loop is taken directly from manufacturer datasheet, in part because the properties of insulation material, referred as LD-PE are not detailed by the manufacturer in order to calculate the capacitance using the general equations for coaxial conductor. For this reason, the value reported as 42,5 [pF/m] is calculated for the length of loop as:

$$C_L = 42{,}5 * \frac{2 * \pi * 0.15}{1} = 40{,}05[pF]$$

Using the calculated values of loop antenna, it is possible simulate his behaviour in the frequency range of interest. The transfer function of loop antenna was modelled using the values calculated in the maximum frequency of interest 30 [MHz].

From the equivalent circuit of antenna and using the definition of antenna factor:

$$K_E = \frac{E}{V_L} \tag{29}$$

Is possible calculate the antenna factor (equivalent to relation between input (in this case the electric field strength) and output voltage) as:

$$K_H = \frac{1}{S^2 * L_L * C_L + S * ((R_{Rad} + R_{AC}) * C_L) + 1} \quad (30)$$

Calculation of antenna factor was developed in Matlab® software. The frequency response of circuit model is shown in Figure 66. Is possible denote form the figure that:

- Frequency response of loop presents a constant gain until 30 [MHz] approximately,
- The gain in the maximum frequency of range of interest is 1,52 [dB], and
- The peak of gain and consequently decrease of gain is in 64,7 [MHz] that results the double of maximum frequency of interest and do not affect the signals in the range of interest.

This results shown that frequency response and corresponding antenna factor is adequate in the range of interest, being suitable and accurate for lightning measurements. Finally, for the specific case of lightning loops, the electric field *E* must be converted into the magnetic field *H* using the free-space wave impedance.

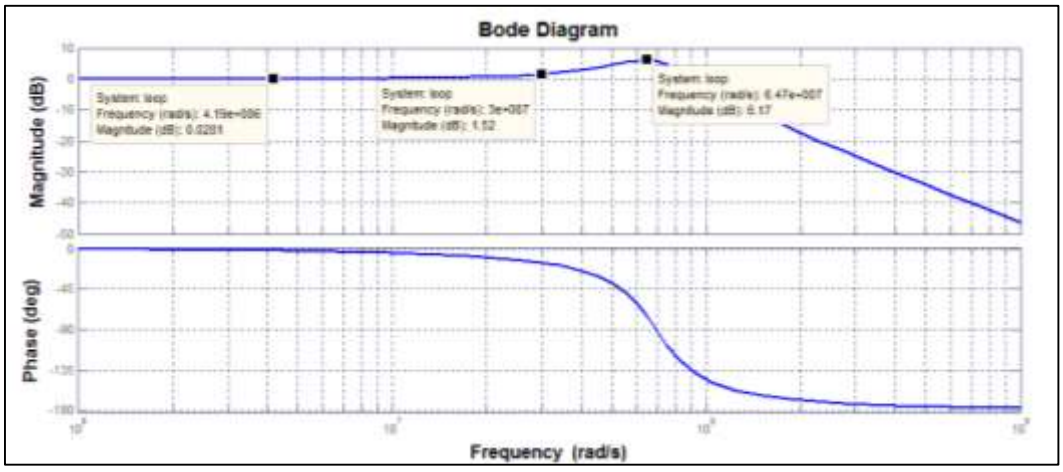

Figure 66. Frequency response of loop antenna transfer function.

A15. Impedance Method Calibration

In order to obtain a better accuracy in the factor between measured voltage and incident magnetic field, the magnetic antenna factor is defined as (See Figure 67):

$$FM(f) = \frac{H(f)}{V_0(f)} \tag{30}$$

This antenna factor is defined as the ratio of an incident electric field to the corresponding output voltage across the matched load. In order to obtain (30), the electric field *E* must be converted into the magnetic field *H* using the free-space wave impedance, based in the fact that electromagnetic signals received by the loop are from far-field condition.

The Impedance Method Calibration developed by Ishii *et al.* [75] was applied to loop antennas. This method is widely used for the easiness of procedure test compared with traditional methods as three antennas or far-field measurements. In traditional methods is necessary the use of two similar antennas and tests fields with lengths superior to wavelength of loop frequency range, for example, in the case of lightning loop antennas constructed for this project, this field must have at least 20 meters for each side and without any obstacle that could interfere the measurements.

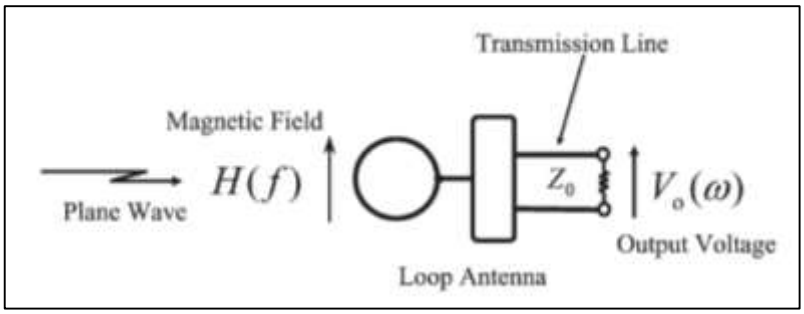

Figure 67. Definition of magnetic antenna factor. Z0 is the load matched to the line impedance, and f is the frequency [75].

Generally, the magnetic antenna factor is defined in far-field condition and in free space. However, it is difficult to apply actual plane wave to a loop antenna and to realize far-field condition in the low frequency because the wave length is more than 20 [m]. Consequently there is non-uniformly distributed magnetic field inside the loop. This traditional method of far-field measurement was implemented in EMC Laboratory and 411 building using a Virtual Network Analyser, nevertheless, the field conditions avoid a correct measurement of variables of interest and the results were not plausible and adequate for antenna calibration. For this reason, the Impedance Method Calibration mentioned above was developed.

The Impedance Method Calibration could be applied to antennas as the developed in this project: Electrically small antennas in the range below to 30

MHz and shielded loops. The objective of method is obtain the magnetic antenna factor of a loop antenna in the far-field without the application of electromagnetic waves to it.

The structure of loop antenna is modelled through an equivalent circuit as is shown in Figure 68 (a) and (b) where:

Z_0: Characteristic impedance of transmission line $(93\ [\Omega])$,

L_1 and L_2: Half-lengths of loop elements $\left(\frac{1}{2} * 2 * \pi * 0{,}15\right) = 0{,}4712\ [m]$,

Z_R: Load impedance at one end of the compensation circuit $(0\ [\Omega])$,

Z_L: Matched load to the line impedance $(93\ [\Omega])$,

Z_{in}: Input impedance of the loop antenna element alone,

Z'_R and Z'_L are expressed as:

$$Z'_R = Z_0 * \left(\frac{Z_R + Z_0 * \tanh(j * k * L_2)}{Z_0 + Z_R * \tanh(j * k * L_2)}\right) \quad (31)$$

$$Z'_L = Z_0 * \left(\frac{Z_L + Z_0 * \tanh(j * k * L_1)}{Z_0 + Z_L * \tanh(j * k * L_1)}\right) \quad (32)$$

Where $k=2*\pi/\lambda$ is the wavenumber and λ is the wave length in the cable.

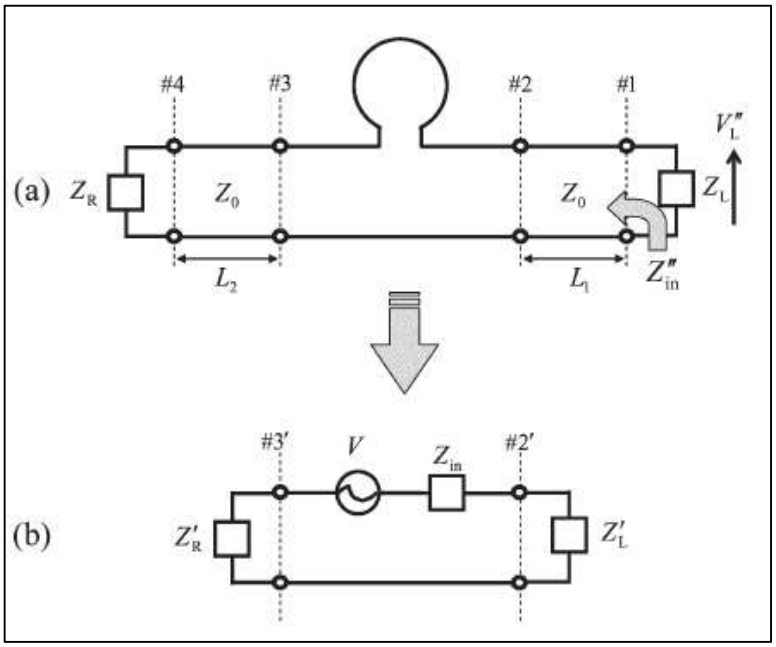

Figure 68. Equivalent circuits of shielded loop antenna. (a) Equivalent circuit and (b) Remodelled circuit of (a). For meaning of symbols, see text. Taken from [75].

On the other hand, the open-circuit output voltage *V* of the loop antenna element is expressed by Faraday's law as was defined in (9) and retyped with the names of variables as:

$$V = -j * \omega * \pi * r^2 * \mu_0 * H \tag{33}$$

Where ω is the angular frequency, *r* the radius of loop antenna, μ_0 the permeability of free space and *H* the magnetic-field strength of the incident plane wave.

Using equation (33) and based in configuration shown in Figure 68, the magnetic antenna factor of the loop antennas is expressed as:

$$FM(\omega) = \frac{H}{V_L''}$$

$$= j * \frac{Z'_R + Z_{in} + Z'_L}{\omega * \mu_0 * \pi * r^2 * Z_L} * \frac{Z_L + Z_0}{Z'_L + Z_0} * e^{j*k*L_1} \tag{34}$$

Where:

$$Z_{in} = \frac{Z_0 * (Z''_{in} - Z'_R) + (Z''_{in} * Z'_R - Z_0^2) * \tanh(j * k * L_1)}{Z_0 - Z''_{in} * \tanh(j * k * L_1)} \tag{35}$$

From this equations, Z''_{in} is the unknown. Measuring the input impedance of the loop antenna system, the magnetic antenna factor could be calculated using (31), (32), (34) y (35).

In order to obtain the input impedance of loop antenna, a Fluke RLC Meter PM 6306 with frequency range until 1 [MHz], was used and input impedance of loop antenna was obtained. Measurements were made in defined frequencies in steps of 100 [Hz] from 100 to 1000 [Hz], 1 [kHz] from 1 to 10 [kHz], 2 [kHz] from 2 to 20 [kHz] and specific points in 100 [kHz], 500 [kHz] and 1 [MHz] according the characteristics of RLC meter.

Using a code programmed in a commercial software, a routine for calculate the magnetic antenna factor was implemented. Calculations were made using the measurements and equations mentioned above and transformation to dB was the final step. Results of magnetic antenna factor are shown in Figure 69.

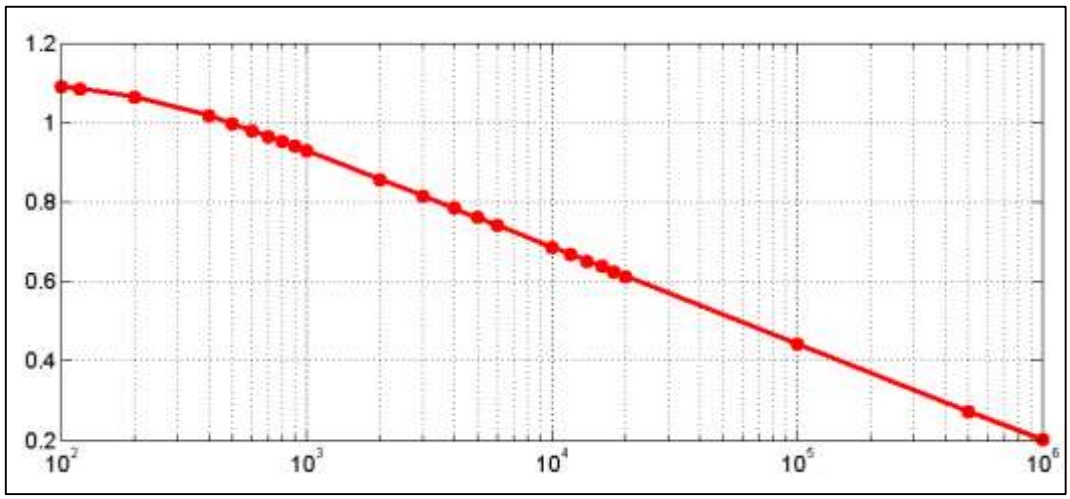

Figure 69. Magnetic Antenna Factor for loop antenna.

Using the calibration obtained with Impedance Method, was possible obtain a better resolution of factor in lower frequencies than 1 [Mhz] respect to circuit model that provides only a value near to zero (See Figure 66). Figure 69 shows that difference between very low frequencies and 1 [MHz] is near to 0,9 [dB] that represent a difference of 18 %, between 100 [Hz] gain of 1,288 and 1 [MHz] gain of 1,047.

Using two calibrations made with circuit models and complemented with measurements of input impedance, the calibration in all the frequency range selected was made obtaining the multiplicative factor that allows the conversion between magnetic field strength and voltage across a load impedance.

The calibration of a loop antenna requires that factor FM must be determined for each frequency on the entire loop frequency band [76]. According to this definition, the antenna factor was obtained for all the frequency range selected for loop antenna and combination between circuit model and Impedance Calibration Method. In both cases the calculation were developed using the antenna factor in relation with electric field and output voltage, being necessary the conversion to magnetic field through use of the free-space wave impedance. This calculation to obtain the final antenna factor for calibration in all the frequency range was used for processing method developed in Chapter 3.

Annex 2: Additional Features

Some characteristics that could be measured and analysed with the lightning electromagnetic field system proposed and constructed during this thesis are related in this section. This processes are not totally developed because exceed the objectives of work, but are subject to expansion for future improvements of measuring system.

A21. Cloud-ground and Cloud-cloud discrimination

In order to obtain reliable statistics of lightning events, the discrimination between cloud to cloud and cloud to ground flashes should be performed. More than 75% of total lightning are cloud to cloud or intra-cloud (See Section 1.1) and statistics related to direct impacts to ground could be obscured if discrimination is not evaluated.

The location and discrimination of lightning flashes is a complete brand of research due to the importance of recognize the lightning characteristics and evaluate the statistics for flash impacts to ground, main input for lightning protection projects and structures safety. Several algorithms for discrimination had been developed using information of multiple measuring stations [67]-[68].

The differences between cloud to ground and cloud to cloud flashes are not easily identifiable using only one measuring station. Nevertheless, some algorithms and techniques that use the information of only one station had been tested assuming several conditions obtaining acceptable results [57]-[69]-[70].

Between the different discrimination techniques that use the information of only one measuring station, the classification according the signature in high frequencies (above than 5 MHz) is the most reliable and studied in the last years. Mäkelä [71] analysed lightning signals from one station using a high frequency acquisition system and suggest the main differences between events cloud to ground and cloud to cloud and intra-cloud flashes.

Taking advantage of bandwidth of Lightning Electromagnetic Field Measuring System constructed and tested in this project, could be possible evaluate the captured signals to discriminate between CG and CC flashes, using small sampling times to obtain adequate resolution to analysis.

In order to evaluate the accuracy of this proposed feature, it is necessary the comparison with a lighting network capable of discriminate between CC and CG flashes. By the date of this document, the LINET network installed in Colombia claim for an accuracy of 90% in CG and CC discrimination, being probable a comparison with this system using GPS time stamp for coordination.

A22. Lightning Location

Lightning location techniques have been applied at the same time of lightning measurement techniques have been developed. Lightning location using one single-station is an approach used in recent years through the use of several instruments as GPS and based in Satellite LLS, discriminating the lightning direction and calculating, based in Satellite LLS, the peak current of flashes.

During this project, an approximation to use the Measuring Station as LLS was developed, obtaining locations and relative peak current magnitudes. Nevertheless, was not possible the comparison with other LLS systems, being necessary for future developments and functions for Lightning Measuring Station.

REFERENCES

[1] V. Cooray, "The Lightning Flash", *Institute of Electrical and Electronic Engineers*, England, 2003.

[2] V. Rakov and M. Uman, "Lightning: Physics and Effects", *Cambridge University Press*, United Kingdom, 2003.

[3] M. Uman, "The Lightning Discharge", *Academic Press Inc.*, International Geophysical Series, Volume 39, United Kingdom, 1987.

[4] H. Norinder, "Rapid variations in the magnetic field produced by lightning discharges", *Proceedings of Physical Society* 49 364, 1937.

[5] F. Horner, "Very-Low-Frequency Propagation and Direction-Finding", *The Proceedings of the Institution of Electrical Engineers*, Vol. 104, Part B, No. 14, 1957.

[6] J, Schoene, A. Uman, A. Rakov, V. Kodali, J. Rambo, and G.H. Schnetzer, "Statistical characteristics of the electric and magnetic fields and their time derivatives 15 m and 30 m from triggered lightning," *Journal of Geophysical Research*, Vol. 108, No D6, 4192, 2003.

[7] G. Diendorfer, A. Mosaddeghi, D. Pavanello, H. Pichler, F. Rachidi and M. Rubinstein, "Electric and Magnetic Field Measurements at Very Close Range Associated with Lightning Strikes to the Austrian Gaisberg Tower", *European COST Action P18 'The Physics of Lightning Flash and Its Effects"*, 2009.

[8] A. Mahanfar, R. Moini, R. Sadeghi, and S. Bonyadi-Ram, "A Novel Automated Detection Of Electromagnetic Fields Due To Lightning Strokes", *IEEE International Symposium on Electromagnetic Compatibility*, pp. 205-209, 2001.

[9] F. Rachidi, "Indirect Estimation of Lightning Currents from Remote Electromagnetic Field Measurements", *Proceedings of IX International Symposium on Lightning Protection*, 2007.

[10] E. Bazelyan, M. Chichinskiy, "Recovery of the Parameters of a Lightning Current Pulse from Measurements of the Electromagnetic Field in the Far Wave Zone", *Plasma Physics Reports,* Vol. 35, No. 9, pp. 794–801, 2009.

[11] E. Olarte, I. Santoyo, D. Aranguren, E. Pérez, J. Herrera and H. Torres, "Sistema Colombiano de Información de Tormentas Eléctricas Soportado en Renata", *Universidad Nacional de Colombia*, 2008.

[12] H. Bernal, J. Castro, "Medición de la radiación electromagnética proveniente de descargas eléctricas atmosféricas mediante una antena de placas paralelas", Undergraduate Thesis *Universidad Nacional de Colombia – Sede Bogotá, Departamento de Ingeniería Eléctrica*, 1991.

[13] A. Cáceres, O. López, "Medición del campo magnético radiado por el rayo mediante una antena bucle", Undergraduate Thesis, *Universidad Nacional de Colombia – Sede Bogotá, Departamento de Ingeniería Eléctrica*, 1993.

[14] Betz, H; Schumann, U; *Lightning: Principles, Instruments and Applications*, Springer Science+Business Media, United States of America, 2009.

[15] "Website of Keraunos S.A.S" Available at: http://keraunos.co/, 23 November 2012.

[16] O. Puerta, "Diseño de antena de lazos para medición de campo magnético producido por descargas atmosféricas", Undergraduate Thesis, *Universidad Nacional de Colombia – Sede Medellín, Escuela de Ingeniería Eléctrica y Mecánica,* 2009.

[17] F. Santamaría, "Medición de Campo Eléctrico de Rayos con una antena de placas paralelas en la Ciudad de Bogotá y comparación con otras zonas del mundo", MSc Thesis in Electrical Engineering, *Universidad Nacional de Colombia – Sede Bogotá, Departamento de Ingeniería Eléctrica*, 2005.

[18] F. Santamaría, C. A. Cortés, and F. Roman, "Noise reduction of measured lightning electric fields signals using the wavelet transform," in X International Symposium on Lightning Protection (SIPDA), 2009.

[19] H. E. Rojas, C. A. Cortes, and F. Santamaria, "Denoising of Lightning Electric Field Signals Using Fractional Fourier Transform,"

in *31st International Conference on Lightning Protection (ICLP),* 2012, pp. 1–9.

[20] M. Chen, N. Takagi, T. Watanabe, D. Wang, Z. I. Kawasaki, and X. Liu, "Spatial and temporal properties of optical radiation produced by stepped leaders", *Journal of Geophysical Research*, No. *104*, pp. 27573–27584, 1999.

[21] F. Heidler, W. Zischank, Z. Flisowski, C. Bouquegneau, and C. Mazzetti, "Parameters of Lightning Current given in IEC 62305 – Background, Experience and Outlook," in *29th International Conference on Lightning Protection*, 2008, June, pp. 1–22.

[22] U. Sonnadara, V. Cooray, and M. Fernando, "Lightning radiation field spectra of cloud flashes," *in 27th International Conference on Lightning Protection (ICLP)*, 2004.

[23] A. Nag, V. a. Rakov, and J. a. Cramer, "Remote Measurements of Currents in Cloud Lightning Discharges," *IEEE Transactions on Electromagnetic Compatibility*, vol. 53, no. 2, pp. 407–413, May 2011.

[24] A. M. Hussein, W. Janischewskyj, J. S. Chang, V. Shostak, W. A. Chisholm, P. Dzurevych, and Z. I. Kawasaki, "Simultaneous measurement of lightning parameters for strokes to the Toronto Canadian National Tower", *Journal of Geophysical Research*, vol. 100, pp. 8853-61, 1995.

[25] G. Diendorfer, M. Mair, W. Schulz, and W. Hadrian, "Lightning current measurements in Austria-experimental setup and first results" in *25th International Conference on Lightning Protection (ICLP)*, Rhodes, Greece, 2000, pp. 44-47.

[26] M. Manhardt, F. Heidler, and K. Stimper, "The Electric Field Of Negative Upward Lightning Strikes At The Peissenberg Tower, Germany", in *31st International Conference on Lightning Protection (ICLP)*, Vienna, Austria, 2012.

[27] A. Rubinstein, C. Romero, M. Paolone, F. Rachidi, M. Rubinstein, P. Zweiacker, and B. Daout, "Lightning measurement station on Mount Säntis in Switzerland," in *X International Symposium on Lightning Protection (SIPDA)*, Curitiba, Brazil, 2009, pp. 463–468.

[28] T. Miki, T. Shindo, A. Asakawa, H. Motoyama, Y. Suzuhigashi, and M. Chihara, "Measurement of Lightning Currents at TOKYO SKYTREE and Observation of Electromagnetic Radiation Caused by Strikes to the Tower," in *31st International Conference on Lightning Protection (ICLP)*, 2012, pp. 1–5.

[29] E. Cano, "Protección contra descargas atmosféricas: 1. Física del rayo", Grupo de Redes de Distribución y Potencia- GREDyP, *Universidad Nacional de Colombia*, 2008.

[30] J. E. Jerauld, "Properties of natural cloud-to-ground lightning inferred from multiple-station measurements of close electric and magnetic field and field derivatives" PhD Dissertation University of Florida, 2007.

[31] K. Berger, R. B. Anderson, and H. Kroninger, "Parameters of lightning flashes", *Electra*. no., vol. 41, pp. 23-37, 1975.

[32] D. Aranguren, "Estudio de las tormentas eléctricas a través del campo eléctrico ambiental" MSc Dissertation Universidad Nacional de Colombia, 2006.

[33] V. Rakov, "Characterization of lightning electromagnetic fields and their modeling" Downloaded in June 2011 from http://www.lightning.ece.ufl.edu/PDF/Zurich/1T01.pdf, 2000.

[34] E. M. Thomson, P. J. Medelius, and M. A. Uman, "A remote sensor for the three components of transient electric fields," *IEEE Transactions on Industrial Electronics*, vol. 35, no. 3, pp. 426–433, 1988.

[35] D. Pavanello, "Electromagnetic radiation from lightning return strokes to tall structures," PhD Dissertation École Polytechnique Fédérale de Laussane, 2007.

[36] P. Krider and C. Noggle, "Broadband Antenna Systems for Lightning Magnetic Fields", *Journal of Applied Meteorology*, March 1975, pp. 252.

[37] D. P. Williams and M. Brooke, "Magnetic measurements of thunderstorm currents: 1. Continuing currents in lightning", *Journal of Geophysical Research*, 68(10), pp. 3243–3247, 1963.

[38] Nelson, L.N. Magnetographic Measurements of Charge Transfer in the Lightning Flash. Geophysical Research Vol. 73(19), pp. 5967-5972, 1968.

[39] C. E. Baum, S. Member, E. L. Breen, F. L. Pitts, G. D. Sower, and M. E. Thomas, "The Measurement of Lightning Environmental Parameters Related to Interaction with Electronic Systems," *IEEE Transactions on Electromagnetic Compatibility*, vol. EMC-24, no. 2, pp. 123–137, 1982.

[40] S. Bernal and F. Román, "Design of a Multigap Loop (MGL) sensor for lightning magnetic field measurement," in *XI International Symposium on Lightning Protection (SIPDA)*, 2011, pp. 2–6.

[41] H. L. Jones, R. L. Calkins, and H. W. L., "Review of the Frequency Spectrum of Cloud to Cloud and Cloud to Ground Lightning," *IEEE Transactions on Geoscience Electronics*, vol. GE-5, no. 1, pp. 26–30, 1967.

[42] J. C. Willett, J. C. Bailey, C. Leteinturier and E. P. Krider, "Lightning electromagnetic radiation field spectra in the interval from 0.2 to 20 MHz", *Journal of Geophysical Research* 95 (D12), 20, 367-320, 387, 1990.

[43] M. Chen, Y. Du, J. Burnett, and W. Dong, "The Electromagnetic radiation from lightning in the interval of 10 kHz to 100 MHz.", Report of *The Hong Kong Polytechnic University, Hong Kong SAR of China.*

[44] V. A. Rakov, S. Mallick, and A. Nag, "Lightning Observatory in Gainesville (LOG), Florida: A Review of Recent Results," in *31st International Conference on Lightning Protection (ICLP)*, 2012.

[45] Y. T. Lin, M. A. Uman, J. A. Tiller, R. D. Brantley, and W. H. Beasley, "Characterization of Lightning Return Stroke Electric and Magnetic Fields from Simultaneous Two-Station Measurements," *Journal of Geophysical Research*, vol. 84, no. C10, pp. 6307–6314, 1979.

[46] V. A. Rakov, "Characterization of lightning electromagnetic fields and their modeling," Report of *University of Florida*, Gainesville, USA, 1999.

[47] J. Cerra, A. L. Pinzón, "Influencia de las Estructuras en la Propagación de los Campos Electromagnéticos Producidos por los Rayos", Bachelor Thesis in Electrical Engineering, *Universidad Nacional de Colombia – Sede Bogotá, Departamento de Ingeniería Eléctrica*, 2012.

[48] J. Kraus, R. Marhefka, "Antennas for All Applications", *Tata McGraw Hill Publishing Company Limited,* Second Edition, 1998.

[49] C. E. Baum, E. L. Breen, J. Giles, J. O'Neill, and G. Sower, "Sensors for electromagnetic pulse measurements both inside and away from nuclear source regions," *IEEE Transactions on Electromagnetic Compatibility*, vol. AP-25, no. 1, p. 15, 1978.

[50] D. M. Le Vine, "Review of Measurements of the RF Spectrum of Radiation from Lightning," *Meteorology and Atmospheric Physics*, vol. 37, pp. 195–204, 1987.

[51] J. C. Willet, J. C. Bailey, C. Leteinturier, and E. P. Krider, "Lightning electromagnetic radiation field spectra in the interval from 0.2 to 20MHz", *Journal of Geophysical Research*, No. 95, 1990.

[52] E. Paschal, "The design of broad-band VLF receivers with air-core loop antennas," 1988.

[53] C. Balanis, "Antenna Theory, Analysis and Design", *Wiley Interscience, John Wiley & Sons*, Third Edition, 2005.

[54] S. Mallick, A. Nag, and V. A. Rakov, "Measurements of Radiation Field Signatures of Rocket-Triggered Lightning," in *2010 International Conference on High Voltage Engineering and Application (ICHVE)*, 2010, pp. 40–43.

[55] V. Cooray and C. Gomes, "Estimation of peak return stroke currents, current time derivatives and return stroke velocities from measured fields," *Journal of Electrostatics*, vol. 43, no. 3, pp. 163–172, May 1998.

[56] W. A. Lea, "Immediate-Readout Lightning Direction Finders," *Northwest Science*, vol. 38, no. 4, pp. 109–133, 1964.

[57] M. Chen, T. Lu, and Y. Du, "Experimental study of single-station lightning locating technique," *2011 7th Asia-Pacific International Conference on Lightning*, pp. 59–64, Nov. 2011.

[58] M. Loboda, H. D. Betz, P. Baranski, J. Wiszniowski, and Z. Dziewit, "New Lightning Detection Networks in Poland - LINET and LLDN," *The Open Atmospheric Science Journal*, vol. 3, no. 1, pp. 29–38, Jan. 2009.

[59] K. Theobald, "On the Properties of Loop Antennas", *Sensor and Simulation Notes IV,* p. 5, 1964.

[60] G. S. Smith, "Chapter 5: Loop Antennas," in *Antenna Engineering Handbook*, Second Edition, McGraw Hill Book Company.

[61] Y. T. Lo and S. W. Lee, "Antenna Handbook: Vol. II Antenna theory", *Van Nostrand Reinhold,* 1993.

[62] J. M. Drake, "Tema III: El amplificador de instrumentación" in *Instrumentación Electrónica de Comunicaciones*, Cantabria University, 2005.

[63] J. Rai and P. K. Bhattacharya, "Impulse magnetic flux density close to the multiple return strokes of a lightning discharge," *Journal of Applied Physics*, vol. 4, pp. 1252–1255, 1971.

[64] ICONTEC: Colombian Institute of Technical Standards and Certification (Spanish: Instituto Colombiano de Normas Técnicas y Certificación), "NTC 4552-1: Protección contra descargas eléctricas atmosféricas (rayos), Parte 1: Principios generales", *ICONTEC*, Bogota, 2008.

[65] H. E. Rojas and C. A. Cortes, "Adaptive Filtering for Lightning Electric Field (LEF) Signals in Fractional Fourier Domain," in 2012 IEEE Statistical Signal Processing Workshop, 2012, pp. 213–215.

[66] X. Zhou, Z. Zhao, L. Li, and X. Cui, "The acquisition and analysis system for lightning electromagnetic wave based on LabVIEW," *2010 Asia-Pacific International Symposium on Electromagnetic Compatibility*, pp. 1482–1485, 2010.

[67] H. D. Betz, K. Schmidt, W. P. Oettinger, and M. Wirz, "Total VLF/LF - Lightning and pseudo 3D-Discrimination of intra-cloud and

cloud-to-ground discharges," in *18th International Lightning Detection Conference*, 2004, no. 33, pp. 1–9.

[68] A. B. Weerasekera, R. Lelwala, T. R. Ariyaratne, and S. Namasivayam, "Locating cloud-to-ground lightning flashes with simultaneous two-station measurements," vol. 1, pp. 11–22, 2000.

[69] C. Mackay and a. C. Fraser-Smith, "World coverage for single station lightning detection," *Radio Sci.*, vol. 46, no. 3, Jun. 2011.

[70] W. I. Ibrahim and M. R. Ghazali, "Measurements of electric and magnetic fields due to lightning strokes based on single-station detection," *2012 IEEE Asia-Pacific Conf. Appl. Electromagn.*, no. Apace, pp. 268–273, Dec. 2012.

[71] J. Mäkelä, "Electromagnetic Signatures of Lightning near the HF frequency band," University of Helsinki, 2010.

[72] BEDEA, "RG-Kabel für höchste Anforderungen RG-Cables for highest demands", *BEDEA Berkenhoff & Drebes GMBH Catalog*.

[73] A. DiPaola and S. Dipaola, "Introduction to Low Voltage Systems", *Electronics Technicians Association*, 2nd Edition.

[74] F. Grover, "Inductance Calculation, Working Formulas and Tables", *Instrumentation Systems*, 1982.

[75] M. Ishii and K. Komiyama, "Impedance Method for a Shielded Standard Loop Antenna," *IEEE Transactions on Instrumentation and Measurement*, vol. 56, no. 2, pp. 422–425, Apr. 2007.

[76] A. Aykan, "Calibration of circular loop antennas," *IEEE Transactions on Instrumentation and Measurement*, vol. 47, no. 2, pp. 446–452, Apr. 1998.